Check for updates

small methods
www.small-methods.com

Ambient Fabrication of Organic–Inorganic Hybrid Perovskite Solar Cells

*Yuan Zhang, Ashleigh Kirs, Filip Ambroz, Chieh-Ting Lin, Abdulaziz S. R. Bati, Ivan P. Parkin, Joseph G. Shapter, Munkhbayar Batmunkh, and Thomas J. Macdonald**

Organic–inorganic hybrid perovskite solar cells (PSCs) have attracted significant attention in recent years due to their high-power conversion efficiency, simple fabrication, and low material cost. However, due to their high sensitivity to moisture and oxygen, high efficiency PSCs are mainly constructed in an inert environment. This has led to significant concerns associated with the long-term stability and manufacturing costs, which are some of the major limitations for the commercialization of this cutting-edge technology. Over the past few years, excellent progress in fabricating PSCs in ambient conditions has been made. These advancements have drawn considerable research interest in the photovoltaic community and shown great promise for the successful commercialization of efficient and stable PSCs. In this review, after providing an overview to the influence of an ambient fabrication environment on perovskite films, recent advances in fabricating efficient and stable PSCs in ambient conditions are discussed. Along with discussing the underlying challenges and limitations, the most appropriate strategies to fabricate efficient PSCs under ambient conditions are summarized along with multiple roadmaps to assist in the future development of this technology.

1. Introduction

Developing clean energy that is readily accessible and deployable is essential in order to decouple from fossil fuels, which is one of the major contributors to global warming.[1,2] Unlike fossil fuels, the sun is an inexhaustible energy source that delivers more energy to the earth in 1 h than the entire planet consumes in one year. Energy can be harvested from the sun using photovoltaics (PV) and stored (e.g., batteries), meaning solar energy can be used as and when required.[3,4] Currently, the commercial PV market is dominated by single-junction crystalline silicon (c-Si) PV which deliver power conversion efficiencies (PCE) of over 26% under 1 Sun illumination (AM 1.5 standard).[5,6] Despite their high efficiencies, the fabrication of c-Si PV is nontrivial and lacks electronic tunability. Furthermore, the record efficiency for c-Si PV is 26.7%[5] which is very close to the theoretical limit of 29.4%.[7] This clearly indicates that c-Si PV is a mature technology and there is limited room for improvement.[8] Over the past two decades, third-generation solar cells such as dye-sensitized solar cells,[9,10] quantum dot solar cells,[11,12] organic solar cells,[13,14] and perovskite solar cells (PSCs)[15,16] have been developed as alternatives to c-Si technologies. Of these third-generation solar cells, single-junction PSCs have generated significant attention due to their intense visible to near-infrared absorptivity,[16–18] long diffusion lengths of the charge carriers,[19,20] high efficiency,[21,22] electronic and physical tunability,[23,24] and low manufacturing costs.[25,26] After the first report by Miyasaka's group in 2009,[27] the PCE for single junction devices increased considerably from 3.8% to 25.2%,[27,28] making it the fastest advancing PV technology to date. This has uniquely placed PSCs as the frontrunner technology to potentially replace or coexist with c-Si PV.

The term "perovskite" refers to a group of compounds that share the same lattice structure as calcium titanium oxide ($CaTiO_3$). All PV perovskite materials have the general chemical formula ABX_3, as illustrated in **Figure 1**a. Organic–Inorganic hybrid PSCs are typically made using an organic/inorganic cation (A = methylammonium (MA) $CH_3NH_3^+$, formamidinium (FA) $CH_3(NH_2)_2^+$, or cesium), a divalent cation (B = Pb^{2+} or Sn^{2+}) ,[29] and an anion (X = Cl^-, Br^-, or I^-), illustrated in Figure 1b.[16,30] A is surrounded by eight lead halide octahedra (B in the center of octahedra) and forms a cubic perovskite structure. When the size of A or/and X is changed, the structure of perovskite will distort. The Goldschmidt tolerance factor (t)[31] of perovskite is an empirical index for

Y. Zhang, A. Kirs, F. Ambroz, Prof. I. P. Parkin, Dr. T. J. Macdonald
Department of Chemistry
University College London
20 Gordon St, London WC1H 0AJ, UK
E-mail: t.macdonald@imperial.ac.uk
Dr. C.-T. Lin, Dr. T. J. Macdonald
Department of Chemistry and Centre for Plastic Electronics
Imperial College London
London W12 0BZ, UK
A. S. R. Bati, Prof. J. G. Shapter
Australian Institute for Bioengineering and Nanotechnology
The University of Queensland
St Lucia, Queensland 4072, Australia
Dr. M. Batmunkh
Centre for Clean Environment and Energy
Griffith University
Gold Coast, Queensland 4222, Australia
The ORCID identification number(s) for the author(s) of this article can be found under https://doi.org/10.1002/smtd.202000744.

© 2020 The Authors. Published by Wiley-VCH GmbH. This is an open access article under the terms of the Creative Commons Attribution License, which permits use, distribution and reproduction in any medium, provided the original work is properly cited.

DOI: 10.1002/smtd.202000744

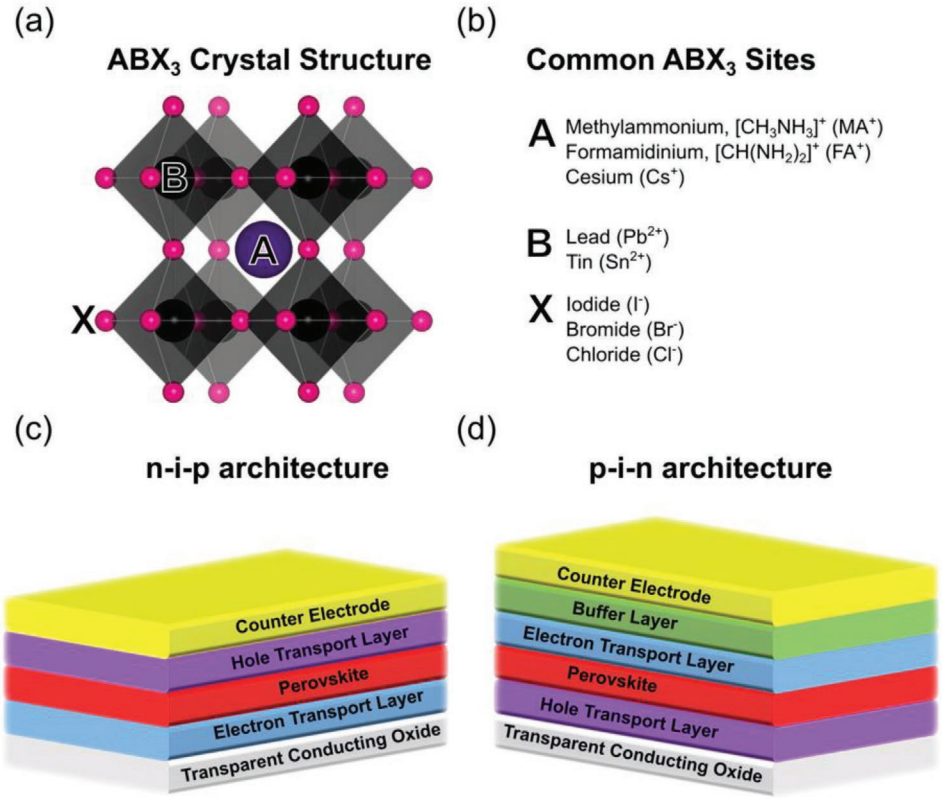


Figure 1. a) ABX_3 crystal structure of a perovskite with cation A neighbored by eight BX_6 octahedra. Crystal structure was drawn using visualization for electronic structural analysis (VESTA).[321] b) The common site occupation of monovalent cation A, divalent cation B and anion C in a photovoltaic perovskite. c) The conventional n–i–p architecture of PSCs. d) The inverted p–i–n architecture of PSCs.

predicting stable crystal structures of perovskite materials, as shown in Equation (1)

$$t = \frac{r_A + r_X}{\sqrt{2}\,(r_B + r_X)} \tag{1}$$

where r_A is the ionic radii of A; r_B is the ionic radii of B; r_x is the ionic radii of X.

The structure is expected to be cubic if t is close to 1. If $0.7 < t < 0.9$, the structure will deviate into the orthorhombic or tetragonal phases characterized by lead halide octahedral distortion and tilting. For methylammonium lead iodide ($MAPbI_3$), formadinium lead iodide ($FAPbI_3$), and cesium lead iodide ($CsPbI_3$), their tolerance factors are 0.89 (tetragonal), 1.02 (cubic) and 0.79 (orthorhombic), respectively.[32] Importantly, a revised system for the tolerance factor was introduced in 2016 by Travis et al.[33] who used a revised set of ionic radii for cations that are anion dependent. The revised system is necessary due to the increased covalency in metal–halide bonds for heavy halides paired with fluoride and metal-oxide bonds which are used to calculate Shannon radii.[34,35] The tolerance factor can be modified by varying the ratios of cations and halides with different radii. Such structural modifications have previously been shown to improve the performance and stability of PSCs and will be discussed in Section 3 of this review.

Typically, single junction PSCs can be fabricated with two main configurations, namely conventional (n–i–p) (Figure 1c) and inverted (p–i–n) (Figure 1d) architectures. In n–i–p cells, the electron transport layer (ETL) is below the perovskite absorber and for p–i–n cells, it is on the top. While n–i–p PSCs hold the highest reported PCE,[28] p–i–n PSCs are increasingly becoming more popular due to their high operating stability and are now achieving efficiencies over 22%.[36] In addition to PV devices, perovskites have also been used in a variety of applications including x-ray detectors,[37] light emitting diodes,[38] photodetectors,[39] and transistors.[40]

High efficiency PSCs high efficiency PSCs are mainly fabricated with small device area (<0.1 cm^2) and are fabricated in a glovebox under inert conditions.[41,42] Although great progress has been made on the fabrication of large area PSCs,[43–47] the long-term stability under ambient operating conditions remains to be one of the significant challenges in PSCs. This is because of the numerous factors affecting the degradation of PSCs including moisture, oxygen, ultra-violet light, and temperature.[48–51] To fabricate PSCs without an inert environment, the growth of perovskite films must be well controlled in an ambient atmosphere allowing for good crystallinity and well-defined morphology. This would also stimulate the ability to scale up PSCs in large quantities, where roll-to-roll processing could be coupled with state-of-the-art industrially printable techniques. Similar concepts which support both stability and scale up have been demonstrated,[52–57] however, a majority of the large printable and stable PSCs do not surpass 20% in efficiency. While there has been some excellent progress in the

© 2020 The Authors. Published by Wiley-VCH GmbH

fabrication of perovskite films in an ambient atmosphere,[58–61] their efficiencies are usually lower than PSCs fabricated in an inert environment. Importantly, there have also been studies which have discussed the benefits of an ambient atmosphere.[58,62] Therefore, in order to further promote the development of PSC technology, there is an urgent need to discuss both the limitations and benefits from an ambient atmosphere when fabricating PSCs without a glovebox.

In this review, we provide an extensive overview of the most recent developments in PSCs produced in an ambient atmosphere as well as a summary of their degradation processes in ambient environments. This will be of significant interest to laboratories without inert processing facilities such as a dry box or glovebox. Such an overview is important to the future development of stable PSCs, providing greater insights into what is required for their scale-up and commercialization. This review is arranged as follows: 1) effects of ambient exposure (moisture, oxygen, light, and temperature), 2) ambient fabrication strategies, 3) structure and architecture engineering, and 4) perspectives and important roadmaps for the future development of ambient PSCs.

2. Ambient Exposure on Perovskite Films

A high-quality perovskite thin film which exhibits high surface coverage, large grain size, low defect concentration, and consistent crystal orientation, is essential for efficient PSCs.[63–66] Despite their tolerance to defects,[67,68] severe blemishes in the perovskite crystals and voids in the film can cause significant charge recombination and short-circuiting in the device, which deteriorates the charge transport and collection.[69] In most cases, PSCs are fabricated in an inert atmosphere such as a dry box or glovebox where nitrogen or argon is used to partially or fully replace air. This controlled dry environment protects the perovskite thin film from water and oxygen in the atmosphere, and while degradation is suppressed, the requirement of an inert atmosphere increases the fabrication cost. Promisingly, many research groups have succeeded in the fabrication of efficient and stable PSCs in ambient air over the past few years,[42] but many challenges remain. Throughout this review, the terms low, medium, and high humidity will refer to humidity values of <30%, 30–50%, and >50% relative humidity (RH), respectively. Where possible, exact humidity values will be quoted. If the referring literature clearly states that the PSCs were fabricated without a glovebox but fails to quote the exact humidity, the RH value will be quoted as N/A. When the fabrication conditions are not clearly reported, it will be assumed that a glovebox has been used and thus not included in this review. In this section, the impacts of ambient exposure on perovskite thin films, both post fabrication and during fabrication are discussed.

2.1. Ambient Exposure Post Fabrication

The most established perovskite absorber used in solar cells, $MAPbI_3$, is usually synthesized by reacting methyl ammonium iodide (MAI) with lead iodide (PbI_2) in an inert atmosphere as shown in Equation (2). However, under ambient conditions, the perovskite film will incur an accelerated degradation process due to the presence of water as provided in Equation (3)

$$CH_3NH_3I + PbI_2 \rightarrow CH_3NH_3PbI_3 \quad (2)$$

$$CH_3NH_3PbI_3 \xleftrightarrow{H_2O} CH_3NH_3I + PbI_2 \quad (3)$$

Frost et al.[70] demonstrated a decomposition pathway of $MAPbI_3$ as shown in **Figure 2**a. Here, water acted as an initiator to form a hydrated intermediate phase, $[(CH_3NH_3^+)_{n-1}(CH_3NH_2)nPbI_3][H_3O]$. Then, the decomposition was driven by the phase changes of hydrogen iodide (soluble in water, step b) and methylammonium (volatile and soluble in water, step c). Finally, the yellow phase PbI_2 remained (water and PbI_2, step d). Other hydrated intermediate phases, such as $MA_4PbI_6 \cdot 2H_2O$[48,71] and $MAPbI_3 \cdot H_2O$[72,73] were also previously reported.

Equation (4) shows the decomposition products MA and hydrogen Iodide (HI), where moisture, oxygen and light also contribute to the degradation of HI which is described by Equations (5) and (6). The water generated in Equation (6) creates a cyclic process leading to further moisture degradation.[74] To verify these reactions, MAI degradation experiments under different conditions were performed by Niu et al.[75] As shown in

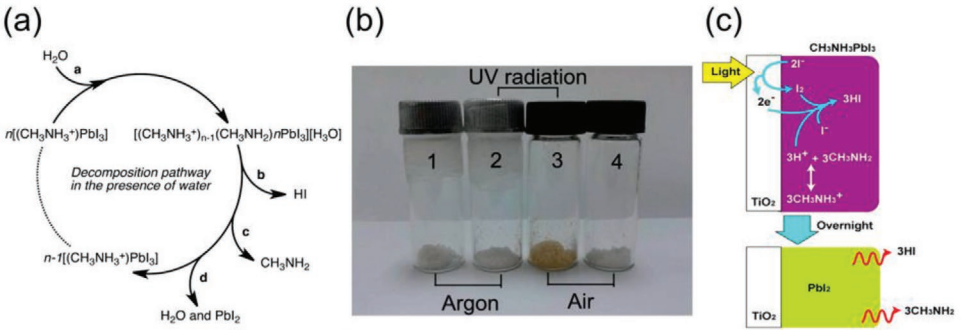


Figure 2. a) Proposed decomposition pathway of $MAPbI_3$ in the presence of water whereby water initiates the process and the decomposition is driven by phase changes of HI and CH_3NH_2 to form degradation product PbI_2. Reproduced with permission.[70] Copyright 2014, American Chemical Society. Further permissions related to the material excerpted should be directed to the publisher. b) The degradation of MAI under different conditions: Tube 1: Argon atmosphere without UV radiation. Tube 2: Argon atmosphere with UV radiation. Tube 3: Air conditions with UV radiation. Tube 4: Air conditions without UV radiation. c) Degradation process of PSCs under UV exposure. Reproduced with permission.[80] Copyright 2014, American Chemical Society.

© 2020 The Authors. Published by Wiley-VCH GmbH

Figure 2b, the color of MAI in tube 3, which was exposed to oxygen and UV radiation, changed from white to brown, indicative of the presence of degradation product (I_2).

$$CH_3NH_3I \leftrightarrow CH_3NH_2 + HI \quad (4)$$

$$2HI \xleftrightarrow{h\nu} H_2 + I_2 \quad (5)$$

$$4HI + O_2 \leftrightarrow 2H_2O + 2I_2 \quad (6)$$

Previous studies have demonstrated that when $MAPbI_3$, is exposed to oxygen and light, a photodegradation process occurs via the formation of superoxide species.[76–78] The decomposition of the perovskite film was light activated and required oxygen as shown in Equations (7)–(9) below.[77] In a moisture-free environment, the superoxide generated through electron transfer from the photoexcited $MAPbI_3$ to oxygen broke down the $MAPbI_3$ by deprotonating the methylammonium cation, and finally formed CH_3NH_2, PbI_2, I_2, and water. Also, the degradation induced by oxygen and/or light can be independent of moisture and faster than the degradation induced by moisture alone.[76,79,80] A decomposition pathway induced only by UV exposure was reported by Ito et al.[80] The process shown in Figure 2c deconstructed the $MAPbI_3$ layer (Equations (10)–(12)) and finally resulted in CH_3NH_2, PbI_2 and HI as shown in the Equation (13)

$$CH_3NH_3PbI_3 \xleftrightarrow[\text{No moisture}]{\text{Light}} CH_3NH_3PbI_3^* \quad (7)$$

$$O_2 \xleftrightarrow{CH_3NH_3PbI_3^*} O_2^{\bullet -} \quad (8)$$

$$CH_3NH_3PbI_3 + \tfrac{1}{2}O_2^{\bullet -} \xleftrightarrow{\text{Deprotonation}} CH_3NH_2 + PbI_2 + \tfrac{1}{2}I_2 + H_2O \quad (9)$$

$$2I^- \leftrightarrow I_2 + 2e^- \left[\text{at the interface between } TiO_2 \text{ and perovskite}\right] \quad (10)$$

$$CH_3NH_3^+ \leftrightarrow CH_3NH_2 + H^+ \quad (11)$$

$$I^- + I_2 + 3H^+ + 2e^- \leftrightarrow 3HI \quad (12)$$

$$CH_3NH_3PbI_3 \leftrightarrow CH_3NH_2 + PbI_2 + HI \quad (13)$$

$$CH_3NH_3PbI_3 \xrightarrow{\text{heat}} NH_3 + CH_3I + PbI_2 \quad (14)$$

In accordance with the International Electrochemical Commission (IEC) 61215:2016,[81] PSCs must be able to withstand 85 °C/85% RH under operating conditions. Notably, the first PSC to pass the IEC61215:2016 test was reported in 2017, which was a tandem silicon/perovskite cell fabricated in a dry air box.[82] However, exposing PSCs to high temperatures usually induces degradation of the perovskite layer. Philippe et al.[83] found that all the $MAPbI_3$ molecules (on the $MAPbI_3$/titanium dioxide (TiO_2)/fluorine doped transparent oxide (FTO) film) were degraded into PbI_2 after annealing at 200 °C for 20 min, and 30% of $MAPbI_3$ was degraded at 100 °C after 20 min. Interestingly, the authors showed that under inert conditions, this process can be slowed down but not prevented. The proposed degradation mechanism of perovskite films under high temperature and vacuum is provided in Equation (13). Conings et al.[84] investigated the thermal stability of $MAPbI_3$ films by annealing the $MAPbI_3/TiO_2$/FTO film at 85 °C for 24 h in different atmospheres (O_2, N_2, and ambient conditions). It was found that when compared with a N_2 and O_2 environment, the perovskite film annealed under ambient conditions exhibited a significant structural change and a much faster degradation rate. Juarez-Perez et al.[85] demonstrated that the final product of thermal degradation was ammonia (NH_3) and CH_3I under an inert atmosphere, as shown in Equation (14).

Although several degradation mechanisms have been provided in the literature, it is clear that products of degradation bring impurities to the remaining perovskite layer and strongly affect the microstructure of the film, which causes a significant decrease in the optical absorption in the visible region.[86–88] Therefore, achieving a high moisture resistant perovskite composition is an essential step for ambient fabrication and commercialization of PSCs.

2.2. Ambient Exposure During Fabrication

One-step and two-step spin-coating are the two most commonly used methods in the fabrication of PSCs and their typical processes are outlined in **Figure 3**.[89] In the one-step method (Figure 3a), the perovskite precursors (MAI and PbI_2) are typically dissolved into a mixture of coordinating solvents and spin-coated onto a charge transport material (such as TiO_2 or tin oxide, SnO_2). During this process, the strong ionic interactions between halogen anions and the metal cations allow the perovskite layer to form via convective self-assembly owing to fast solvent evaporation and a final annealing step. A generous volume of antisolvent is dynamically dropped onto the substrate containing the perovskite precursor, which washes away excess coordinating solvent (without dissolving the perovskite) and enables the formation of a smooth and uniform transparent layer.[86] The formation of the intermediate phase is important for smoothing the surface (achieved via antisolvent

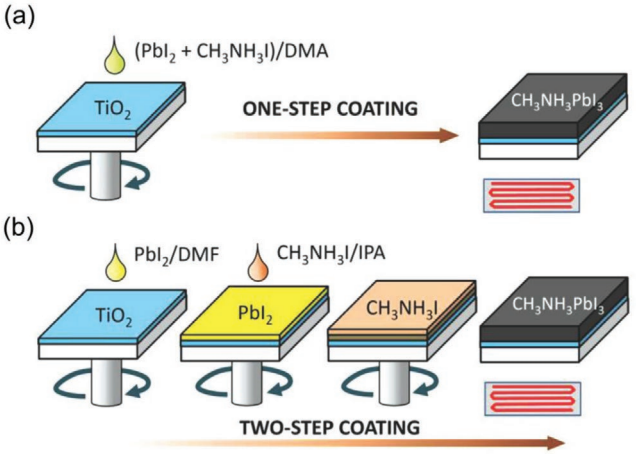


Figure 3. a) One-step and b) two-step spin-coating methods to the fabricate perovskite layer. Reproduced with permission.[89] Copyright 2014, Wiley-VCH GmbH.

© 2020 The Authors. Published by Wiley-VCH GmbH

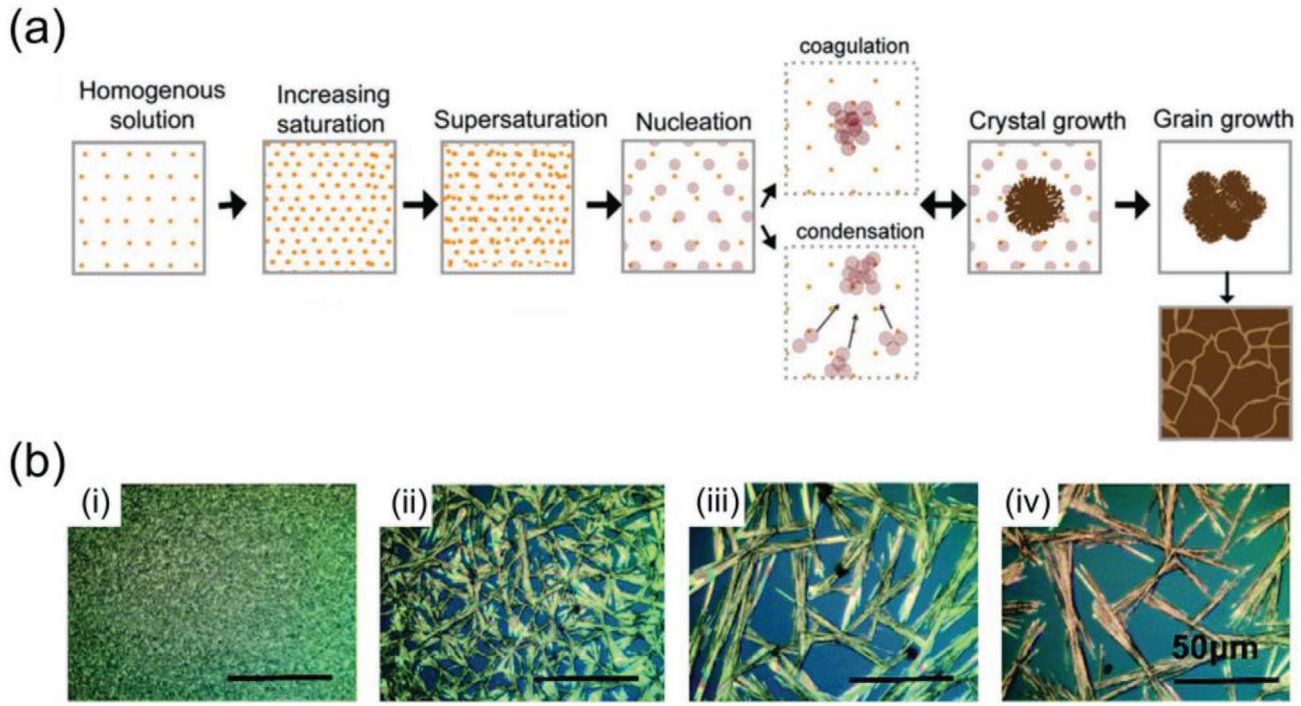


Figure 4. a) The formation mechanism of perovskite film assisted with antisolvent. Reproduced with permission.[93] Copyright 2019, Wiley-VCH GmbH. b) SEM images of perovskite films fabricated under RHs of i) 0%; ii) 50%; iii) 70%; iv) 90%. Reproduced with permission.[98] Copyright 2019, The Royal Society of Chemistry.

treatment), which results in the formation of a compact and uniform thin layer. After antisolvent treatment, the thin films are annealed and the transparent film becomes dark rapidly due to the crystallization and formation of the active perovskite layer.

For the two-step method (Figure 3b), PbI_2 in a coordinating solvent is first spin-coated onto the charge transport material, followed by annealing to form a thin film of PbI_2. A solution containing MAI in a hydrophilic solvent is then spin-coated on top of the PbI_2 film, resulting in a dark color, indicating the formation of perovskite. Finally, the perovskite film is annealed to complete the crystallization and remove excess solvent.[89]

2.2.1. Ambient Exposure: One-Step Spin-Coating

Spin-coating perovskite precursor on a substrate and annealing it in a humid environment significantly affects the properties of the final thin-film, as it can increase the grain size of the perovskite crystal but reduce the coverage and film compactivity.[90–95] Several papers have illustrated that a humid environment during the annealing process can control the crystallization of perovskite films. It was proposed that humid environments promoted Ostwald ripening, reduced the supersaturation of the precursor solution, slowed down the crystallization process, assured fewer nucleation centers formed and provided more time for grain coarsening, and thus resulted in the large grain size.[91,96,97] Angmo et al.[93] also found that water from the atmosphere can sequester Lewis base solvents like dimethyl sulfoxide (DMSO), dimethylformamide (DMF), and *N*-methyl-2-pyrrolidone (NMP), causing heterogeneity during nucleation and crystal growth of the perovskite film. The formation mechanism of the perovskite film assisted with antisolvent treatment can be seen in **Figure 4**a. Usually, a low humidity or humidity-free environment can promote the nuclei formation which results in a dense nuclei with a small grain size. However, a high humidity environment promotes the growth of nuclei, which results in a larger grain size with poor coverage (Figure 4b).[98] The mild humid environment of 30–50% RH was considered as the optimal condition for perovskite film fabrication.[63,96,97,99,100] For example, the perovskite films annealed at a RH of 30–40% obtained the PCE of 17.1%, but when the humidity was increased to 80%, the PCE was reduced to 12.1%.[63] A water-vapor annealing (WVA) method was used to create more specific mild humidity by putting a water droplet in the center of the petri dish as shown in **Figure 5**a.[99] The humidity of the petri dish was controlled by the amount of water and 36–43% RH was found to be the optimal environment. Under appropriate water vapor pressure, $MAPbI_3$ at the grain edge and void area can decompose into PbI_2 and MAI, and then regenerate the perovskite crystal again as shown in Figure 5b. Through this dissolution and recrystallization process, void free perovskite films with large grain sizes were obtained as shown in the scanning electron microscopy (SEM) images in Figure 5c. Similarly, Lv et al.[101] found that a low humid condition of 28% RH was the ideal environment for fabricating $MAPbI_3$ films. The slight difference in the optimal RH could come from the different perovskite composition, precursor fabrication method and precursor solvent. Gao et al.[92]

© 2020 The Authors. Published by Wiley-VCH GmbH

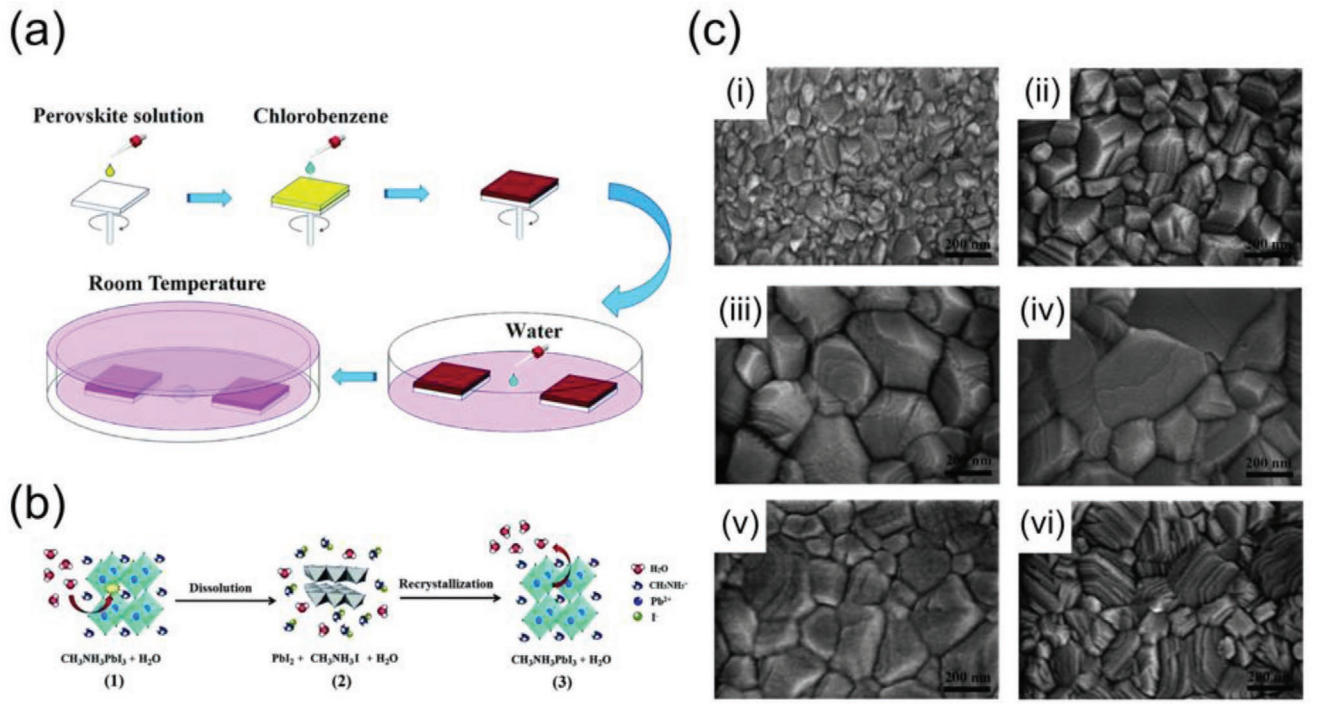


Figure 5. a) The spin-coating and WVA method. b) The mechanism of WVA method showing the crystal growth processes in the perovskite film; 1) absorption of water on the perovskite surface forming strong hydrogen bonds between MA cations and the Pb-I cage; 2) hydrolysis of the perovskite into PbI_2 and CH_3NH_3I; 3) once the water evaporates, CH_3NH_3I and PbI_2 react to reform the perovskite. Reproduced with permission.[99] Copyright 2016, The Royal Society of Chemistry. c) SEM images of the perovskite film; i) Placed in air (25 °C, RH < 10%) without annealing process, ii) WVA under the 33–36% RH (5 mL water), iii) WVA under the 33–42% RH (10 mL water), iv) WVA under the 36–43% RH (15 mL water), v) WVA under 36–51% RH (20 mL water) for 1 h, respectively, and vi) Annealed at 100 °C for 10 min in air (RH < 10%).

demonstrated that the fabrication of perovskite films required a relatively low humidity during the spin-coating process and a relatively high humidity environment at the annealing step. The hygroscopic perovskite phase can adsorb moisture in a humid environment, which prolonged the evaporation of solvents and delayed the supersaturation of the solution. A reduced supersaturation induced low nucleation density and large critical nucleus radius, resulting in an isolated perovskite crystal. However, in the annealing process, low supersaturation enabled full crystal growth of the perovskite, which reduced the crystal defect density and improved the crystallinity of the perovskite film. These findings can also be confirmed by the higher photoluminescence, the longer lifetime and the increased open circuit voltage (V_{oc}) of the perovskite films formed under moisture exposure, due to reduced defects and suppressed recombination.[95,100,102]

Moisture showed a healing effect on the perovskite film due to the partial hydration from water molecules.[95,103] Water in the atmosphere can solubilize and mobilize excess methylammonium, accelerate its removal from the perovskite film, and thus reducing the trap state density and enhancing the performance.[95] Zhou et al.[103] also found that water vapor can change deep-level defects to shallow-level defects by forming hydrogen bonding with iodine in the perovskite. However, this process was fully reversible which meant the deactivation effect was lost if water was evaporated.

Benefits of Water: Interestingly, the addition of water or the use of hydrated lead precursors has been reported to have beneficial effects on the formation of the perovskite film and thus resulted in improved device performance.[102,104] Gong et al.[104] found that trace amounts of water (2%) in DMF can improve the high vapor pressure and lower the boiling point.[104] Similarly, He et al.[105] fabricated PSCs with water (1.5%) added in the DMF precursor solution under 40% RH. In both cases, a hydrated complex $MAPbI_{3-x}Cl_x \cdot nH_2O$ was detected in the annealing process which promoted the crystallization process, improved the surface coverage and enhanced moisture tolerance of the perovskite film. Liu et al.[106] used an aqueous-containing precursor solution to deposit the perovskite films and reported that while water in the precursor did not affect the performance of PSCs, it improved the tolerance of fabrication in a humid environment. There was a negligible difference between the performances of PSCs fabricated by anhydrous (PCE 18.6 ± 0.5%) and 20%-water contained (PCE 18.7 ± 0.7%) precursor solution as shown in **Figure 6**a,b. However, the sensitivity of humidity during the deposition process was greatly suppressed as the PSCs fabricated by an aqueous-containing precursor remained at 18% when the RH of the fabrication environment increased from 16 ± 4% to 57 ± 3% (Figure 6c). Water in hydrated lead acetate ($PbAc_2$) can also affect the morphology of the perovskite film. It was found that a hydration water concentration of $x = 1.5$ for $3CH_3NH_3I{:}1PbAc_2 \cdot xH_2O$ was considered to be the optimal precursor, providing the lowest surface roughness, highest photocurrent and good balance between nonradiative recombination pathways and surface porosity.[102]

© 2020 The Authors. Published by Wiley-VCH GmbH

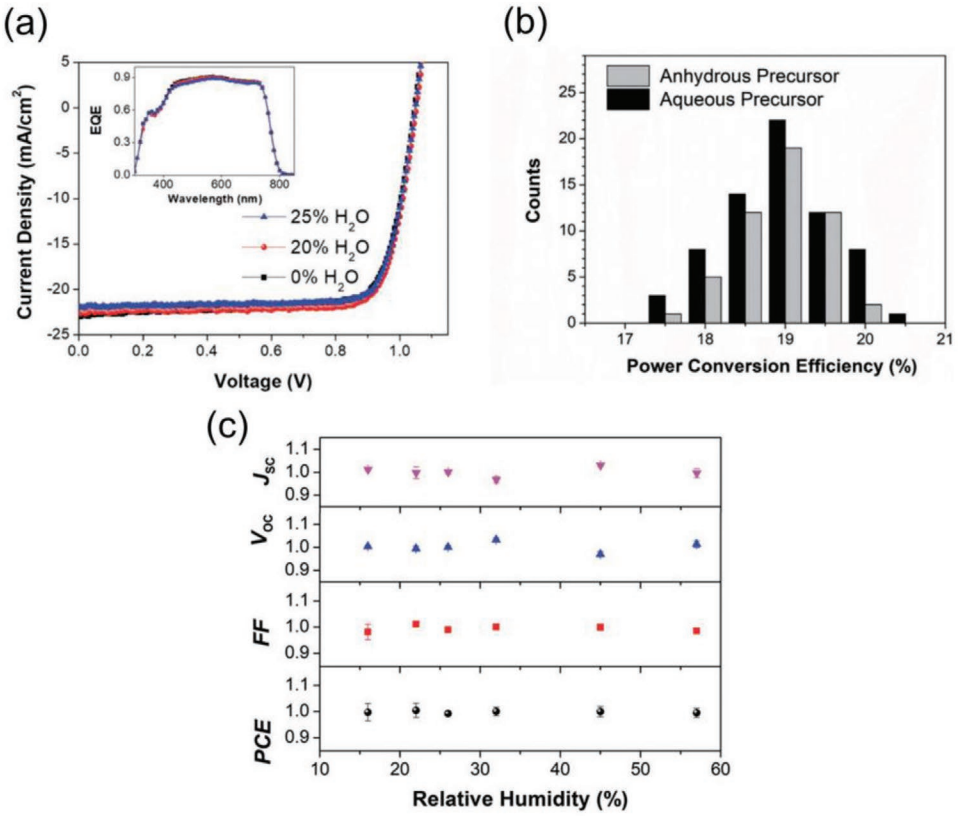


Figure 6. a) The *J–V* curves and EQE spectra of PSCs fabricated with 0%, 20%, and 25% water containing precursor. b) The histograms of PCE for anhydrous and 20% water containing precursor PSCs. c) Normalized parameters; PCE, FF, V_{oc}, short-circuit current (J_{sc}) of PSCs fabricated under different RH from 10%–60%. Reproduced with permission from.[106] Copyright 2017, Wiley-VCH GmbH.

In addition to moisture, it has been previously shown that oxygen also has an impact during the fabrication of perovskite films. Exposing a perovskite film under oxygen or dry air has been used as a post-treatment strategy to reduce the defect density, and this strategy has been described in both the one-step[107] and two-step spin-coating methods (discussed in Section 2.2.2).[108] Brenes et al.[107] demonstrated that superoxide O_2^- can form at iodide vacancies under the exposure of light and oxygen which can remove the shallow surface states of the perovskite layer and suppress ion migration. Oxygen is also used as a passivation method for inorganic PSCs.[109,110] Liu et al.[109] reported oxygen passivation under room temperature which can passivate the surface defect by adsorbing on the film surface. Additionally, oxygen passivation during the dry-air annealing process was shown to passivate both surface and bulk defects by incorporating into the whole perovskite film as shown in **Figure 7**a. The increased photoluminescence (PL) intensity of the glass side, as well as the longer lifetime proved the suppression of nonradiative recombination in the bulk of perovskite film (Figure 7b–d).

2.2.2. Ambient Exposure: Two-Step Spin-Coating

In similar circumstances with the one-step spin-coating method, moisture exposure during the formation of the PbI_2 film in the two-step spin-coating procedure results in large grain sizes and increased surface roughness due to the low supersaturation and reduced nucleation density.[60,111–113] Huang et al.[114] and Zhai et al.[113] attributed this phenomenon to the poor hydrophilicity of the TiO_2 surface, and the water from humid conditions discretely distributed on the surface. Water molecules can attract PbI_2 by hydrogen bonding, leading to the island growth of PbI_2 film. It was also found that moisture can promote the conversion of PbI_2 to perovskite in the second step of the spin-coating process.[60,111,115–117] Yang et al.[115] hypothesized that a metastable and more active hydrate intermediate phase, $MAPbI_3 \cdot H_2O$, was formed under humid conditions, which accelerated the perovskite conversion. Hydrated intermediates $MA_4PbI_6 \cdot 2H_2O$ and $MAPbI_{3-x}Cl_x \cdot yH_2O$, which can activate the perovskite conversion, were also reported by Xu et al.[117] in $MAPbI_3$ and $MAPbI_{3-x}Cl_x$, respectively. It was proposed by Xu et al.[117] and Wu et al.[111] that exposure below 60% RH can result in moisture being dissolved on the surface of the film, facilitating MAI ionization, and thus accelerating the growth of the perovskite crystal. Since moisture exposure is detrimental in the first step but beneficial in the second step, Wu et al.[111] did a series of experiments under different humidity using the two-step spin-coating method, and achieved the best device with an average PCE of 12.48% at 15% RH, which proved the benefit of a controlled humidity environment.

© 2020 The Authors. Published by Wiley-VCH GmbH

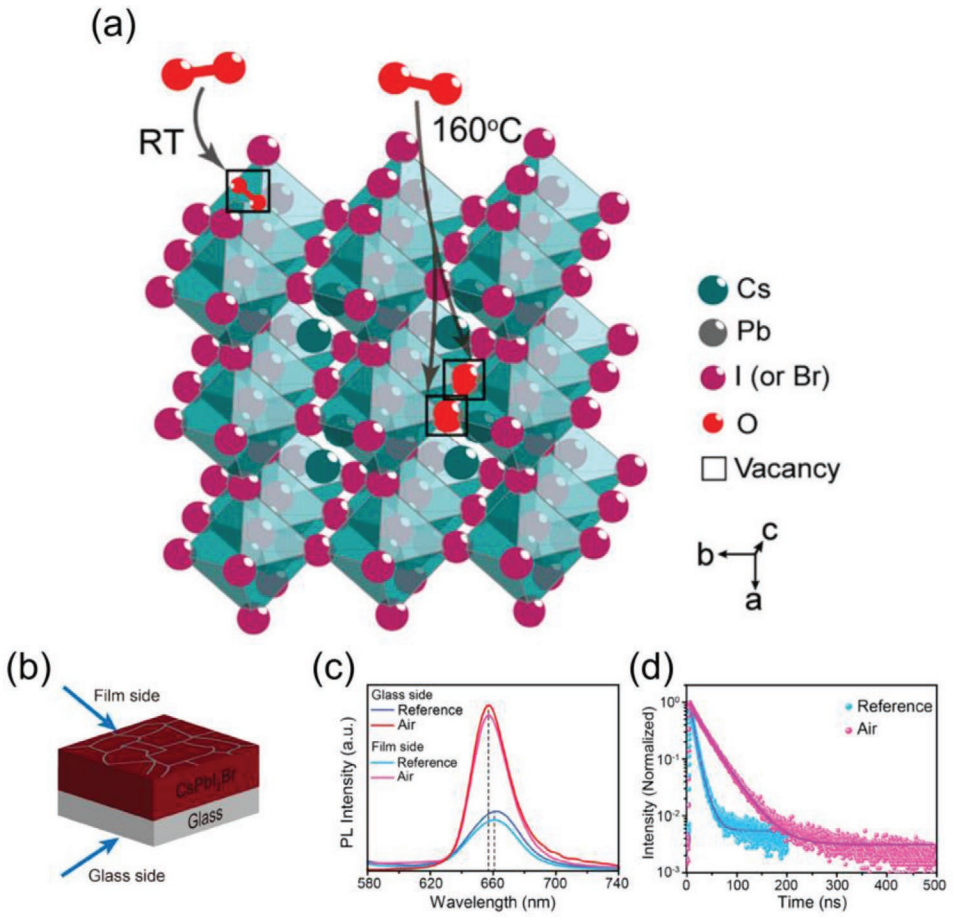


Figure 7. a) The schematic of adsorbed O_2-passivation and incorporated O-passivation at 160 °C in an all-inorganic halide perovskite. b) The $CsPbI_2Br$ film side and glass side setup to be used for PL measurement. c) The PL spectra of the dry-air processed perovskite from the film and glass side compared to the reference films. d) The normalized Time-resolved PL decay profiles for dry-air processed perovskite films compared to the reference films. Reproduced with permission from.[109] Copyright 2019, American Chemical Society.

Water is also used as an additive in the PbI_2 precursor solution. Wu et al.[118] found that after adding 0.5–4 vol% water, the PbI_2/DMF solution became homogenous (see **Figure 8**a). It was proposed that water can change the properties of DMF, such as dielectric constant, polarity and solubility and partially dissolve PbI_2, resulting in completely dissolved PbI_2. With 2 vol% water as the additive, PSCs fabricated under ambient conditions achieved a PCE of over of 18% with a high fill factor (FF) of 0.85. The enhanced performance was attributed to the homogeneous PbI_2 precursor, which helped the formation of compact PbI_2 and large grain size perovskite film as shown in the SEM images in Figure 8b–e.

Oxygen can also make a difference in the two-step spin-coating method. Ren et al.[108] used a postdeposition treatment by annealing FTO/ETL/$MAPbI_3$/HTL film under 65 °C. They found that oxygen can diffuse into the perovskite layer and the interface, passivating the under-coordinated cation. It was also reported that oxygen can suppress the wetting of the PbI_2 precursor solution on a hydrophobic organic HTL, resulting in poor coverage of the PbI_2 film and subsequent perovskite film.

As discussed in Sections 2.2.1 and 2.2.2., fabricating perovskite films under ambient conditions has both positive and negative effects. On the one hand, moisture can increase the grain size of the perovskite crystal and promote the reaction of PbI_2 and MAI. Also, perovskite films fabricated under humid conditions (30–40%) usually show higher moisture resistance compared with those fabricated in an inert environment. On the other hand, high humidity (>70%) during the fabrication can lead to pinholes in the film and increased roughness, which is detrimental to PSC performance. The effect of oxygen was also discussed as a post treatment strategy to reduce defect density in perovskite films. Therefore, taking these measures into account would be a useful strategy to maximize the quality of perovskite films fabricated in an ambient environment.

3. Approaches for Ambient Fabrication

The first PSC fabricated in ambient air was published by Liu and Kelly[119] in 2013. A thin film of zinc oxide (ZnO) nanoparticles (NPs) instead of conventional mesoporous TiO_2 was used as the ETL. All the fabrication steps were carried out in an uncontrolled environment (outside the glovebox) and the best device obtained a PCE of 15.7%. Since the first ambient publication of PSCs,

© 2020 The Authors. Published by Wiley-VCH GmbH

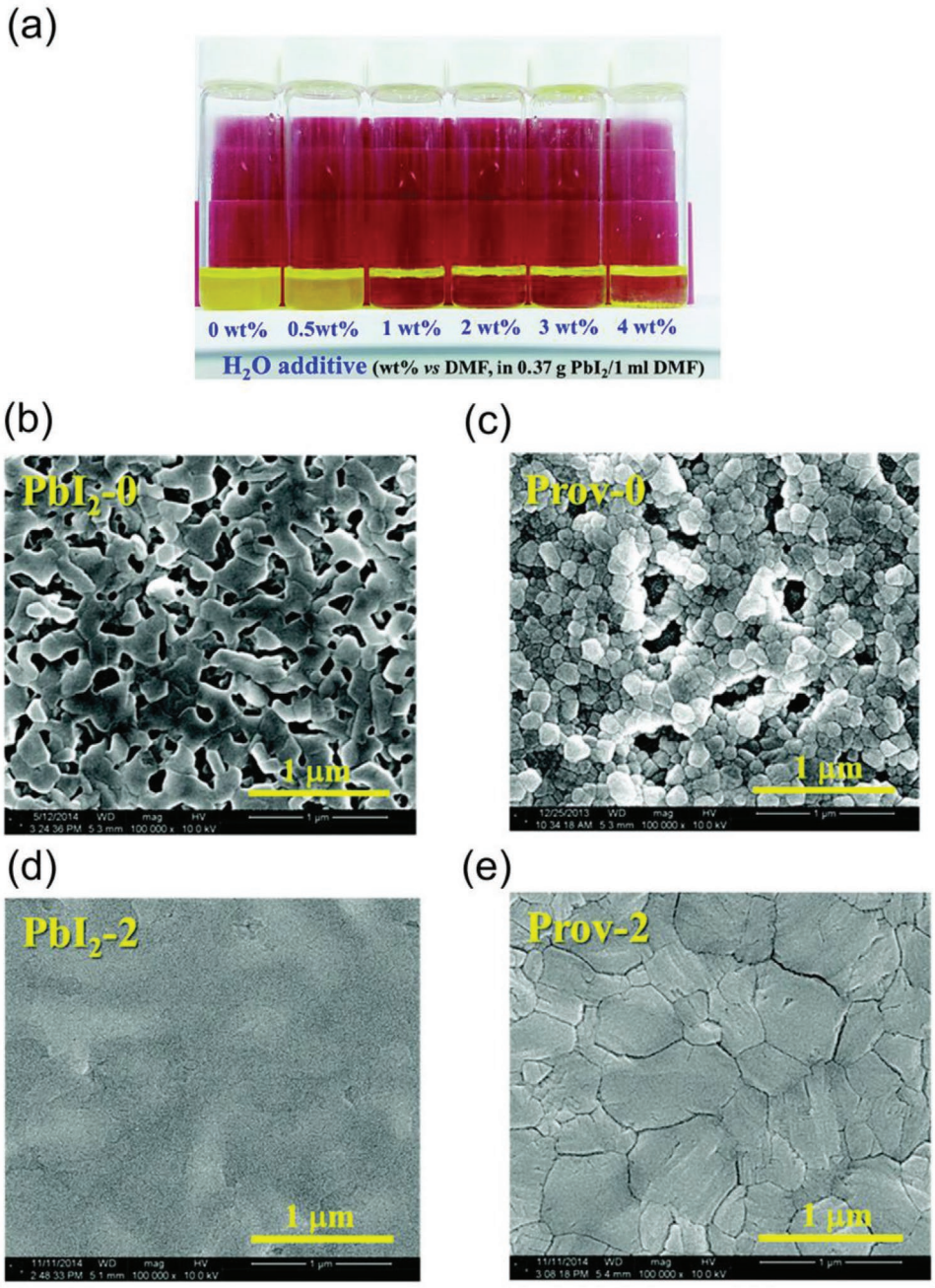


Figure 8. a) PbI_2/DMF solution with varying amounts of water additive up to 4 wt%. SEM images of b) PbI_2 film without water additive, c) Perovskite film without water additive, d) PbI_2 film with 2 vol% water additive, and e) Perovskite film with 2 vol% water additive. Reproduced with permission.[118] Copyright 2015, The Royal Society of Chemistry.

other groups have also advanced in the fabrication of PSCs under ambient air.[58,120] Despite this, the performance and stability of PSCs fabricated in ambient air are typically lower than those fabricated in an inert atmosphere. In order to improve the performance and stability of ambient processed PSCs, various techniques such as composition engineering, additive engineering, solvent engineering, interface engineering, and other methods have been employed. The following sections describe each of these techniques with reference to recent state-of-the-art progress in the fabrication of PSCs in ambient conditions.

3.1. Composition Engineering

Currently, the most commonly used perovskite is $MAPbI_3$ and PSCs using this absorber can now achieve over 20% in PCE.[15,121–123] However, as discussed in Section 2, the hygroscopic nature and high temperature vulnerability of $MAPbI_3$ makes it more difficult to prepare in ambient conditions and thus making scale up for commercialization unlikely.[84] For example, it was reported that $MAPbI_3$ undergoes a phase transition between ordered tetragonal and disordered cubic

© 2020 The Authors. Published by Wiley-VCH GmbH

structure at around 57 °C.[124–126] Apart from conventional $MAPbI_3$, different cations and anions such as A = FA[23] or Cs,[127] X = Br^-,[128] Cl^-,[129] and thiocyanate (SCN^-)[58] have also been investigated. Partial cation and halide substitution forms a mixed-halide perovskite film that provides enhanced stability toward ambient conditions.[130] Despite the phenomenal performance of $MAPbI_3$ based PSCs, the highest performing PSCs are now achieved using a mixed cation and/or mixed-halide composition.[22,131–133] This section will discuss some of the recent progress made by the incorporation of mixed-cations and/or mixed-anions in the ambient fabrication of PSCs.

Duan et al.[134] fabricated PSCs using a double cation perovskite absorber layer under 30% RH and the best device used a perovskite with a composition of, $FA_{0.4}MA_{0.6}PbI_3$, and obtained a PCE of 10.86%. However, PSCs using organic components FA and MA are still sensitive to elevated temperature and light.[135] The relatively small Cs cation is also used to compensate for the large FA. Another mixed-cation perovskite composition $FA_{0.85}Cs_{0.15}PbI_3$ whose tolerance factor is close to 1 was reported by Li et al.[136] and an improvement in thermal stability was observed. Similarly, Lee et al.[137] reported a mixed-cation perovskite $FA_{1-x}Cs_xPbI_3$ which exhibited UV and moisture resistance. Different amounts of Cs were tested by fabricating the perovskite films in 55% RH, and the best device with composition $FA_{0.9}Cs_{0.1}PbI_3$ obtained 16.5% PCE. Although the Cs-FA mixed-cation perovskite device had a better moisture stability than $FAPbI_3$ and $MA_{0.5}FA_{0.5}PbI_3$ PSCs, the long-term stability in the ambient of Cs-FA PSCs still needs to be improved.

Triple cation PSCs composed of Cs, MA and FA have gathered great attention for their improved performance and enhanced stability.[22,138] Singh et al.[138] explored the fabrication of the triple cation PSC by controlling the humidity (RH < 25%). The highest PCE exceeded 20% which interestingly was higher than the same device fabricated in a dry nitrogen environment. Compared with the dry nitrogen environment, the evaporation of solvent was slower under controlled humidity and was further slowed down by covering the substrate with a glass petri dish during the annealing process. Also, moisture from the controlled humidity environment accumulated at the grain boundaries. These two factors were proposed to promote the Ostwald ripening and increase the grain size of the perovskite crystal. $Cs_{0.05}(MA_{0.17}FA_{0.83})_{0.95}Pb(I_{0.83}Br_{0.17})_3$ PSCs obtained a PCE of 20.8%, and still preserved high efficiency (19.5% PCE) after 18 weeks under a RH of 20–35%.

Chlorine (Cl)-based PSCs have also been widely investigated and its influence on nucleation and moisture was briefly discussed in Section 2.[139–143] The addition of chloride ions showed an increase in the electron-hole diffusion length, which has been suggested to be a result of a substantial inhibition of non-radiative electron-hole recombination.[19] The presence of lead chloride ($PbCl_2$) in the evolution of $MAPbI_3$ films has been suggested to change the nucleation dynamics by generating an intermediate methylammonium lead chloride ($MAPbCl_3$) phase, promoting carrier lifetimes and diffusion lengths.[139] It was also found that a porous lead (II) iodide chloride (PbICl) structure was formed in the precursor film after the introduction of $PbCl_2$.[142] This structure can improve the quality of the perovskite film after the dipping of MAI by releasing the structural stress generated during the phase conversion. However, whether Cl can in fact be incorporated into the crystal lattice of a perovskite is still under debate.[144,145] Colella et al.[129] reported that Cl incorporation was only possible at 3–4% but otherwise can be used as an additive/dopant to improve the charge transport of the perovskite film. Raga et al.[146] reported that compared with a nitrogen environment, excess Cl ions can be more easily removed in the form of methylammonium chloride (MACl) during annealing in air. The water in the air prevented the formation of $MAPbCl_3$ and favored the crystallization of $MAPbI_3$, meaning $MAPbCl_3$ was only obtained in samples that were annealed in N_2.

Compared with conventional $MAPbI_3$, replacing iodide with bromide (i.e., methylammonium lead bromide, $MAPbBr_3$) has shown higher resistance against environmental humidity.[128,147–149] In addition, the partial substitution of iodide for bromide has shown longer operational lifetimes due to an increased resistance to moisture.[128,150] Pont et al.[128] found that higher ratios of bromide in mixed-halide perovskites $MAPb(I_{1-x}Br_x)_3$, resulted in higher moisture stability. The pure $MAPbBr_3$ PSC demonstrated improved stability when only exposed to light and oxygen, but the mixed-halide perovskite degraded rapidly under such conditions. Strong degradation was detected by Noh et al.[151] in $MAPbI_3$ films after storing in high humidity. However when the amount of bromide increased to 20% (x = 0.2, perovskite was $MAPbI_{2.4}Br_{0.6}$), the PSC maintained high efficiency under a high RH of 55%. It was proposed that smaller bromide atoms substituted the larger iodide atoms which reduced the lattice parameter and transferred the crystal into a cubic phase. This made the microstructure of the perovskite more compact and stable, thus making it less sensitive to the moisture. Despite this, excess bromide has been reported to result in phase segregation.[152,153] Recent work by Aziz et al.[154] showed that as the content of bromide was increased, the amount of superoxide species decreased, which resulted in an increase in material stability toward oxygen and light.

Tai et al.[58] reported the successful fabrication of $MAPbI_{3-x}(SCN)_x$ PSCs in ambient air which achieved an average PCE of 13.49% under a RH exceeding 70%. A two-step spin-coating method was used with a lead (II) thiocyanate ($Pb(SCN)_2$) precursor due to its higher moisture resistance. In comparison to the $MAPbI_3$ based PSCs, $MAPbI_{3-x}(SCN)_x$ based devices had an improved film morphology and higher PCE (see **Figure 9**a) due to their low trap density and long carrier lifetime. Moreover, the device stability was also increased because of the intrinsic stability of the perovskite material. Zhang et al.[155] introduced alkali thiocyanates (potassium thiocyanate, KSCN and sodium thiocyanate, NaSCN) as an additive to fabricate $MAPbI_{3-x}(SCN)_x$ based PSCs under ambient conditions. A two-step spin-coating method was used and the alkali thiocyanates were added in the $Pb(SCN)_2$ precursor solution. As shown in the SEM images in Figure 9b–d, the grain size of perovskite crystal was increased from 250 nm to 500 nm, thus enhanced charge transport and suppressed charge recombination. The best device which used 3.5% KSCN obtained 16.59% PCE and maintained 97% of its efficiency after exposure to 70% RH for 45 days.

Recently, Tang et al.[156] investigated the solidification process of single-cation ($FAPbI_3$) and a mixed-cation mixed-halide

© 2020 The Authors. Published by Wiley-VCH GmbH

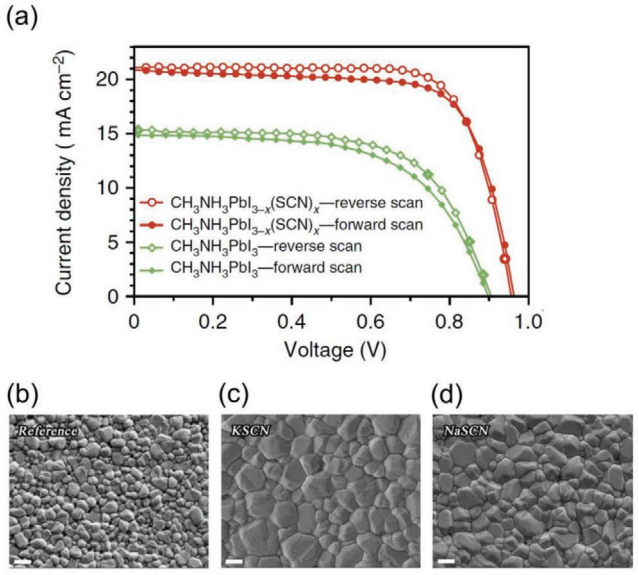


Figure 9. a) J–V curves of $MAPbI_{3-x}(SCN)_x$ and $MAPbI_3$ PSCs. Reproduced with permission.[58] Copyright 2016, Nature Publishing Group. Top and cross-sectional SEM images $MAPbI_{3-x}(SCN)_x/TiO_2/FTO$/glass films with 400 nm scale bars of b) The reference film, c) KSCN additive, and d) NaSCN additive. Reproduced with permission.[155] Copyright 2018, Elsevier.

perovskite ($FA_{0.8}MA_{0.15}Cs_{0.05}PbI_{2.55}Br_{0.45}$) using grazing incidence wide-angle X-ray scattering (GIWAXS). It was reported that the addition of Br^- into $FAPbI_3$ to obtain $FAPbI_{2.55}Br_{0.45}$, can promote the formation of the desired black phase (cubic 3C (100), α phase), and suppress the formation of yellow nonperovskite phase (hexagonal 2H (100), δ phase). To prevent the concurrently formed PbI_2 and segregation of halides, MA^+ and Cs^+ were incorporated to obtain $FA_{0.8}MA_{0.15}Cs_{0.05}PbI_{2.55}Br_{0.45}$ under elevated temperature, which suppressed all the nonperovskite intermediate phase and enhanced the perovskite environmental stability. The perovskite film that was simultaneously incorporated with a mixed-cation mixed-halide composition also showed reduced trap states and improved carrier mobility. PSCs fabricated with this composition achieved a maximum PCE of 18.2% under 23 °C and 50% RH through blade coating without using an antisolvent.

Despite the promising results from the addition of chloride or use of alkali thiocyanates, the most promising perovskite composition is the triple-cation based absorber, $Cs_{0.05}(MA_{0.17}FA_{0.83})_{0.95}Pb(I_{0.83}Br_{0.17})_3$, which has been demonstrated to produce a PCE of 20.8% in 25% RH. Low humidity conditions were shown to promote the Ostwald ripening and increase the grain size of the perovskite crystal. It should also be mentioned that with higher humidity (e.g., 50% RH), the approach by Tang et al.[156] using single-cation ($FAPbI_3$) and a mixed-cation mixed halide perovskite ($FA_{0.8}MA_{0.15}Cs_{0.05}PbI_{2.55}Br_{0.45}$), reduced trap states and improved carrier mobility. This approach successfully produced PSCs with a PCE of 18.2% at a RH of 50%.

It is worth mentioning that the most efficient PSCs rely significantly on lead containing compounds, which are highly toxic and brings potential environmental issues. It has been suggested that the release of lead from PSC modules is negligible and the lead concentration in soil has been reported to only increase by ≈4.0mg kg^{-1} (based on a PSC module containing 0.8 g of lead per square meter), compared with the 250 mg kg^{-1} limitation for lead regulation in agriculture.[157] However, Li et al.[158] found that due to the high bioavailability of perovskite, lead from a PSC module is more dangerous than other lead contaminants that are already present in the soil. The organic cations from perovskite increase the lead uptake ability of plants, and thus can increase the adverse impact on the environment and humans. Tin, as one of the most popular alternatives to lead, has been shown to be less dangerous than lead.[158] Although in some circumstances the toxicity of tin can be higher than lead,[159] tin is less bioavailable because of the low solubility of Sn^{4+} in water.[160] However, the performance of tin-based PSCs is limited with the highest PCE record of 13%, which is lower than lead-based PSCs.[161] In addition, tin-based PSCs are highly unstable in an ambient atmosphere and hence have not been discussed in this review. Future work should focus on the stabilization of tin-based PSCs, the development of new perovskite compositions without heavy metal divalent cations, and novel encapsulation strategies to limit the release of toxic cations in PSCs.

3.2. Solvent Engineering

Solvent engineering in PSCs can either refer to refining the solvents used in the perovskite precursor solution, or the dynamic dripping of an antisolvent during the spin-coating procedure (as discussed in Section 2).[86] This section is predominately focused on the antisolvent used in the one-step spin-coating method, and the solvent used to modify the underlying PbI_2 surface in the two-spin spin-coating method. The morphology of the perovskite plays an important role in the performance of PSCs, and it is the major challenge for ambient fabrication. Perovskite films fabricated without dynamically dripping an antisolvent have been previously shown to result in nonuniform films with poor surface coverage.[86] Thus, various solvent engineering techniques have been investigated to modify and benefit the microstructure of the perovskite film.

3.2.1. Solvent Engineering: One-Step Spin-Coating

In one-step spin-coating, antisolvent is used to control the growth rate of the perovskite film and remove residual solvent. More specifically, applying antisolvents can reduce the solubility of the perovskite in other solvents and accelerate its nucleation due to supersaturation and therefore provide a compact and pinhole-free perovskite film with large grain sizes.[162] In general, antisolvents which have a low boiling point, low polarity, low dielectric constants and low perovskite solubility are ideal for the formation of high quality perovskite films. Based on this mechanism, a series of antisolvents such as isopropyl alcohol (IPA),[127] diethyl ether (DE),[90,162] chlorobenzene (CB),[163] and acetate-based solvents were considered as potential candidates for solvent engineering.

Wang et al.[90] demonstrated that the moisture effect during fabrication can be suppressed with DE antisolvent. The PCE of

© 2020 The Authors. Published by Wiley-VCH GmbH

PSCs which used DE remained at 15% and almost unchanged when the RH was increased from 0 to 60%. The low moisture sensitivity can be attributed to the rapid crystal growth, whereby the solvent of the precursor solution was extracted and spun away when the DE was dripped, which shortened the grain growth process and minimized the influence of humidity. The best device fabricated under 50% RH achieved the highest PCE of 16.9%. Acetate group molecules including methyl acetate (MeOAc),[164] ethyl acetate (EtOAc),[165–168] propyl acetate (PrOAc),[93] and butyl acetate (BuOAc) are also considered favorable antisolvents for ambient fabrication. When DMSO, a common solvent for perovskite precursors, is used for perovskite film fabrication, it can slow down the reaction between MAI and PbI_2 and formed a MAI–PbI_2–DMSO intermediate, as shown in **Figure 10**a. Antisolvent toluene was dripped to remove the excess DMSO and induce the formation of a uniform MAI–PbI_2–DMSO intermediate thin layer. DMSO in the intermediate phase was removed in the annealing process and

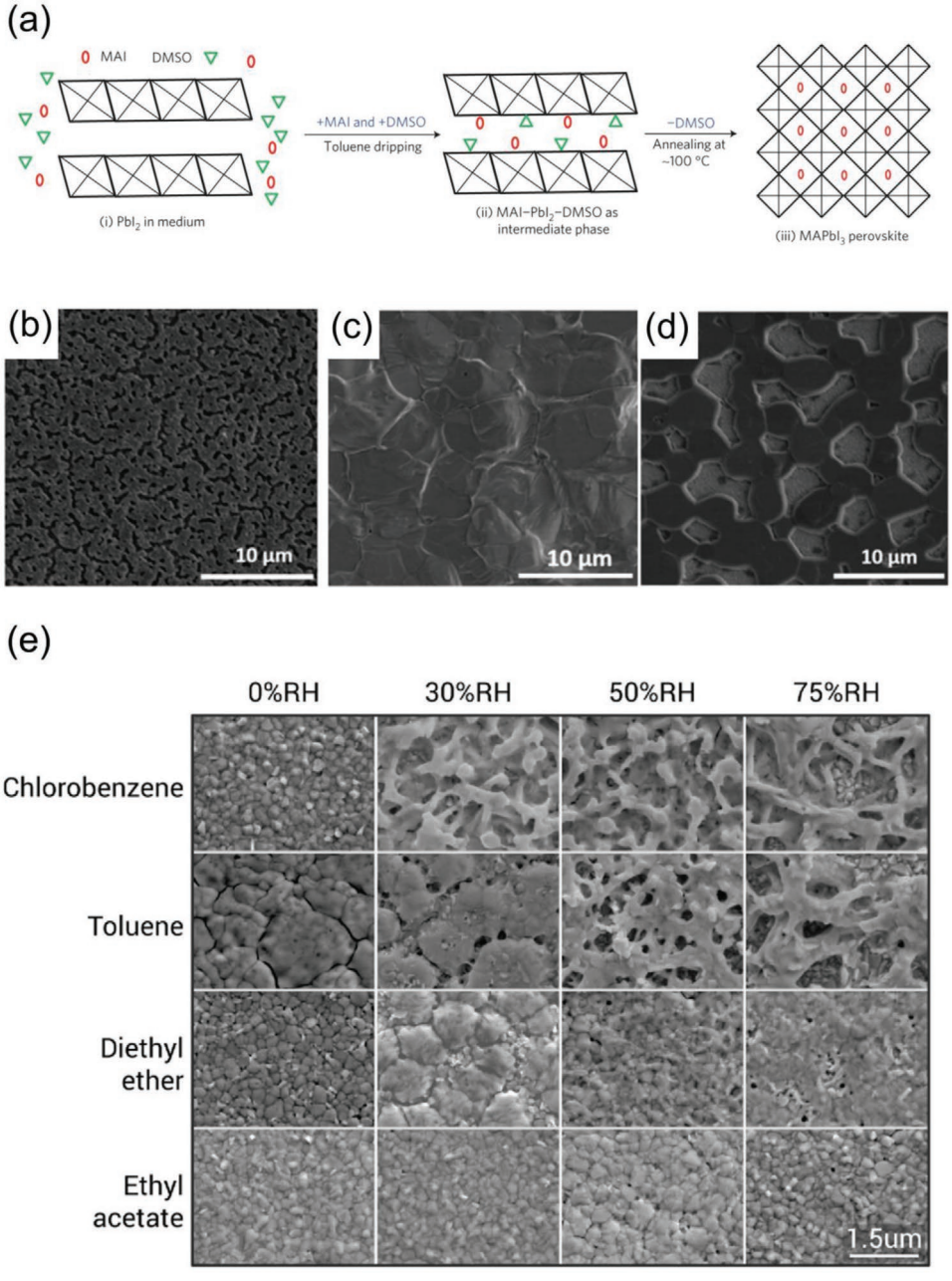


Figure 10. a) The mechanism showing the formation of $MAPbI_3$ with DMSO and toluene solvent via octahedral [PbI_6^{4-}] layers in i) PbI_2 which then form a ii) MAI-PbI_2-DMSO intermediate to give iii) a uniform perovskite phase with corner-sharing octahedra via extraction of DMSO. Reproduced with permission.[86] Copyright 2014, Nature Publishing Group. Microstructure of perovskite films treated with b) 100% CB, c) 100% ethanol, and d) 25% ethanol and 75% CB. Reproduced with permission.[171] Copyright 2018, Nature Publishing Group. e) SEM of $MAPbI_3$ PSCs fabricated with CB, Toluene, DE and EA under 0%, 30%, 50%, and 75% RH. Reproduced with permission.[165] Copyright 2017, Elsevier.

© 2020 The Authors. Published by Wiley-VCH GmbH

a smooth and uniform perovskite layer was obtained.[86] While acetate group molecules are used as the antisolvent, the intermolecular force between DMSO and acetate can suppress the evaporation of acetate, thus promoting the regular growth of MAI–PbI_2–DMSO intermediate and slowing down the crystallization of the perovskite. Also, acetate functioned as a water absorber which trapped the moisture in the air and protected the perovskite intermediate phase.[165] Yang et al.[164] compared $MAPbI_3$ PSCs fabricated under 60–70% RH using a group of acetate based antisolvents. The best device which used MeOAc reached a promising PCE of 16.3%. The high-quality perovskite film was attributed to the higher water solubility of MeOAc which prevented the perovskite intermediate phase from moisture. Meanwhile, the higher vapor pressure and lower boiling point can accelerate the evaporation of DMF and control the crystallization of the perovskite.[169] However, Shi et al.[167] found that for $FA_{0.1}MA_{0.9}PbI_3$ PSCs under relatively low humidity (20-30% RH), the performance of the best PSCs fabricated with EtOAc (16.24%) was better than that with MeOAc (15.78%). It was proposed that the hydration of MeOAc was too strong under 20–30% RH.

CB is also used in the ambient fabrication of perovskite films. Yang et al.[170] reported an antisolvent washing treatment with CB to fabricate ZnO-based PSCs in a humid environment (exact humidity not disclosed). It was discovered that during the deposition of perovskite thin films on the ZnO layer, the MAI in the precursor solution reacted with the $Zn(OH)_2$ which came from ZnO and water, thus etched the ZnO film, as shown in Equation (15). To solve this, CB was added after the perovskite precursor solution was spin-coated for 5s to freeze the MAI into the perovskite crystal. Moreover, CB covered the wet perovskite layer and prevented water from reaching the interface of MAI and ZnO. To avoid water and hydroxyl groups in the ZnO film, a relatively high temperature (160 °C) was used in the annealing process of the ZnO film. Gedamu et al.[171] demonstrated a mixed solvent strategy that combined antisolvent (CB) and ethanol together to fabricate PSCs in ambient conditions (RH ≈ 40%). A CB approach usually gives large grain perovskite films with a lot of large pinholes and poor surface coverage as shown in the SEM image in Figure 10b. The film treated with ethanol resulted in better surface coverage with fewer and smaller pinholes but also much-reduced crystal grains (see Figure 10c). A mixture of 75% CB and 25% ethanol was considered as the best antisolvent to produce uniform and large grain size perovskite films (see Figure 10d), which obtained the PCE of 14.0%

$$Zn(OH)_2 + 4CH_3NH_2 \cdot HI \rightarrow \left[Zn(CH_3NH_2 \cdot HI)_4\right]^{2+} + 2OH^- \quad (15)$$

3.2.2. Solvent Engineering: Two-Step Spin-Coating

In the two-step spin-coating method, solvents have been used to improve the quality of the initial underlying PbI_2 film and promote the transfer of PbI_2 into the perovskite phase. Wang et al.[172] spin-coated a series of solvents with different polarities such as toluene, IPA, and water onto the PbI_2 film to obtain a smooth and small crystalline PbI_2 film. The dispersion of PbI_2 was determined by the polarity of the solvents where toluene and water resulted in a much poorer dispersion of PbI_2 than IPA as shown in **Figure 11**a. IPA was the most suitable solvent due to its partial affinity for PbI_2 and smaller crystal arrangement in the precursor solution, thus forming a uniform PbI_2 film as shown in Figure 11b.

Cheng et al.[173] demonstrated that ethanol can control the morphology of the PbI_2 film and help its conversion into perovskite. In the second step of spin-coating, MAI was deposited on the PbI_2 film where it diffused through the film forming the perovskite. However, this intercalation process can expand the surface of PbI_2 and form a compact perovskite layer which can prevent the MAI from reacting with inner PbI_2. This process resulted in residual or excess PbI_2 and lowered the performance of the PSCs.[174–176] In order to overcome this, ethanol was used to modify the PbI_2 film and make it easier to intercalate.[173] The PbI_2 precipitated and crystallized rapidly because of the low solubility in ethanol, forming a dendrite-like or flake-like surface morphology with nanosized voids. The conversion of PbI_2 to perovskite was achieved more easily and a high-quality perovskite film was obtained where PSCs achieved an average PCE of 11.22 ± 0.65% (average of 30 devices).

In brief, precise solvent engineering enables the formation of high quality PbI_2 or perovskite films under ambient conditions. Due to their high volatility and low perovskite solubility, the addition of antisolvents can control the growth rate of the perovskite crystal, remove the residual solvent and protect the intermediate phase film from oxygen and water in an ambient atmosphere. From this work, it is clear that the one-step spin-coating method has a larger variety of approaches when fabricating ambient PSCs. This is primarily due to the large window of antisolvents which can be used in this approach. For example, the one-step spin-coating method has a large window of nonpolar/low polar and low boiling point antisolvents to choose from, which in turn provides high quality perovskite films in one simple step. This, in comparison to the two-step spin-coating method, is quite different. For instance, the two-step spin-coating method usually requires dissolving MAI or formadinium iodide (FAI) salts in a polar solvent, and this choice of solvent is somewhat limited due to the solvent's effect on the underlying PbI_2 film (and thus, the eventual perovskite formation). Thus far, the solvent of choice for almost all the literature is IPA, due to its mild polarity and only partial affinity for PbI_2 molecules. This promotes the arrangement of PbI_2 as small grains of lower crystallinity in the film. When using solvents from low and high polarities (see Figure 11), PbI_2 arranges itself from mid to large sizes. Therefore, exposure to IPA results in the formation of smaller PbI_2 chunks, which then provides the ideal platform of small ordered PbI_2, leading to smooth and highly crystalline $MAPbI_3$.[172] Thus far, no other mild polar solvent has been as successful in the two-step deposition as IPA. When fabricating PSCs in ambient conditions using the one-step spin-coating method, DE or acetate-based antisolvents is recommended. The antisolvent which gave the highest PCE under medium humidity (<40% RH) conditions was EtOAc, due to its influence on the growth of the MAI-PbI_2-DMSO intermediate and control of perovskite crystallization.[166] When the humidity is high (>60% RH), MeOAc is more suitable due to its high

© 2020 The Authors. Published by Wiley-VCH GmbH

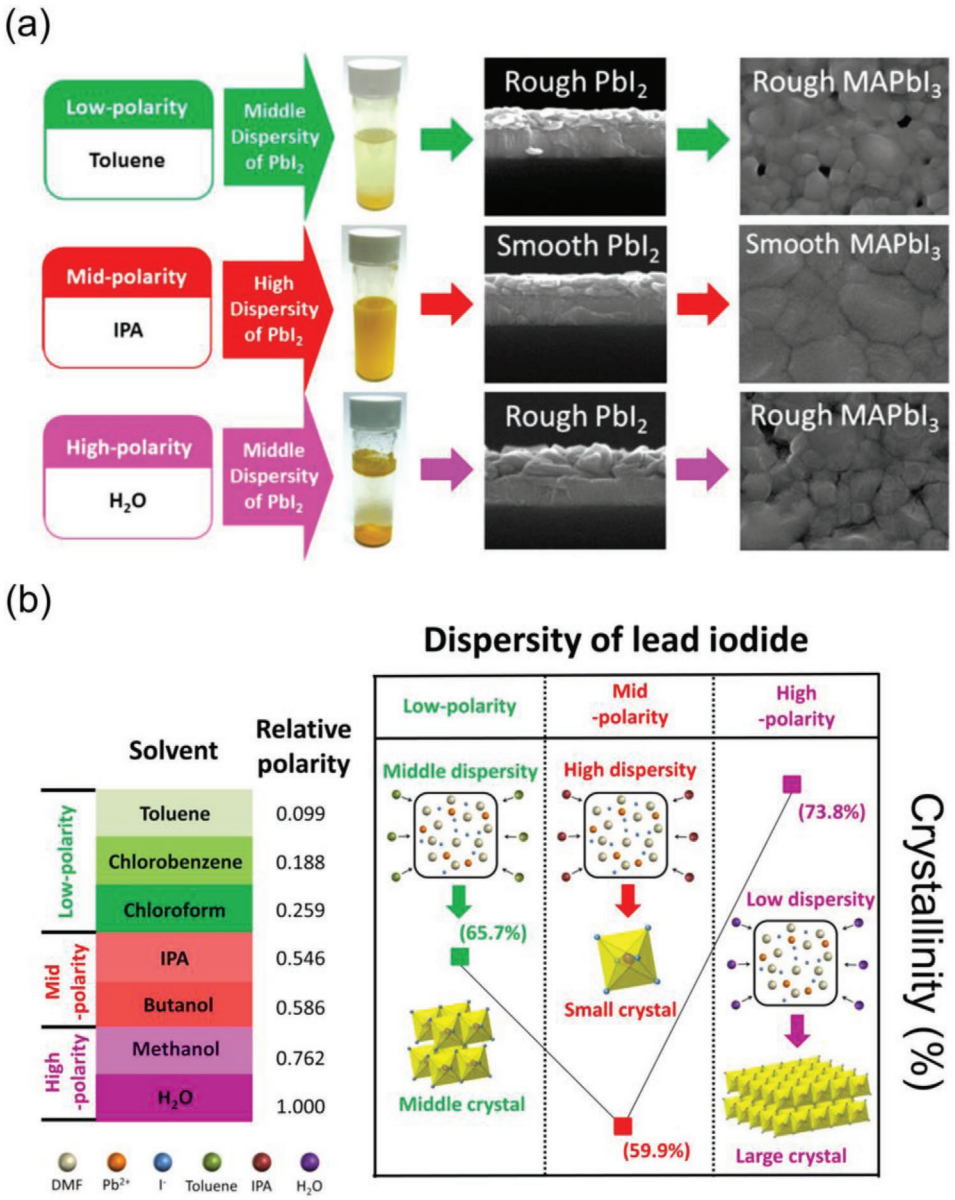


Figure 11. a) Cross-sectional and top view SEM images of PbI_2 films and the corresponding disparity as a result of different polarity solvents. b) Polarity of various solvents and the corresponding formation process of the PbI_2 crystal when treated with each polarity group. Reproduced with permission.[172] Copyright 2017, American Chemical Society.

vapor pressure, high water solubility and low boiling point.[164] As for the two-step spin-coating procedure, IPA should be used as the solvent to disperse MAI or FAI salts since it has been shown to have the least negative effects on the underlying PbI_2 film and final perovskite film.[172]

3.3. Additive Engineering

Additive engineering refers to the introduction of additives into the perovskite precursor to improve crystallization and film formation, defect passivation, and/or influence the interface tuning.[177] More specifically, additives have been effective for facilitating homogenous nucleation or modulating crystallization kinetics. Controlling nucleation and crystal growth during film formation is vital to obtain good surface coverage and crystal size, which reduces electrical shunt pathways, probability of recombination, and bulk trap states.[178] In this section, additives which are utilized in the ambient fabrication of PSCs and their impact on the morphology and moisture resistance of perovskite films are discussed. In brief, the additive has three specific functions: 1) to work as a modifying reagent during the spin-coating method and form high quality perovskite/PbI_2 film; 2) to coordinate with the composition of perovskite to control the growth of the film and protect it from environmental moisture; and 3) to exist in the perovskite film

© 2020 The Authors. Published by Wiley-VCH GmbH

to enhance the device performance and inhibit the degradation process. This section is divided into one-step and two-step spin-coating procedures and highlights the benefits of additives for each approach.

3.3.1. Additive Engineering: One-Step Spin-Coating

The additive can coordinate to the perovskite precursor or form an additive-perovskite intermediate to affect the formation of the perovskite film. 2-Pyridylthiourea is used as a Lewis base additive.[29] Since 2-pyridylthiourea contains both S and N-donors from thiourea and pyridine respectively, it can strongly coordinate to the Lewis Acid, PbI_2.[179] Fourier-transform infrared spectroscopy (FTIR) is shown in **Figure 12**a where the stretching vibrations of C=S and C=N in 2-pyridylthiourea were blue-shifted and further shifted to lower wavenumbers with the increase of additive amount. The interactions between 2-pyridylthiourea and PbI_2 contributed to the perovskite formation, reduced the film roughness and enhanced the stability. Also, it slowed down the formation of the perovskite, thus providing a compacted perovskite film with large grain sizes and fewer pinholes. It was found that DMSO, as the additive solvent of the precursor solution, can suppress the influence of moisture.[180] DMSO has also been shown to compete to coordinate with the lead atom, forming the PbI_2:MAI:$DMSO_n$:H_2O_m intermediate during the spin-coating process.[181] When $m + n \approx 1.5$, the best crystallinity was obtained, which meant the ratio of PbI_2:MAI:DMSO needed to change according to different RH. Rong et al.[182] demonstrated a moisture-induced transformation of perovskite crystals by adding ammonium chloride (NH_4Cl) to assist in the crystallization of the perovskite. Figure 12b shows a schematic overview of the crystal growth process of $MAPbI_3$ in the presence of NH_4Cl and moisture. Ammonium lead trihalide dehydrate, $NH_4PbX_3(H_2O)_x$, was dominantly formed during the evaporation of the solvent (steps i–ii). NH_3 was released in the annealing process and $NH_4PbX_3(H_2O)_x$ was partially transforming to $MAPbX_3$ by combining with MA^+ (steps ii–iii). During the 45% RH exposure, moisture contributed to the removal of NH_4^+ (steps iii–iv) and promoted the crystallization of $MAPbX_3$ (step v), which finally resulted in the growth of perovskite crystals along the [110] direction. They obtained printable $MAPbI_3$ based PSCs with the highest PCE of 15.6% and a lifetime of 130 days in ambient conditions (30% RH).

Some additive can remain in the PSCs to improve the device performance by filling the defects. A light sensitive additive, diiodomethane (CH_2I_2), was used by Ankireddy et al.[183] to fabricate PSCs with an intense pulsed light (IPL) process. The perovskite film was prepared under low humidity (less than 10%) and then processed in an IPL apparatus under 60% RH. PSCs fabricated with CH_2I_2 obtained a reduced defect density as the disassociated iodide ions from the CH_2I_2 during the IPL process participated in the formation of the perovskite crystal and resulted in the reduction of iodide vacancies as shown in Figure 12c,d. Also, CH_2I_2 can control the growth of the grains and improve the solvent-precursor interaction, leading to a pinhole-free and fully covered perovskite film. Yang et al.[184] reported that a 5% addition of polysaccharide agarose can negate the effects of moisture-induced degradation of the perovskite film during synthesis. The formation of agarose-LiTFSI complexes decreased the hygroscopicity of LiTFSI, thus reducing water uptake and leading to less corrosion of the perovskite. Also, $MAPbI_3$-agarose complexes passivated the grain boundaries and provided continuous carrier transporting pathways. Huang et al.[185] used MA solution in ethanol and MACl as the additives in the perovskite fabrication under ambient condition (RH 10–15%). During their preparation of $MAPbI_3$ films, the presence of weak hydrogen bonding within the CH_3NH_2-$CH_3NH_3^+$ dimers, whereby dissociation of CH_3NH_2 from the intermediate encouraged a fast, spontaneous phase transition of the intermediate/perovskite from δ-$MAPbI_3$ to α-$MAPbI_3$. Using this knowledge, an all wet-chemistry route by spin-coating MA liquid presolutions in ethanol solvent and using an MACl additive in the intermediate was devised and the impact of the additive assessed. It was found that the additive altered the initial phase-transition route, whereby the ambient conditions prompted dissociation of CH_3NH_2 and created a slow transition from δ to α, which upon annealing (110 °C), produced pure α-$MAPbI_3$ as a highly crystalline and pinhole-free film. The optimal device fabricated under ambient conditions, giving an appreciable PCE of 20.3% (10–15% RH), entailed an addition of 0.15 mol MACl. Potential for large scale fabrication of these films was then evaluated using a simple dip-coating method under ambient conditions to produce a module (12 cm^2 aperture area) from 4×4 cm^2 films. This method successfully produced uniform films with a PCE of 16% suffering minimal stability diminution.

Halogen based additives are one of the commonly used additives in the one-step spin-coat method. Pan et al.[186] used dry-hydrogen chloride (HCl) as the additive to fabricate PSCs in a N_2-filled glove box where HCl gas was directly dissolved into the DMF solvent. HCl bonded to the PbI_2 and became an inhibitor in the crystallization process, leading to a deceleration of nucleation and nucleus growth, thus obtaining good and uniform coverage of the perovskite film. However, Yang et al.[187] reported that HCl remaining in the film can lead to morphology and electronic defects, and resulted in a low efficiency. To completely remove HCl, Yang et al.[187] expanded on previous work by implementing an antisolvent washing process using chloroform and successfully fabricated PSCs with the highest PCE of 17.72% in ambient conditions (30% RH). Chloroform was expected to protect the intermediate film from oxygen and water in the air and remove the excess HCl in the film (atomic ratio of HCl to lead decrease from 1:5 to less than 1:100). Li et al.[188] used 33 wt% hydrochloric acid (aqueous HCl) as an additive to fabricate moisture tolerant PSCs in ambient conditions with a RH of up to 60%. The one-step and two-step spin-coating methods were used, and both achieved a PCE exceeding 14%. The two-step method will be discussed in Section 3.3.2. The highest PCE obtained from the one step method was 14.28% under 60%. A proposed explanation was based on its high moisture resistance in which the HCl molecules can preferentially bond to PbI_2 or $MAPbI_3$, protecting the perovskite film from water. Hydrogen iodide (HI) was used as an additive to enhance the stability of perovskite under ambient conditions. The perovskite film degraded when exposed to moisture and finally decomposed into PbI_2, CH_3NH_2 and HI. The additive HI can suppress this process by recovering the CH_3NH_2 into MAI, preventing the

© 2020 The Authors. Published by Wiley-VCH GmbH

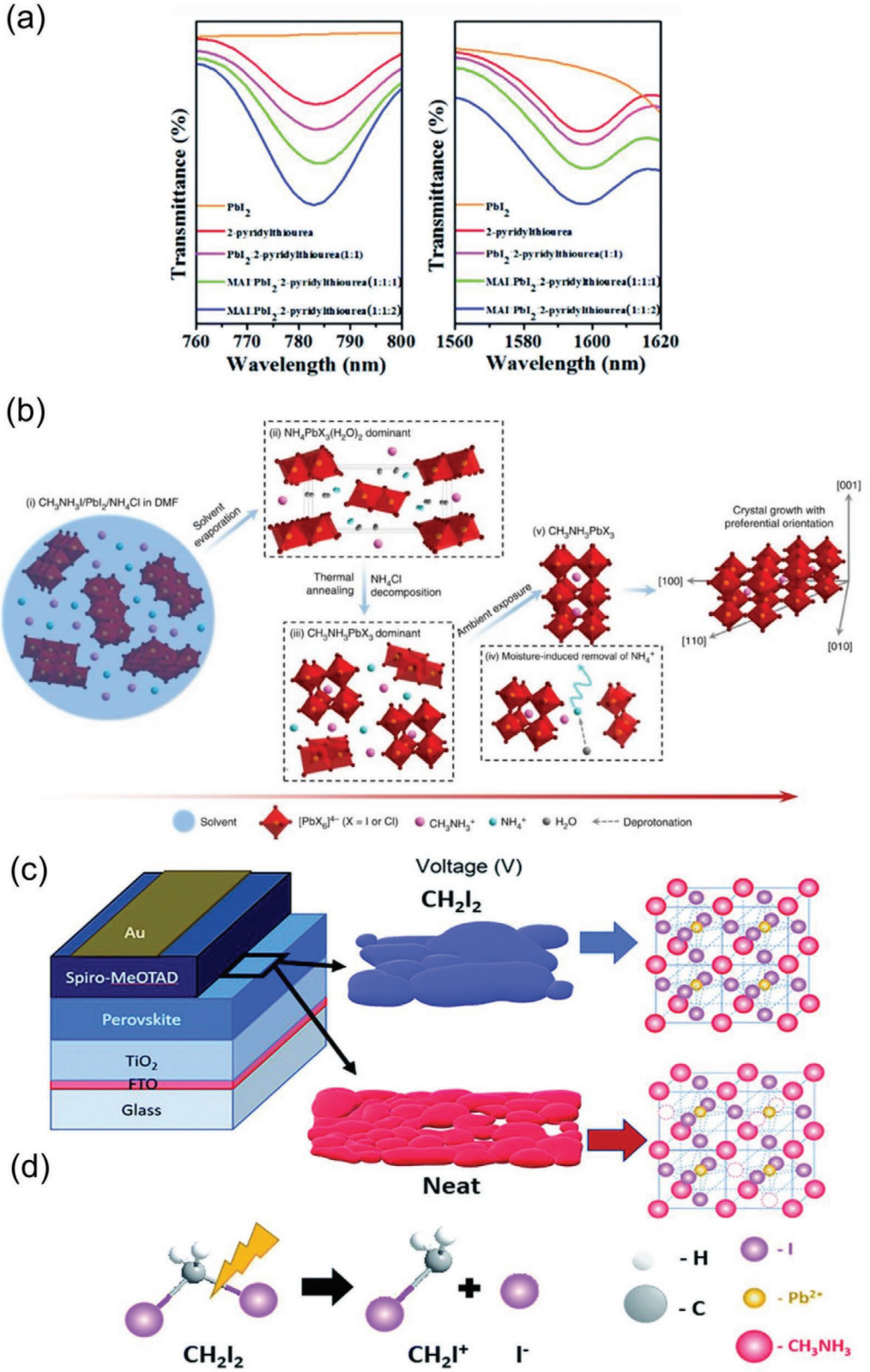


Figure 12. a) The FTIR spectra of the perovskite precursor with different molar ratios of 2-pyridylthiourea. Reproduced with permission.[29] Copyright 2017, The Royal Society of Chemistry. b) The schematic of the crystal growth process of $CH_3NH_3PbX_3$. Reproduced with permission.[182] Copyright 2017, Nature Publishing Group. c) The structure of PSCs synthesized with and without CH_2I_2. d) The cleavage of CH_2I_2 under UV releasing a free iodide ion. Reproduced with permission.[183] Copyright 2018, The Royal Society of Chemistry.

© 2020 The Authors. Published by Wiley-VCH GmbH

decomposition process. In addition, $MAPbI_3$ had a higher solubility in DMF with HI which provided a more concentrated precursor solution, resulting in a denser perovskite film with full coverage and less pinholes.

3.3.2. Additive Engineering: Two-Step Spin-Coating

As discussed in Section 2.2.2, it was concluded that moisture induced a poor-quality PbI_2 film with isolated distribution but promoted the formation of the perovskite film in the second step.[111] To fabricate a high quality PbI_2 film, previous research groups have used additives in the PbI_2 precursor solution. A strong Lewis base, *n*-butylamine (BTA), was used to fabricate PSCs with a PCE of 16.0% under low RH of 25%.[111] Due to the moisture effect, the PbI_2 film exhibited a poor morphology with a rough surface and large grain size. Because of the strong Lewis base nature and good infiltrative property, BTA made the PbI_2 solution homogeneously spread out on the substrates, slowed down the formation of the PbI_2 film and protected it from the water in the atmosphere. Similarly, Zhang et al.[143] used BTA as the additive to reduce the moisture effect and further improve the conversion of PbI_2 to perovskite film. As shown in **Figure 13**a, BTA was added into the PbI_2 solution to form a smooth and uniform PbI_2 film which guaranteed a high-quality perovskite layer.[189] These PSCs achieved the highest PCE of 17.56% under a high RH of 60–80%.

4-*tert*-butylpyridine (tBP) was used as a surface modification agent to increase the hydrophobicity of PbI_2 film and enhance its moisture resistance.[190] As shown in Figure 13b, tBP is hydrophobic because of its tertiary butyl group and the N atom on the pyridyl group of tBP can strongly coordinate with the Pb^{2+} in the PbI_2, which results in the formation of a hydrophobic layer (see Figure 13c). The water contact angle measurements are shown in Figure 13d, where the increased contact angle indicated an improvement of hydrophobicity of the PbI_2 and perovskite droplet, aiding its protection against water.[191] While this approach produced a PSC with improved stability, it was still strongly affected by moisture. Notably, when the RH increased from 50% to 70–80%, the PCE of PSC decreased from 12.6% to 7.21%. Further work by, Cheng et al.[192] introduced a poly(3,4-ethylenedioxythiophene) polystyrene sulfonate (PEDOT:PSS) interlayer to tBP added PSCs. The PCEs of the best devices fabricated under 40–50%, 50–60%, and 60–70% RH were 16.16%, 14.11%, and 10.73%, respectively. The presence of PEDOT:PSS as an interlayer acted as a reduction active-flexible polymer which enhanced the tBP morphology-modifying effect of the $MAPbI_3$ film. A uniform and porous $PbI_2 \cdot x$tBP film was obtained, which resulted in a compact $MAPbI_3 \cdot x$tBP with large grains. Also, compared with reference PSCs which almost lost all the PCE after 10 days under 50% RH, PSCs fabricated with this method retained 80% PCE, proving its enhanced ambient stability. Similarly, tetrahydrofuran (THF) as an oxygen donor (O-donor) additive can enhance the stability and reproducibility of PSCs in a humid atmosphere.[193] O-donor THF was found to interact with PbI_2 which resulted in a homogeneous, dense and pinhole-free layer of PbI_2. The resulting perovskite layer was therefore compact and resulted in a significant reduction in defects as shown in the SEM image in Figure 13e. The best PSC fabricated with the THF additive obtained a PCE of 15% with high reproducibility and retained 80% of its PCE after exposure to 50% RH for 20 days (see Figure 13f).

Wang et al.[112] used zinc oxide ZnO NPs as an additive to control the formation of the PbI_2 film. The homogeneously dispersed ZnO NPs in the PbI_2 precursor solution can provide more nucleation sites and accelerate the nucleation process, resulting in large grain and pinhole-free PbI_2 films. It was proposed that the small domains grown from ZnO NPs filled the pinholes on the large grain film formed under ambient conditions. This method obtained PSCs with an average efficiency of 18.34% under 60% RH.

As discussed in Section 3.3.1, Li et al.[188] also introduced HCl (from 33 wt% HCl) into the DMF precursor solution of PbI_2 and formed an $HCl \cdot PbI_2$ intermediate film with excess PbI_2. This intermediate film exhibited a high crystallinity and can rapidly be converted to a smooth $MAPbI_3$ film after dipping in a MAI solution. It is also demonstrated that HCl can be completely removed during the annealing step. The PCE for the two-step method was 14.76%, slightly higher than the 14.28% reported for the one-step method.

In summary, the most promising approach in utilizing additive engineering in the one-step spin-coating method is the addition of 2-pyridylthiourea, which promotes film morphology and stability of the PSCs. At a high RH of 50–60%, the addition of 2-pyridylthiourea resulted in PSCs with a PCE of 18.2%. As for the two-step spin-coating method, the addition of BTA slows down the crystallization rate due to its strong Lewis base nature and further protects the PbI_2 film from water in the atmosphere. Impressively, using BTA as an additive was shown to produce PSCs with a PCE of 17.56% under a high RH of 60–80%. Finally, the use of ZnO NPs were shown to promote the formation of the PbI_2 film where PSCs with a PCE of 18.34% were fabricated at a RH of 60%.

3.4. Large-Scale Fabrication

To promote the commercialization of PSCs, several large-scale fabrication methods such as slot-die coating,[194] doctor blading[195] and spray coating[196] methods have been investigated (see **Figure 14**a–c). Substrate preheating is another promising technique which has been used in parallel with large scale fabrication methods as it provides assisted formation and protection of the perovskite layer.[197] Considering the production environment and need to reduce the fabrication cost, it is necessary to conduct these methods under ambient conditions. Also, to obtain better performance, composition engineering, additive engineering, and solvent engineering have also been implemented in these fabrication methods. Such methods have all been outlined in the sections above, however this section will focus on current state-of-the-art large-scale fabrication methods and the commonly used substrate heating method in the large-scale ambient fabrication of PSCs.

3.4.1. Substrate Preheating

In spin-coating, preheating the substrate before deposition or heating the substrate during the deposition is used

© 2020 The Authors. Published by Wiley-VCH GmbH

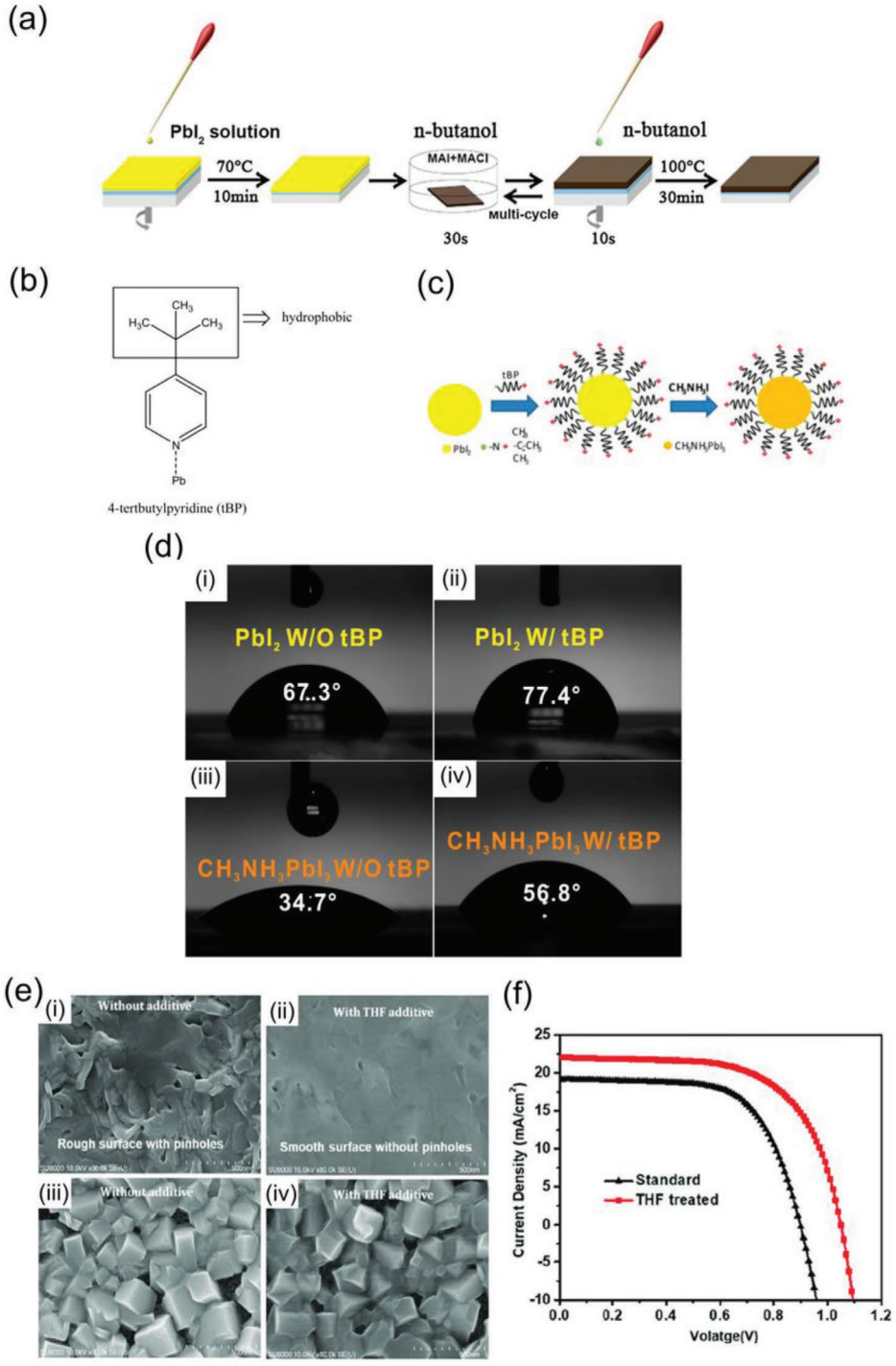


Figure 13. a) Multicycle short-time dipping reaction protocol to synthesize $MAPbI_{3-x}Cl_x$ film. Reproduced with permission.[143] Copyright 2017, Elsevier. b) The hydrophobic 4-*tert*-butylpyridine coordinated to lead. c) The hydrophobic layer (tBP) on the surface of PbI_2 and $MAPbI_3$. d) The contact angle water droplets on PbI_2 i) without and ii) with tBP, and on $MAPbI_3$ solution iii) with and iv) without tBP. Reproduced with permission.[190] Copyright 2017, American Chemical Society. e) Top-view SEM images of PbI_2. i) with THF additive and ii) without THF and the iii,iv) corresponding perovskites films, respectively.[193] f) *J–V* curve of THF treated PSCs and control group. Reproduced with permission.[193] Copyright 2019, Wiley-VCH GmbH.

to improve the quality of PbI_2 film. The increase in temperature accelerates the vaporization of solvent, which can increase the supersaturation degree of PbI_2 and promote the crystallization process.[198] Furthermore, the solvent vapor can suppress the ingress of oxygen and moisture in the air,[60] thus a compact and fully covered PbI_2 film fabricated under ambient conditions can be obtained with the substrate heating method.

© 2020 The Authors. Published by Wiley-VCH GmbH

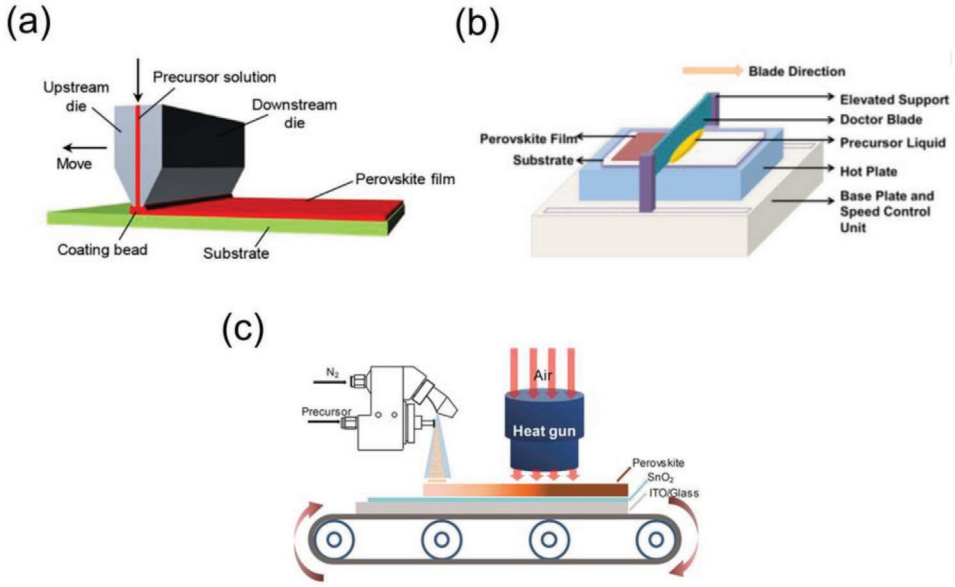


Figure 14. a) Slot-die coating process. Reproduced with permission.[194] Copyright 2018, American Chemical Society. b) Doctor blading process. Reproduced with permission.[195] Copyright 2016, Elsevier. c) Spray coating method. Reproduced with permission.[196] Copyright 2019, American Chemical Society.

Ko et al.[198] used a substrate heating treatment to fabricate PSCs with a best PCE of 15.76% under 50% humidity. The substrate was preheated at 40, 50, and 60 °C respectively, and was kept at 60 °C during the spin-coating, then dried at 40 °C for 3 min and 100 °C for 5 min. It was found that the thickness of the PbI_2 film increased with higher temperature. Huang et al.[199] used an in situ substrate-heating-assisted deposition method to fabricate PSCs under 40% RH. The substrates were maintained at constant temperature (from 20 to 80 °C) through in situ heating and further heating for 30 min in air. With the increase of temperature, the PbI_2 film became more uniform and the grain size decreased gradually as depicted in **Figure 15**a, which shows the SEM images with temperatures from 20 to 80 °C (as detailed in the figure caption). It was proposed that under the high temperature, the volatilization of solvent was accelerated which increased the supersaturation degree of PbI_2. The nucleation was faster than the growth of the crystal, forming small grain sized PbI_2. Subsequently, the surface morphology of the perovskite films shows a similar trend to that of the PbI_2 film described above. Figure 15b shows the surface morphology of the perovskite films as the temperature increases from 20 to 80 °C. As temperature increased, continuous films with uniform coverage are achieved, while grain size decreased (also shown in Figure 15a). One possible explanation was that the dense PbI_2 crystal provided more nucleation sites for the perovskite but reduced the crystal growth space. While there was no clear trend in surface roughness measurements shown in Figure 15c–g, the roughness immediately decreased upon heating of the film where the lowest root-mean-square (RMS) value was reported as 57 nm at 50 °C. This was attributed to a balance between the reduced number of pinholes and increase in film disorder. Using this approach, the best PSCs fabricated under 40% RH obtained a PCE of 18.38% at 50 °C. Cheng et al.[60] also used the substrate heating method to fabricate PSCs with a highest PCE of 18.11% under 70% RH. The authors found that moisture can accelerate the PbI_2 crystallization process and resulted in an isolated and poor coverage film. The oxygen changed the surface energy of the interface materials and reduced the wettability of PbI_2 on the substrates, which significantly affected the coverage of the PbI_2 film. To address this, preheating treatment was used and the high vapor pressure of DMF formed a DMF filled environment which protected the PbI_2 film from oxygen and moisture.

The substrate preheating method is also performed in the one-step spin-coating method. Inorganic $CsPbI_3$ PSCs were fabricated under ambient conditions using the preheating method assisted with anti-solvent MeOAc.[200] Preheating the substrate at an elevated temperature (85 °C) for 5 min was considered an efficient strategy to control the nucleation and crystal growth of the perovskite film and resisted the erosion and damage from environmental humidity. The best device of $CsPbI_3$ based inorganic PSCs achieved a PCE of 15.91% under 50% RH. As discussed in Section 2.2.1, Wang et al.[98] reported that the atmospheric humidity can steer the crystallization process of perovskite films through affecting the evaporation of the precursor solvent. It was also found that the conventional antisolvent method, which was aimed at controlling the solvent evaporation, failed when the RH was higher than 70%, as the evaporation of solvent was strongly suppressed under high RH. Thus, the film was preheated to reduce the humidity sensitivity of the anti-solvent. The substrate at elevated temperatures (70 °C) can increase the critical free energy of nucleation and critical nucleus radius, facilitating the nucleation. Finally, the best PSCs fabricated under 90% RH using DE as the anti-solvent achieved a PCE of 19.5%, which was the best PCE fabricated under high RH. Singh et al.[201] fabricated flexible triple cation PSCs using the preheating method under 15–25% RH and achieved a highest PCE of 18.0%. The substrates were

© 2020 The Authors. Published by Wiley-VCH GmbH

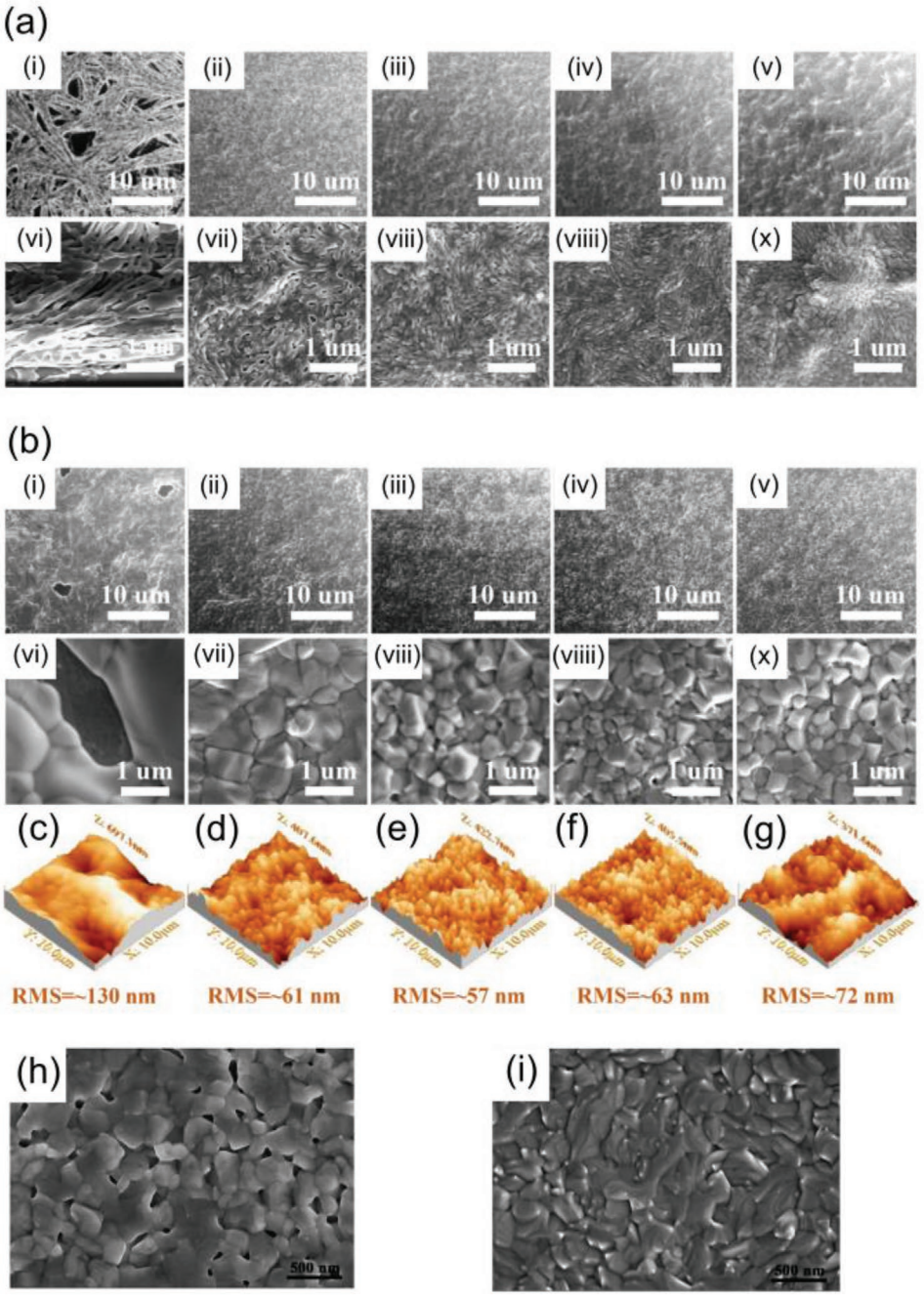


Figure 15. a) The morphology (SEM) of in situ substrate-heating-assisted deposited during the spin-coating of PbI_2 films fabricated under ambient conditions (40%) at the different temperatures of i,vi) 20 °C, ii,vii) 40 °C, iii,viii) 50 °C, iv,viiii) 60 °C, and v,x) 80 °C, respectively. b) The morphology (top-view SEM) of $Cs_{0.21}FA_{0.56}MA_{0.23}(I_{0.98}Br_{0.02})_3$ perovskite films fabricated under ambient condition (40% RH) at the different temperature of i,vi) 20 °C, ii,vii) 40 °C, iii,viii) 50 °C, iv,viiii) 60 °C, and v,x) 80 °C, respectively. The surface roughness (AFM images) of $Cs_{0.21}FA_{0.56}MA_{0.23}(I_{0.98}Br_{0.02})_3$ perovskite films fabricated by in situ substrate heating-assisted method under ambient conditions (40% RH) at the different substrate temperatures of: c) 20 °C, d) 40 °C e), 50 °C f) 60 °C, g) 80 °C, respectively. Reproduced with permission.[199] Copyright 2019, Wiley-VCH GmbH. h) The top-view SEM image of a perovskite film fabricated under 50% without preheating method. i) The top-view SEM image of a perovskite film fabricated under 50% with preheating method. Reproduced with permission.[200] Copyright 2019, The Royal Society of Chemistry.

preheated to 100 °C to reduce the adsorption of atmospheric moisture, thus obtaining a uniform film with large grain size. In brief, substrate heating is a simple and useful strategy to reduce the impact from ambient environment and improve the performance of PSCs.

3.4.2. Slot-Die Coating

In order to develop PSCs toward industrialization, slot-die coating is used in the large-scale fabrication of PSCs.[202–205] Also, with slot-die coating, films with different thicknesses

© 2020 The Authors. Published by Wiley-VCH GmbH

can easily be achieved with little wastage.[206] Ciro et al.[206] used slot-die coating to fabricate perovskite films under high humidity of 65% but only achieved a PCE of 2.4% with the active area of 12 mm^2. The poor efficiency was attributed to poor perovskite crystallization which resulted in a rough absorber layer with pinholes. A similar one-step slot-die system was also reported by Jung et al.[207] to produce fully printable PSCs with the highest PCE of 12.52% in ambient air with the active area of 10 mm^2. A synergistic binary processing additives system containing, *N*-cyclohexyl-2-pyrrolidone (CHP) and DMSO, was used to fabricate uniform and homogeneous $MAPbI_3$ films. CHP remained in the film and facilitated homogeneous nucleation which further modified the morphology of the perovskite film.[208] However, CHP coordinated with PbI_2 to form an intermediate MAI–PbI_2–CHP with a spread dendritic morphology, which resulted in poor film coverage and reduced device performance. DMSO prevented this negative influence by preferentially coordinating with PbI_2 for its higher polarity and basicity. A near-infrared radiation method was used to shorten the annealing time after the two-step slot-die coating process.[209] The substrate was heated to 70 °C to suppress the influence of moisture and oxygen on the PbI_2 film, PSCs with the highest PCE of 12.3% achieved under 60% RH with the active area of 30 mm^2. The triple cation MA/FA/Cs PSCs were fabricated under 40% RH and obtained a highest PCE of 10.57% with total area of 15×15 mm^2 and the active area of 7 mm^2.[210] Mixed MA/FA organic halide salts were used as additives to prevent the overgrowth of PbI_2 from ambient fabrication conditions and to promote the transformation in the next step, and a nitrogen gas knife was employed to accelerate the evaporation of solvent and improve the film quality. Gao et al.[61] developed a novel multiflow air knife (MAK) to control the formation of large area perovskite films in ambient conditions. The introduction of multiple gas flow rapidly dried the solution and enabled the production of large-area perovskite films in air. Using MAK technology, high quality perovskite films with a low roughness of 4.98 nm over a large 10×10 μm^2 area were fabricated. Large area (1.0 cm^2) PSCs achieved highly reproducible efficiencies of 11.70%, while small area (0.1 cm^2) PSCs achieved an efficiency of 17.71%.

3.4.3. Doctor-Blade Method

The doctor-blade method can be used in conjunction with other continuous deposition approaches and is suitable for processing under ambient conditions. In addition, this method provides good control over the film thickness, which suggests great potential to promote the scale up of PSCs. Yang et al.[69] prepared a series of perovskite films using the one-step doctor-blading method under relative humidity from 15–25% to 60–70%. With the increase of humidity, the performance of the PSC device reduced dramatically, which was attributed to the interaction between MA^+ and H_2O being a much stronger interaction than PbI_3^- and MA^+. However, the PSCs with a total area of 15×15 mm^2 and an active area of 10mm^2 annealed in 15–25% humidity exhibited an average PCE of 10.44 ± 0.23%, which was close to the PSCs fabricated by the spin-coating method in a glove box (PCE 11.04%). A proposed explanation was that under the low humidity, the incoming and evaporating water molecules came to equilibrium so that the moisture did not affect the recrystallization process of the perovskite film.

It was reported that increasing the temperature of the substrate can increase the grain size of the perovskite film using the doctor blading method.[195] PSCs with a large area (1 cm^2) obtained a PCE of 7.32% under 25–40% RH when the substrate temperature was 120 °C. Similarly, Wu et al.[211] reported planar heterojunction PSCs with the highest PCE of 11.29% fabricated under 45% humidity, and 120 °C was also found to be the most suitable in situ substrate temperature for the crystallization of the perovskite film. Peng et al.[212] improved this method using cosolvents (DMSO and DMF) for precursor inks and an excess of MAI. The cosolvent enlarged the grain size of the perovskite film and slowed down the crystallization process, thus improving the perovskite morphology. During the annealing process in an ambient environment, some of the MAI released from the perovskite film, resulting in PbI_2 remaining in the grain boundaries. The excess MAI was proposed to embed in the intermediate film and function as a reservoir which facilitated the reformation of $MAPbI_3$.[213] These improvements achieved a compact and uniform perovskite film with a large grain size and small grain boundary, and the best device obtained the highest PCE of 10.92% under 40% RH (active area of 9 mm^2). Wang et al.[214] improved the performance of PSCs using the doctor-blade method by optimizing the precursor and HTL. In this work, 15 vol% DMSO was used in conjunction with DMF (DMF:DMSO = 8.5:1.5), which was shown to delay the crystallization and improve the flatness of the perovskite film. However, PSCs based on PEDOT:PSS only achieved a PCE of 13.83% due to a low open circuit voltage of 0.908 V. To mitigate this issue, PEDOT:PSS was replaced with NiO_x which provided good wettability and a higher work function. The PSCs with the active area of 1.5×1.5 mm^2 based on NiO_x brought the open circuit voltage to 1.12 V and the best device obtained an improved PCE of 15.34% in a RH of 45%. The final perovskite films had large grain domains sized up to 200 μm, low surface roughness and less obvious boundaries between grain domains, all of which contributed to preferential nucleation and crystallization of the perovskite film.

In 2018, Bi et al.[215] used the doctor-blade method to produce PSCs from nontoxic solvents, which is a large step forward for the commercialization and scale-up of this technology. In most doctor-blading methods, DMF is used as it plays a pivotal role in dissolving the perovskite precursor solution. Instead, the authors incorporated a mixture of γ-butyrolactone (GBL) and DMSO, and the perovskite layer was formed via a supersaturation regime following spherulitic growth. PSCs fabricated in ambient conditions (RH 45 ± 10%) via the doctor blading method achieved an average PCE of 15.6%. When the same technique was carried out in a dry box (0.01 vol% H_2O), the PCE improved to 18.0%. The lower PCE obtained without using a dry box was due to poor morphology and impurities which were attributed to coordinated complexes which formed with H_2O molecules. Such effects were otherwise not detected when a dry box was used. In addition, previous work demonstrated that crystallized water was typically present when devices were fabricated in a RH of ≈45%, which related to the bulk properties of the perovskite films.[96] In addition, large area (1.53 cm^2)

© 2020 The Authors. Published by Wiley-VCH GmbH

PSCs were found to achieve a PCE of 14.2%, further supporting the commercialization of this technique. This study showed that spherulitic growth was beneficial for device performance since chemical defects were confined at the grain boundaries of the spherulites, not limiting charge extraction.

3.4.4. Spray-Coating Method

Using N_2 as the carrier gas, the spray-coating method enables protection of the perovskite from oxygen and moisture in the atmosphere. In 2014, an ultrasonic spray-coating method was introduced to fabricate perovskite films under ambient conditions.[216] The substrates were preheated to 75 °C before spray-coating to accelerate the drying of the perovskite film. The combination of spray-coating and the preheating method can shield the perovskite film from moisture and oxygen. With improved coverage and quality of the perovskite film, the best PSCs achieved 11% PCE (active area of 2.5 mm^2). Similarly, Bi et al.[217] showed that heated substrates can reduce the humidity and nitrogen can suppress the effect of oxygen. As a result, PSCs with a highest PCE of 13.54% (active area of 6.71 mm^2) were obtained under 50% RH using the spray-coating method without annealing process. Under evaluated substrate temperature, a local circumstance with low humidity can be produced, which protects the perovskite film from environmental humidity, and N_2 as the carrier gas can reduce the impact of oxygen. Also, the rapid solvent evaporation due to heated substrate resulted in the formation of pinhole-free perovskite film without the formation of a dendritic crystal. Su et al.[196] employed a hot air blowing strategy to replace the substrate heating during the spray-coating process. If the perovskite precursor was directly deposited on the heated substrate, due to the fast evaporation of solvent and immediate supersaturation, perovskite molecules accumulated rapidly, which resulted in uneven nucleation. Hot air blowing mitigated this by promoting the coalescence of the precursor microdroplets and guaranteed the full coverage of the perovskite film. The best PSCs obtained 13.5% PCE for the active area of 13 mm^2, and 9.8% PCE for the active area of 1 cm^2 under 30% RH.

Clearly, large-scale fabrication is critical for the scale-up of this technology and its compatibility with ambient fabrication is pivotal for commercialization. Thus far, the most promising technique which provides resistance to humidity, high efficiency, and compatibility to scale up is the doctor-blade method. Its simplicity and high performance make it the most promising route to fabricate large-area PSCs in ambient conditions, where PCEs exceed 14% for large area devices (>1 cm^2). In addition to simplicity and scale-up compatibility, the doctor-blade technique produces perovskite films with low surface roughness which assists in the crystallization of the active layer and thus performance of the solar cells.

3.5. Other Ambient Fabrication Methods

Other than the methods mentioned previously, some other approaches have also been proposed to prepare PSCs under ambient conditions. This section will discuss a combination of other methods, which cannot otherwise be sensibly included into the specific sections above.

An air or N_2 blowing method is considered as a potential way to replace the antisolvent method, which while still controlling the growth of the perovskite, can form a high quality film.[218,219] Zhang et al.[218] fabricated the mixed-halide $MAPbI_{2.4}Br_{0.6}$ perovskite by gently drying the film by blowing air in an ambient environment. As shown in **Figure 16**a, different from the conventional one-step spin-coating method, excess precursor solution was first absorbed by a tissue. Then, the wet film was blow-dried by compressed air and annealed for 10 min at 100 °C to remove excess MAI. With the help of the compressed air flow, super-saturation of mixed-halide perovskite was formed in the film which promoted the nucleation and crystal growth. Under the high evaporation rate, the nucleation was extremely fast that prevented ion migration, leading to a uniform and high-performance perovskite film. Zuo et al.[219] used N_2 gas instead of compressed air for the blowing-assisted drop-casting method. With NH_4Cl additive, PSCs fabricated under 45% RH achieved a high PCE of 19.48%. As shown in Figure 16b, this method was also expanded to slot-die coating and the roll-to-roll methods which achieved PCE of 15.57% and 11.16%, respectively.

Similar to the air drying method, a gas flow assisting (GFA) method was reported by Lei et al.[220] A two-step spin-coating method was employed under medium humidity (42–48% RH) and the PbI_2 layer was fabricated by flowing high humidity gas during the spin-coating process of PbI_2. The GFA process promoted the mass transfer and formed a more uniform layer by balancing the disparity of centrifugal force between the center and edge. A hot MAI solution was drip-spun to form the perovskite layer in the second step. Finally, the best device was produced with a dense base of sufficient thickness and exhibited 16.32% PCE.

A novel low-pressure chemical vapor deposition (LPCVD) method was reported and PSCs with a highest PCE of 12.73% were fabricated under 60% RH.[59] MAI was prepared by methylamine and hydroiodic acid and then vacuum-dried into a white powder. The PbI_2 spin-coated film and the MAI powder were put into the tubular furnace as shown in Figure 16c. After pumping down under vacuum for 10 min, the PbI_2 film was heated to 140 °C and MAI was heated to 180 °C at the same time to form the perovskite film. One of the reasons for the low-quality film prepared using the conventional spin-coating method was that the formation of $MAPbI_3$ was too fast which resulted in a rough surface with many pinholes. In the LPCVD method, the reaction rate was much slower as it was limited by a slow gas–solid reaction. In low pressure conditions, MAI vapor had a long molecule free path which eventually eliminated the gas concentration gradient and reacted slowly with the PbI_2 film through layer-by-layer growth. The compact and dense perovskite film can be seen from SEM in Figure 16d. Also, the PSC device fabricated by this method exhibited better moisture resistance, even under high temperature and laser illumination.

Instead of pumping down the deposition container, a vapor assisted film deposition strategy reported which used a heat gun to control the humidity of the deposition conditions as

© 2020 The Authors. Published by Wiley-VCH GmbH

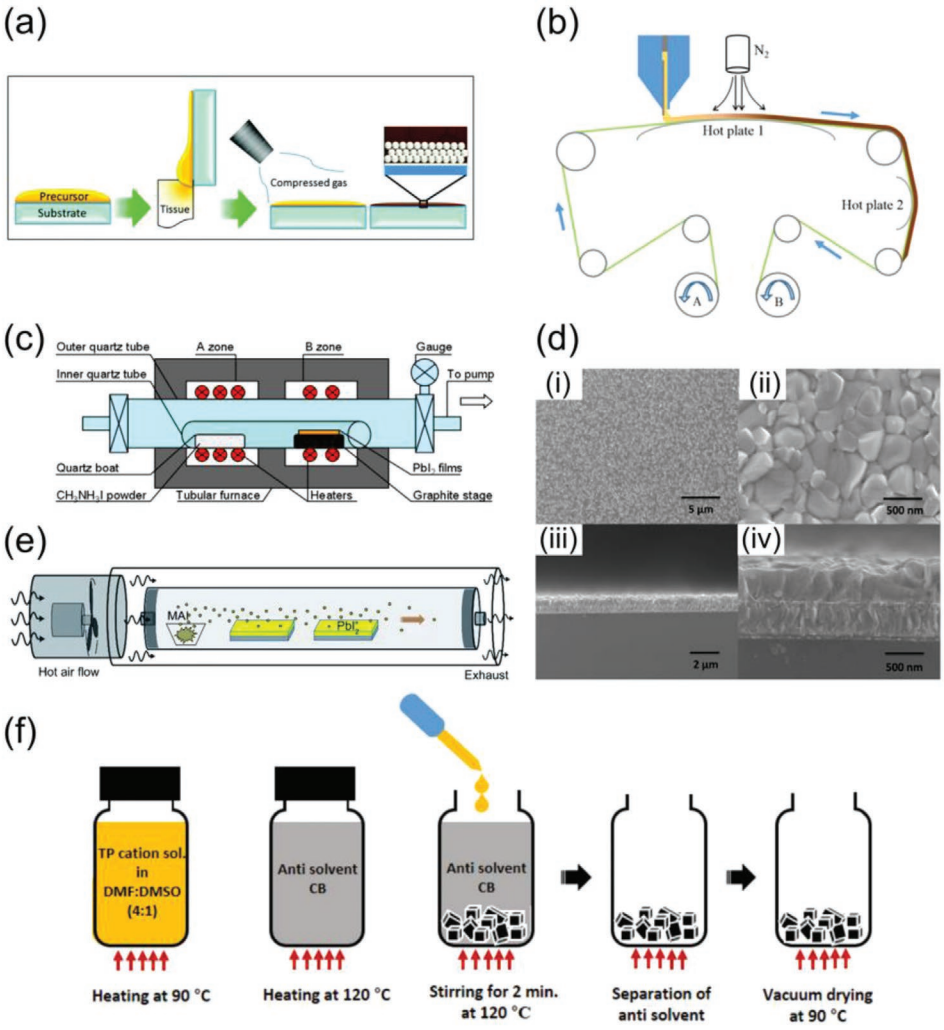


Figure 16. a) The gas blowing method. Reproduced with permission.[218] Copyright 2015, The Royal Society of Chemistry. b) Roll-to-Roll process of perovskite film deposition. Reproduced with permission.[219] Copyright 2018, Elsevier. c) The process of LPCVD method. d) Top-view SEM from LPCVD method at i) low- and ii) high-magnification and cross-sectional SEM at iii) low and iv) high-magnification. Reproduced with permission.[59] Copyright 2015, American Chemical Society. e) The equipment of vapor assisted deposition system conducted in ambient conditions. Reproduced with permission.[221] Copyright 2016, The Royal Society of Chemistry. f) The synthesis of a triple cation perovskite powder precursor solution.

described in Figure 16e.[221] The hot air flow can control the environment of the vapor reaction region which can reduce the RH from 40% to 10%. It also functioned as the heating resource to vaporize MAI powder, and transported the MAI vapor to the PbI_2 film. The best PSCs fabricated by this method obtained a highest PCE of 18.90% (average 17.25%) under 35% RH. Higher long-term air stability was also observed compared with traditional solution processed PSCs.

A highly crystalline perovskite powder was employed to make the precursor solution and it was spin-coated under ambient conditions (22% RH).[222] This perovskite powder was prepared by adding the hot triple-cation perovskite solution (DMF/DMSO 4:1, 1 drop/5 s) to 120 °C antisolvent CB, then stirring overnight at 65 °C. The perovskite powder was dissolved in 4:1 DMF/DMSO solution again to make the powder-based precursor (see Figure 16f). X-ray diffraction (XRD) results revealed less variance in peak positions/intensities between fresh and aged samples indicating a higher stability. This aligned with previous findings where enhanced ambient stability was observed using single-crystal perovskite powders.[223] The higher stability was attributed to superior crystallinity, resulting in strong ionic interactions within the crystal lattices. Compared with the original precursor, an average PCE of the PSCs fabricated with powder-based precursor increased from 15.58% to 18.07% due to improved absorption and better morphology.

Xu et al.[224] reported a PbI_2–$(CsI)_{0.15}$–$(FAI)_x$ intermediate assisted two-step spin-coating method combined with the substrate annealing strategy. The $Cs_{0.15}FA_{0.85}PbI_3$ based PSCs were fabricated under 70 ± 10% RH and achieved a best PCE of 15.56% at $x = 0.3$. In the first step of spin-coating, the precursor solution of PbI_2, cesium Iodide (CsI) and FAI was heated to 80 °C and deposited on a hot substrate (80 °C) to form the intermediate complex. In the second step, FAI was spin-coated on top of the intermediate complex to absorb moisture due

© 2020 The Authors. Published by Wiley-VCH GmbH

to its hygroscopic property. Thus, the detrimental effect from the ambient environment can be suppressed by the FAI and annealed substrate.

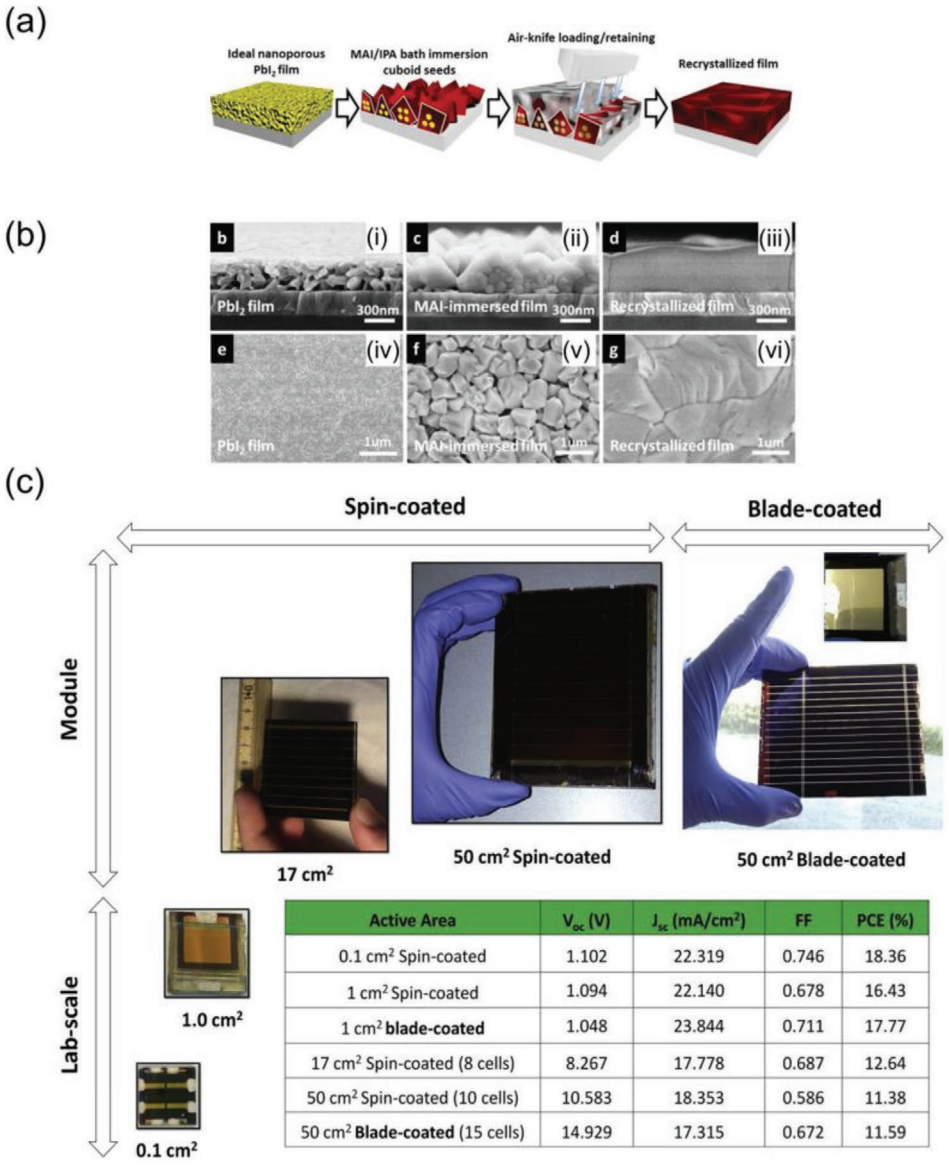
Methylammonium acetate (MAAc), a molten salt, was used as the solvent for perovskite precursor solution and PSCs fabricated under 80% RH achieved a high average PCE of 18.42%.[225] Similar to the preheating treatment, the perovskite film was deposited by spin-coating the perovskite precursor on the substrate which was kept at 100 °C. It was proposed that the solvent MAAc can promote the crystallization of the perovskite as a media and protect the perovskite from humidity for its high viscosity. The PSC devices fabricated by this method also showed excellent long-term stability, retaining 93% of its original PCE after 1000 h exposure under ambient air.

Bath immersion or dipping methods immerse (or dip) a Pb-halide film in a FAI/MAI precursor solution as a method for deposition. This method is a potential strategy to reduce the impact from environmental moisture as the growth of the perovskite film is processed in the solution.[47,226,227] A secondary crystal growth method was reported to fabricate PSCs under ambient conditions (<40% RH).[226] The PbI_2 film was first dipped into the MAI solution at room temperature to form the intermediate perovskite film. After rinsing with IPA, the film was placed at room temperature for 5 min. The intermediate film was again dipped into the MAI solution at 50 °C (secondary crystal growth) for the conversion into perovskite. Finally, the film was dried by spin-coating and annealing. The PSCs with compact and pinhole-free perovskite film obtained the highest PCE of 17.3% and had enhanced environmental stability. An aqueous lead nitrate ($Pb(NO_3)_2$) precursor was used to fabricate flexible PSCs under ambient conditions.[228] The aqueous $Pb(NO_3)_2$ solution was deposited on the substrate by spin-coating, then immersed into the MAI/FAI solution (with IPA as the solvent) to form the perovskite film. The $Pb(NO_3)_2$ residues in the film can act as a water scavenger to help slow the moisture induced decomposition of the perovskite. The best PSCs fabricated under ambient condition with the composition of $FA_{0.1}MA_{0.9}PbI_{0.9}Br_{0.1}$ achieved a PCE of 16.50% (RH N/A).

Similar to the bath immersion method, Cheng et al.[227] used DMSO in a PbI_2 precursor solution and an air knife-assisted recrystallization strategy to improve the film morphology to further complete the perovskite conversion. To form the perovskite layer, the PbI_2 film was dipped into the MAI/IPA solution, however two problems occurred during the immersion process: 1) If the immersion time was too short, a compact perovskite layer can form on the PbI_2 film, which slowed the diffusion of MAI and resulted in incomplete conversion;[175] 2) If the immersion time was prolonged, the conversion can be fully completed, but the slow crystallization and/or recrystallization can result in perovskite film with small grain size. The air knife-assisted recrystallization strategy was to use a strong and ultrathin wind to blow the immersed film. As shown in **Figure 17**a, the air flow can remove the extra MAI solution and retain MAI in the gaps of the perovskite grains. A compact perovskite film was obtained for the completed conversion of loaded MAI and residual PbI_2 and the recrystallization of rough perovskite cuboids is shown in the SEM images in Figure 17b. Impressively, all PSCs fabricated under 20–60% RH obtained over 19% PCE, and the PCE of the best device fabricated under 60% RH reached 19.39%. Nia et al.[229] used a crystal engineering approach in the first step and combined it with the bath immersion method to fabricate perovskite films under ambient conditions. Through spin-coating hot and supersaturated Pb/Cs halide solution (75 °C) on the heated substrate (50 °C), a compact and mesoporous crystalline intermediate film of $PbX_2 \cdot 2DMSO$ was formed. Dipping the intermediate film into an anhydrous IPA solution of FAI/methylammonium bromide (MABr), resulted in an increase of perovskite nuclei (dense nuclei) aiding crystal growth. For complete crystal growth (full surface coverage), the duration of the dipping time had a strong correlation with the humidity in the atmosphere. The higher the humidity, the longer the dipping time and this demonstrated that moisture can have a positive effect on crystal growth. The authors suggested that moisture could accumulate in the grain boundaries of the perovskite film, inducing grain boundary creep and merging the adjacent grains together, thus resulting in full surface coverage. The best device using this method fabricated under 50–75% RH achieved a PCE of 18.4% for 0.1 cm^2 active area, and 16.5% for 1 cm^2 active area, respectively. Subsequently, this method was also applied using the doctor-blading method, and PSCs with an active area of 1 and 50 cm^2 achieved a PCE of 17.8% and 11.6%, respectively. Figure 17c shows the scaling up procedures from small area to large area PSCs, including modules and both spin-coated and blade-coated approaches.

Zhang et al.[62] recently suggested that water could promote the formation of lead complexes, which must be controlled to prevent unfavorable and discontinuous perovskite films. This was done in ambient air by obtaining a dense supply of intermediate nuclei using a prenucleation strategy. They demonstrated that water can induce fast intermediate crystallite growth, suggesting that the concentrations of the lead complexes must be controlled (i.e., the prenucleation clusters) by controlling the solute concentration. The process involved spinning first a wet film at a low spin speed (1000 rpm), followed by a high spin speed of 6000 rpm to form a high concentration of prenucleation clusters to drive the system across the nucleation threshold. Anti-solvent was then dripped multiple times on the wet film to extract solvent in a programmed fashion, keeping the prenucleation cluster concentration above the nucleation threshold. Both the spin-coating and antisolvent treatment process is outlined in **Figure 18**a, where the prenucleation scheme is detailed in Figure 18b. Both the proposed nucleation system and comparison between conventional and prenucleation methods are shown in Figure 18c–f. Specifically, SEM images of the intermediate films prior to annealing and perovskite films after annealing using the conventional method are shown in Figure 18c,d respectively. Figure 18e,f shows the SEM images of the intermediate/perovskite film after ageing without annealing and perovskite films after annealing using the prenucleation method, respectively. The XRD comparison between the conventional and prenucleation method is shown in Figure 18g,h, respectively. Clearly, the prenucleation approach (even without annealing) showed much smoother and compact films where the XRD showed the film was mainly made of perovskite with few intermediate phases. Figure 18i illustrates the spin-coating conditions/dripping time between both the conventional and prenucleation method. Following the prenucleation method in an ambient atmosphere of 40% RH, the best PSC with an efficiency of 19.5% was obtained.

© 2020 The Authors. Published by Wiley-VCH GmbH



Active Area	V_{oc} (V)	J_{sc} (mA/cm^2)	FF	PCE (%)
0.1 cm^2 Spin-coated	1.102	22.319	0.746	18.36
1 cm^2 Spin-coated	1.094	22.140	0.678	16.43
1 cm^2 **blade-coated**	1.048	23.844	0.711	17.77
17 cm^2 Spin-coated (8 cells)	8.267	17.778	0.687	12.64
50 cm^2 Spin-coated (10 cells)	10.583	18.353	0.586	11.38
50 cm^2 **Blade-coated** (15 cells)	14.929	17.315	0.672	11.59

Figure 17. a) Schematic of the air-knife recrystallization strategy used to prepare the perovskite film with micrometer-sized single-layer grain morphology. b) Cross-sectional and top-view SEM images at different fabrication stages of the perovskite film: i,iv) PbI_2 films coated in air giving a nanopore-network connectivity, ii,v) MAI-immersed perovskite films after bath-immersion showing uniform perovskite cuboid seeds, and iii,vi) the recrystallized smooth perovskite films with single-layer grain morphology, respectively. Reproduced with permission.[227] Copyright 2019, Wiley-VCH GmbH. c) Scaling-up procedure from lab-scale small areas to large area PSCs and modules. Spin-coated PSCs and modules are shown along with fully blade-coated large area modules. PV parameters of the best devices are also shown. Reproduced with permission.[229] Copyright 2020, Elsevier.

A new perovskite precursor system which included HCOOCs, $HPbI_3$, and $HPbBr_3$ was used to fabricate inorganic PSCs ($CsPbI_2Br$).[230] This new system provided a platform for high moisture-resistivity and the ability to fabricate perovskite films with an anti-solvent. A metastable complex $HCOOH \cdot Cs^+$ can be obtained where the formation of the perovskite crystal was delayed under ambient conditions and the deposited film was protected from moisture, even under a high RH of 91%. During the spin-coating process at an elevated temperature (50 °C), the intermediate $HCOOH \cdot Cs^+$–PbI_3^- was formed and released HCOOH in the forward annealing process (10 min at 60 °C and 10 min at 250 °C). Due to the energy barrier of decomposition of $HCOOH \cdot Cs^+$-PbI_3^-, the growth of nuclei dominated the crystallization process, resulting in high-quality perovskite film with compact morphology and large grain size. Finally, the best PSCs fabricated under low humidity (30% RH, 25 °C) and high humidity (91% RH, 36 °C) environments achieved PCEs of 16.14% and 15.11%, respectively.

A large variety of ambient fabrication methods for high efficiency PSCs have been developed. This section outlines a clear example of the different techniques being applied to ambient fabrication, where a variety of previously highlighted methods are also included and modified. Not surprisingly, the approaches which produce PSCs with the highest efficiency

© 2020 The Authors. Published by Wiley-VCH GmbH

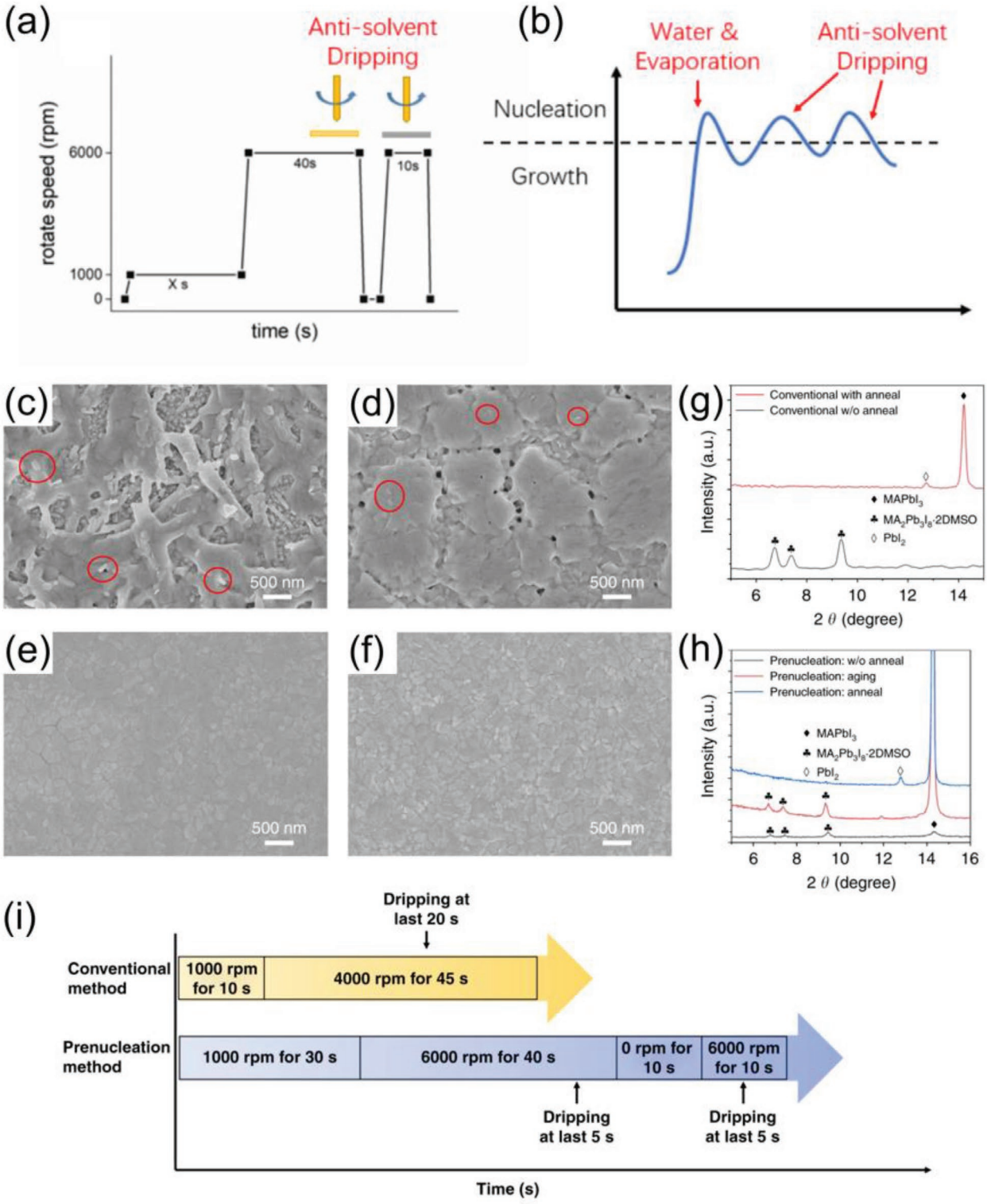


Figure 18. a) The spinning process with programmed antisolvent dripping at two set time intervals. b) Diagrammatic representation of prenucleation scheme for nucleation and growth at the water and evaporation stage and anti-solvent dripping stages. SEM images of films synthesized in ambient conditions at 40% RH of c) the intermediate film without annealing, d) perovskite film after annealing (98 °C, 7 min) using conventional method, e) intermediate/perovskite film after aging and without annealing, and f) perovskite films after annealing (98 °C, 7 min) using the prenucleation method. g) XRD of intermediate (black curve) and the perovskite film (red) synthesized via conventional method. h) XRD of intermediate (black curve), aged intermediate (red curve) and perovskite film (blue curve) synthesized via prenucleation method. i) Comparison of conventional and prenucleation method. Reproduced with permission.[62] Copyright 2020, Nature Publishing Group.

© 2020 The Authors. Published by Wiley-VCH GmbH

require several steps. These several steps provide an excellent platform to both protect the perovskite from moisture and better control the nucleation of the perovskite layer. The two most promising approaches are introduced by Cheng et al.[227] and Zhang et al.[62] where the former uses a bath immersion method and the latter uses multiple spin-coating steps. Importantly, both of these approaches emphasize the importance of complete perovskite crystallization using either assist air-knife techniques, or solvent evaporation control. With a large processing window of humidity (20–60% RH), the approach by Cheng et al. obtained PSCs with PCEs over 19%. The approach by Zhang et al. obtained a PCE of 18.8% at a moderate RH of 40%. This demonstrates that a variety of processing techniques can result in high performance PSCs with good resistance to RH.

4. Charge Transport Layers in Ambient PSCs

Upon illumination, free electrons and holes are photogenerated in the perovskite material where carriers are then selectively directed to their respective electrodes via charge transport layers (CTLs). In PSCs, the perovskite absorber layer is sandwiched between the respective CTLs, meaning both the ETL and HTL play an important role when fabricating PSCs in ambient conditions. This section will discuss the commonly used CTLs, their interface engineering with perovskite layer and the impacts that they can have on an ambient environment. Finally, we summarize the best combination of CTLs when fabricating PSCs in ambient conditions.

4.1. Electron Transport Layer

In n–i–p PSCs, the ETL is typically made up of air-stable metal oxides such as TiO_2 or SnO_2, since they are still the front runners for the highest efficiency PSCs. Metal oxides are typically fabricated in ambient conditions using simple annealing procedures. Oxygen has been shown to fill oxygen vacancies on the surface of TiO_2 or SnO_2, either during the annealing process or upon oxygen plasma treatment which can be beneficial for the operation of PSCs.[231–233] Despite this, ZnO has often been introduced as an alternative metal oxide ETL due to its low processing temperature[170] and high electron mobility.[234] Unlike TiO_2 and SnO_2, ZnO has been found to have undesirable side effects with $MAPbI_3$ where the nature of the ZnO surface leads to proton-transfer reactions at the ZnO/$MAPbI_3$ interface. The proton-transfer reactions result in decomposition of the perovskite film, which is driven by deprotonation of methylammonium, leading to a loss of methylamine and the formation of PbI_2.[235] Yang et al.[235] discussed how this decomposition process is accelerated by surface hydroxyl groups and/or residual acetate ligands but can be reduced by high calcination temperatures. It is therefore clear that the functional groups on ZnO play a crucial role in the formation of the perovskite layer, which is important for ambient fabrication. Guo et al.[236] demonstrated a facile aging step for a ZnO film to enhance the moisture stability and achieved 9.4% PCE. Before depositing the PbI_2 solution in the two-step spin-coating method, the ZnO film was aged at room temperature for 24 h in ambient air to improve the quality of ZnO film and reduce the hydroxyl groups and/or residual acetate ligands. In 2018, the aging method was further developed by using ultrasonication treated ZnO NPs and operated the fabrication under 50% RH.[237] The ZnO solution treated by ultrasonication was more transparent and formed a smoother film. The reduction of hydroxyl groups and residual acetate ligands increased the hydrophobicity of ZnO film, which suppressed the adsorption of moisture and enhanced the perovskite film stability. The highest PCE also increased from 9.4% to 14.25% with the improved method. Some other examples of ZnO have already been discussed in the solvent engineering section (Section 3.2)

In p–i–n PSCs, the two most common ETLs are phenyl-C61-butyric acid methyl ester (PCBM)[238] and C_{60},[239] where PCBM is solution processable and C_{60} is usually thermally evaporated on top of the perovskite absorber layer. Although fullerene derivatives such as PCBM have been shown to be sensitive to both UV and visible light in an inert atmosphere, they have also been shown to undergo photo-oxidation,[240] where the combination of oxygen and light can form epoxide and carbonyl species on the fullerene cage.[241,242] Early work on organic photovoltaics (OPV) devices discusses how epoxide and carbonyl species can broaden the lowest unoccupied molecular orbital (LUMO) energies around an energy close to the LUMO of pristine PCBM, as well as form deeper electron traps.[243] Thus, the overall density of defect states will increase due to the presence of electron traps. Other work also confirms that oxygen exposure changes the electron structure of fullerenes,[244] which impacts device performance.[245] This therefore suggests that fullerenes that undergo epoxide formation may not be the ideal candidate for ambient device processing. Although this is shown on OPV devices, such limitations are not so dissimilar from PSCs. One limitation of fullerenes in PSCs is that the optimal deposition thickness is thin meaning that it does not form a good protective layer for the underlying perovskite material from moisture in a humid environment. Previous work by Bai et al.[246] has shown that by incorporating a crosslinkable silane-modified fullerene layer, water and moisture stability can be improved by retaining 90% of their original efficiencies after 30 days exposure in an ambient environment. Modifying the perovskite/PCBM interface is a common strategy to improve the operation of PSCs in ambient conditions,[247] however a majority of the literature fabricates the perovskite layer in a nitrogen filled glovebox. Despite this, it is clear that fullerene-based materials have their limitations, especially when used in an ambient atmosphere. This has resulted in the incorporation of additional bilayer/buffer layers on top of PCBM,[238,239,248,249] doping PCBM with inorganic materials,[250] or replacing the fullerene-based materials with ZnO NPs (dispersed in CB),[251] for improved performance and/or stability in ambient conditions. Notably, p–i–n devices using PCBM almost always contain a bilayer ETL (e.g., PCBM/TiO_x, PCBM/ZnO, or PCBM/bathocuproine, BCP) due to the Schottky barrier-type contact between PCBM and metal contact. An additional layer such as TiO_x, promotes efficient electron collection,[44] thus preventing an energy barrier which would otherwise result in the undesirable "s" shape *J–V* curve (attributed to diffusion driven charges against the electric field).[252–255] Despite the high performance

© 2020 The Authors. Published by Wiley-VCH GmbH

of fullerene-based materials, it is clear that their undesirable oxidation can be detrimental to ambient PSCs, meaning that the use of metal oxide transporting layers would be a more favorable alternative for ambient PSC fabrication.

4.2. Hole Transport Layer

For n–i–p PSCs, HTLs such as 2,2′,7,7′-Tetrakis[*N*,*N*-di(4-methoxyphenyl)amino]-9,9′-spirobifluorene (Spiro-OMeTAD) or poly[bis(4-phenyl)(2,4,6-trimethylphenyl)amine (PTAA) with additives bis-(trifluoromethane) sulfonimide lithium salt (Li-TFSI) and tBP are deposited on top of the perovskite layer. Such additives are essential to obtain high hole mobility and conductivity.[256] Since Li-TFSi is hydroscopic, additive solutions as well as both Spiro-OMeTAD and PTAA are typically prepared in a glovebox to reduce risk of moisture reaching the underlying perovskite layer. Cobalt complexes, such as Tris[2-((1*H*-pyrazol-1-yl)-4-*tert*-butylpyridine) cobalt(III) tris(bis(trifluoromethylsulfonyl)imide)] (FK209), a less hygroscopic dopant, have also been used as an additive in Spiro-OMeTAD. The addition of cobalt complex (FK209) has been found to work well with Li-TFSI/tBP by providing reduced carrier recombination and a lower Fermi level of the Spiro-OMeTAD, resulting in higher open circuit voltages.[257] Notably, **Figure 19**a,b shows the effect of leaving both Li-TFSI and cobalt complex (FK209) in ambient conditions from 1 min to 3 h, indicating that Li-TFSI is much more hydroscopic than the cobalt complex.[258] Furthermore, devices with Spiro-OMeTAD require an overnight oxidation step in a dry box to enable complete oxidation, resulting in PSCs with higher fill factors.[259] Wang et al.[260] reported that the conductivity of Li-TFSI doped Spiro-OMeTAD can be improved through oxidation when exposed to oxygen and light. Also, Hawash et al.[261] demonstrated that the water vapor from air can induce the redistribution of Li-TFSI, which further enhanced the conductivity. Therefore, although ambient conditions can be utilized in the oxidation step, processing hole transport material (HTMs) with hydroscopic additives like Li-TFSI in humid environments will undoubtedly cause moisture to find its way into the underlying perovskite layer. Such examples indicate that handling such HTMs under uncontrolled environments can be detrimental to device performance.

Another promising HTL for n–i–p PSCs is poly(3-hexylthiophene) (P3HT) due to it not requiring doping, improving the overall stability of the devices. Despite this, the resulting PSCs typically have low open-circuit voltages due to additional non-radiative recombination at the perovskite/P3HT interface.[262] Until recently, the only high efficiency PSCs using P3HT have been obtained using interface engineering and the devices were prepared in a nitrogen filled glovebox.[263] Compared with poly(3-hexyl thiophene) (P3HT), PSCs using poly(3-thiophene acetic acid) (P3TAA) as the HTL obtained more favorable performance under ambient fabrication conditions. In work by Shit et al.,[264] the PCE of PSCs fabricated under 32 °C and 62% RH increased from 5.85% (P3HT) to 7.38% (P3TAA). The improved PCE was attributed to the −COOH group of P3TAA, which can interact with the lone pair of the nitrogen atom of the NH_3 group from $MAPbI_3$. This led to the interface between the perovskite and HTM becoming more diffused, resulting in the easier injection of holes to P3TAA and the promotion of carrier transport.

In n–i–p PSCs, HTMs which do not require hydroscopic additives or further oxidation steps are preferential for the ambient fabrication of PSCs. For example, triple-layer architectures which incorporate only an ETL, perovskite absorber and carbon layer are promising options for ambient processed PSCs.[265] Mei et al.[57] first proposed a hole-conductor and metal electrode free, fully printable mesoscopic PSCs with a high stability in 2014 and other interesting work has since followed.[266–269] Eliminating the metal electrode is another selling point which prevents migration of metal ions into the perovskite, aiding long term stability by preventing the formation of metal iodides (e.g., AgI or CuI).[270] The HTL-free PSCs with a carbon electrode also attract considerable attention for its high water resistance and improved ambient stability.[57] This work has also been followed by incorporating PSCs fabricated entirely under ambient conditions using triple cation mesoscopic devices. Zhou et al.[271] reported an efficient all-air processed mixed-cation carbon-based PSC which incorporated multiwalled carbon nanotubes (MWCNTs) into the perovskite. The hydrophobic MWCNTs were introduced to mediate the crystallization of the perovskite and prevent erosion by moisture of the perovskite layer. The authors compared

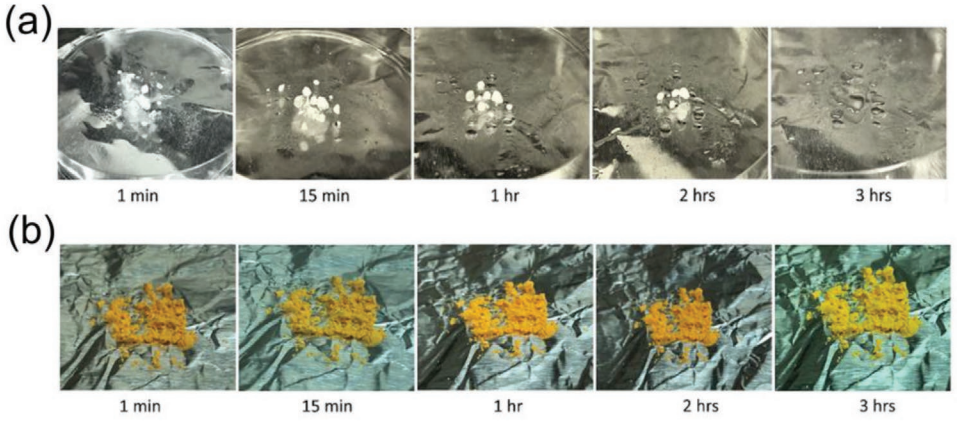


Figure 19. a) Li-TFSI left under ambient conditions (36% RH). b) FK209 left at ambient conditions (36% RH). Reproduced with permission.[258] Copyright 2018, The Institute of Electrical and Electronics Engineers.

© 2020 The Authors. Published by Wiley-VCH GmbH

both 0.5 and 1 wt% MWCNT incorporation and showed that 0.5 wt% is superior for device performance. The incorporation of MWCNTs is shown with SEM and atomic force microscopy (AFM) in **Figure 20**a. The authors reported the device architecture of indium tin oxide (ITO)/SnO_2/perovskite/carbon, which is shown in Figure 20b. The PSCs were fabricated under ambient air conditions and obtained a highest PCE of 16.25% (0.08 cm^2) and 12.34% (1 cm^2). The PSC *J*–*V* curves are shown in Figure 20c, which also highlights the performance for the different wt% of MWCNTs used. Liu et al.[272] incorporated Cs into the perovskite to improve the performance of ambient processed HTM-free carbon-based PSCs where the device schematic is shown in Figure 20d. The authors showed that the incorporation of Cs resulted in a perovskite film with a homogeneous surface and larger grain size as shown in the SEM images in Figure 20e. The work resulted in triple cation

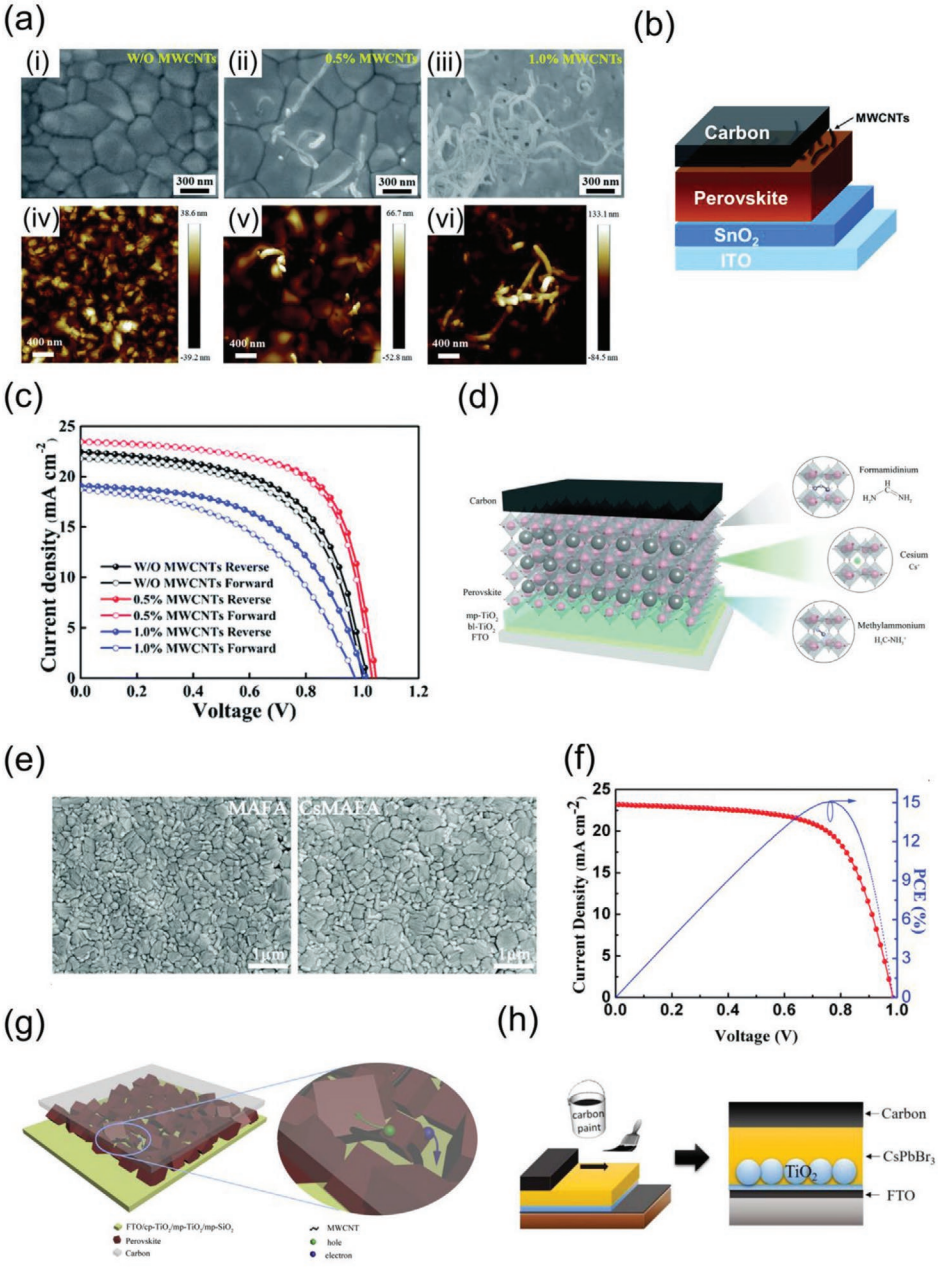


Figure 20. a-i–iii) SEM images and their corresponding iv–i) AFM images of perovskite films with/without MTCNTs. b) The device structure of HTM-free carbon-based PSCs. c) *J*–*V* curve of PSCs with/without MTCNTs. Reproduced with permission.[271] Copyright 2019, The Royal Society of Chemistry. d) The configuration of Cs incorporated into triple cation PSCs. e) SEM morphology of MAFA and CsMAFA PSCs. f) *J*–*V* curve of the best PSC devices with 5% Cs incorporation at a scan rate of 50 mV s^{-1}. Reproduced with permission.[272] Copyright 2019, The Royal Society of Chemistry. g) Schematic of PSC where MWCNTs can provide an electrical highway for charge transport. Reproduced with permission.[273] Copyright 2016, Elsevier. h) Illustration of carbon paint used as top electrode in PSCs without any other additional HTM. Reproduced with permission.[275] Copyright 2016, American Chemical Society.

© 2020 The Authors. Published by Wiley-VCH GmbH

devices fabricated under 50% RH with a best efficiency of 15.06% (see Figure 20f) with superior stability. Cheng et al.[273] demonstrated a HTL-free PSC using MWCNTs as charge transport channel and a carbon electrode. The PSC was fabricated under more than 50% RH and achieved an average PCE of 11.6% which was 15% higher than the HTL-free PSC without MWCNTs. As illustrated in Figure 20g, the authors reported that the MWCNTs will act as an electrical highway for charge transport between individual perovskite NPs, facilitating the hole collection efficiency of the perovskite/MWCNT interface. Papadatos et al.[274] fabricated a HTM-free PSC using a methylammonium/5-aminovaleric acid/phenethylammonium iodide lead perovskite. The HTM-free PSCs utilized a carbon electrode where all processes were conducted under RH of 40 – 60%, achieving an efficiency of 7.11%. Chang et al.[275] fabricated an inorganic $CsPbBr_3$ carbon-based PSCs under 30–50% RH and obtained a PCE of 5%, which was relatively high for early work on fully inorganic PSCs. The carbon ink was directly painted onto the perovskite film as shown in Figure 20h. The authors reported that after 250 h of storage at 80 °C, an 11.7% loss in PCE was observed. Clearly, replacing Spiro-OMeTAD or PTAA (which both require dopants) with carbon is a promising route to fabricate ambient PSCs. While other approaches using copper-based materials have been proposed in both nitrogen[276–278] and ambient[279] conditions, using carbon also replaces the need for the metal top electrode, further benefiting the long-term stability of the PSCs.

In p–i–n PSCs, one of the first materials used as a HTL was PEDOT:PSS.[239] However, PEDOT:PSS is known to undergo irreversible structural modification under ambient conditions when exposed to oxygen and moisture, where its hydroscopic character allows water to diffuse from the PEDOT:PSS through to the metal contacts, reducing the lifetime of the device.[280,281] Other work has also discussed how the gas permeability of PEDOT:PSS allows oxygen to diffuse through, which when combined with light, can quickly decrease the short-circuit current.[282] PEDOT:PSS is also acidic, which can lead to the corrosion at both the ITO and perovskite interface, further limiting stability of ambient PSCs.[283–285] Also, most PSCs employing PEDOT:PSS exhibit considerably lower open-circuit voltages and short-circuit currents, and this has been attributed to the large energy barrier between the PEDOT:PSS and perovskite.[286] To mitigate the poor stability and large energy barrier (high work function) of PSCs using PEDOT:PSS, poly[*N*,*N*′-bis(4-butylphenyl)-*N*,*N*′-bis(phenyl)benzidine] (poly-TPD)[287,288] and poly(triaryl amine) (PTAA)[286,289] have been introduced due to their sustainability to DMF and lower energy barrier. Although poly-TPD and PTAA have poor wetting, Wang et al.[290] suggested this to be beneficial for the nucleation of large grain perovskites. This was attributed to the lower nucleus density and dragging force, leading to large grain growth of the perovskite, which suppressed grain boundary traps and enhanced the PSC efficiency. Interestingly, Cheng et al.[60] reported that oxygen can reduce the wetting of the PbI_2 precursor solution used in the two-step spin-coating method on hydrophobic organic HTLs (including poly-TPD and PTAA). The wetting was however improved in a nitrogen environment meaning that oxygen can impact the final quality of the perovskite film. As previously discussed, Wang et al.[290] described how poor wetting can drive high aspect ratio crystalline grains for highly efficient PSCs, however it is important to note that if wetting is too poor, then insufficient coverage will result in poor PSC performance. This essentially means that that while poor wetting has shown to be favorable for large crystal growth, some degree of wetting is required in order to obtain a sufficient coverage of the perovskite film.

Although the poly(triaryl amine)-based polymers are air stable,[291–293] have favorably high water-contact angels,[290] and can produce high efficiency PSCs,[36,123] their complex synthesis and high cost is still a limiting factor. In contrast, nickel oxide (NiO) is an alternative HTM which retains high chemical stability, hole mobility, low cost, and is simple to synthesize.[294] Tavakoli et al.[295] fabricated p–i–n NiO-based PSCs using a double-cation Cs/FA perovskite absorber layer which was processed in 40% RH. They showed how the grain size, crystallinity, and carrier lifetime of the perovskite films are significantly enhanced due to the humidity. In addition, they employed a thin layer of cadmium-based quantum dots on the back of the device to convert UV-light to visible wavelengths, where the best PSC obtained an efficiency of 20.7%. Finally, while promising developments have been made with high efficiency p–i–n HTM free PSCs,[62,296,297] most of the proposed methods require a nitrogen filled glovebox for the deposition of the perovskite layer.

4.3. CTL Interface Engineering

Two major challenges in PSCs is the poor stability of the perovskite film and chemical incompatibilities of the perovskite layer with the charge transport layers (CTLs).[298] Since the active perovskite layer is sandwiched between two CTLs, an interface forms between the CTL and perovskite layer. Ever since early work showed that perovskite could transport electrons[16] and holes,[17] interface engineering has become a very popular strategy in optimizing the stability and performance of PSCs. Over the past decade it has become apparent that interfaces need to be carefully engineered since they can act as nonradiative recombination centers which can degrade the PSC and restrict the efficiency. Therefore, interface engineering has shown to be a promising strategy to reduce defect-related losses in materials and/or interfaces, where such interface engineering plays a critical role in the ambient fabrication of PSCs. Here, we briefly discuss some appropriate interfacial materials which can enhance both moisture stability and device performance for the ambient fabrication of PSCs.[299]

Zhang et al.[300] introduced an ionic liquid, 1-ethyl-3-methylimidazolium hexafluorophosphate ($[EMIM]PF_6$), modification layer between the perovskite layer and ZnO ETL. The PSCs fabricated under 47.5% RH obtained a highest PCE of 13.5%. The interface layer was formed by spin-coating $[EMIM]PF_6$ on the ZnO layer. The ZnO film modified by $[EMIM]PF_6$ was less rough, which helped the formation of the high-quality perovskite film. As an ionic liquid, the hydrophilicity of $[EMIM]PF_6$ can spread the PbI_2 on the modified ZnO film, further improving the perovskite film. The high stability and reduced hysteresis was attributed to the inhibited ion migration and charge accumulation at the perovskite/ETL interface. The addition

© 2020 The Authors. Published by Wiley-VCH GmbH

of the ionic liquid at the interface layer enables passivation of the underlying ZnO ETL, improving the highest PCE from 10.08% to 13.5% and providing enhanced long-term stability. Zhai et al.[113] anchored dopamine molecules to TiO_2 nanocrystals to modify the ETL. In the two-step spin-coating method, the PbI_2 precursor which was deposited on dopamine-modified TiO_2 (DA-TiO_2) ETL obtained a mesoporous structure, leading to the easier penetration of MAI. PSCs using this method fabricated under 50% RH achieved an average PCE of 16.36% with suppressed hysteresis. Jiang et al.[120] used phenethylammonium iodide (PEAI) interface to passivate the perovskite, which reduced the roughness of the perovskite and suppressed the surface defects. After deposition of the perovskite, PEAI was directly spin-coated onto the fabricated perovskite film without an annealing process. The best PSC fabricated under 30–40% RH achieved 23.32% PCE, which is the highest efficiency ever reported for ambient fabrication. Notably, it was also found that this PEAI thin layer can transfer to PEA_2PbI_4 under elevated temperature, resulting in the quick decrease of PCE (a loss of about 15% of the original PCE in a few h under 85°C)

While small molecules or organic semiconductors have been shown to produce highly efficient PSCs in both n–i–p and p–i–n architectures, high cost and adaptability to ambient fabrication are somewhat limited. Therefore, in order to optimize stability, maintain low fabrication cost, and produce high efficiency PSCs, metal oxide CTLs without additives or dopants are the most promising routes. In addition to metal oxides, carbon-based top contacts which effectively replace the HTM and top electrode, are promising routes to complement the ambient fabrication of PSCs. Therefore, for n–i–p PSCs, ETLs such as TiO_2 or SnO_2 should be used and combined with either carbon-based or copper-based HTMs when fabricating PSCs in ambient conditions. While PTAA is clearly one of the best HTMs for p–i–n PSCs, its high cost and complex synthesis are reasons to suggest NiO as a great alternative when fabricating p–i–n PSCs in ambient conditions. NiO is also a highly stable and robust material, which suggests better long-term stability than its organic counterparts. While in some instances it may be difficult to avoid fullerene-based ETLs in p–i–n PSCs, ZnO NPs are a promising candidate which can either replace organics and/or be used in combination with PCBM (i.e., PCBM/ZnO). Engineering the interfaces between the perovskite absorber layer has been shown to be critical to optimizing the fabrication of PSCs in ambient conditions. Careful interface engineering can modify the underlying layer and prevent ion migration which in combination with preventing moisture and oxygen,[299] undoubtedly improves the performance and long-term stability of PSCs fabricated in ambient conditions.[264] Thus far, PEAI-based PSCs as reported by Jiang et al. in 2019, hold the record for the highest efficiency PSCs fabricated under ambient conditions (30–40% RH).[120]

5. Conclusion and Future Perspectives

This review has summarized the effect of an ambient fabrication environment on the perovskite film and various strategies to fabricate PSCs under ambient conditions. As highlighted in this review, fabricating perovskite films under ambient conditions has both positive and negative effects. High humidity during fabrication can be detrimental to the perovskite film by causing pinholes, increased surface roughness, poor morphology, and thus lead to degradation. Water, oxygen, light, and elevated temperatures in ambient conditions can all induce and accelerate the decomposition of perovskite films. Although no final conclusion has been drawn on the exact mechanism of degradation (aside from the formation of undesirable PbI_2), there is no doubt that products of perovskite decomposition bring impurities to the perovskite layer, strongly affecting the microstructure of the film and causing a significant decrease in device performance. In some cases, moisture was demonstrated to have positive effects on the perovskite film, but this was typically only achieved with low/medium humidity. While low/medium humidity improved the grain size of the perovskite crystal, high humidity promoted the decomposition of perovskite to PbI_2. Where high humidity is unavoidable, it is recommended that the preheating method is used, which accelerates the vaporization of solvents and promotes the crystallization of the perovskite film. Preheating the substrate was also found to reduce the humidity sensitivity of the antisolvent, promoting the critical free energy of nucleation. Remarkably, PSCs fabricated under 90% RH were able to achieve a PCE of 19.5%, which is the highest ever reported for such high humidity.[98] Furthermore, the preheating method was shown to produce high efficiency PSCs in both low and high humidity conditions, indicating the versatility of this approach. Additive engineering, solvent engineering and hot air/vapor assisted deposition were also shown to be successful methods to fabricate high efficiency PSCs in high humidity.

While an inert environment may be preferential for the fabrication of the highest efficiency PSCs, recent progress discussed in this review shows that there have been significant developments fabricating PSCs outside of a glovebox, delivering PCEs over 20%. In order to achieve better quality perovskite films and deliver the highest efficiency PSCs in an ambient environment, methods like additive engineering, solvent engineering, composition engineering, interface engineering, preheating methods, and others should be adopted. Given the diversity of the approaches which can be selected to fabricate high efficiency PSCs in an ambient atmosphere, the following points summarize key findings which are recommended to be adopted for the ambient fabrication of PSCs:

i) For n–i–p PSCs, metal oxides should be selected as preferential ETLs. For example, SnO_2 spin-coated from a NP suspension provides the highest efficiencies.[120] While Spiro-OMeTAD and PTAA have been shown to provide the highest efficiency as HTLs in n–i–p PSCs, their necessary hygroscopic dopants remains a challenge. Alternatives such as carbon pastes or dopant free inorganic materials do not achieve as high efficiencies, however, should be considered as a favorable approach to ambient fabrication and stability.
ii) For p–i–n PSCs, PTAA is recommended as the HTL since it is stable in ambient conditions, requires no doping and provides high efficiency. Although publications using PTAA in ambient PSCs are lacking, there is no reason it should be not utilized. As a cheaper alternative, NiO could also be used as it has shown to provide efficiencies of over 20% at a RH of 40%.[295] For the ETL, ZnO NPs (in CB) is recommended as the ETL.

© 2020 The Authors. Published by Wiley-VCH GmbH

iii) Mixed-cation perovskites show enhanced stability and promising PCE when fabricated under ambient conditions. Specifically, $FA_{1-x}MA_xPbI_3$ PSCs with PEAI (interface engineering) post-treatment achieved a high initial PCE of 23.32% at 30–40% RH.[120] In addition, mixed-cation mixed-halide $Cs_{0.05}(MA_{0.17}FA_{0.83})_{0.95}Pb(I_{0.83}Br_{0.17})_3$ based PSCs obtained a PCE of 20.8%, and preserved a high efficiency (19.5% PCE) after 18 weeks under 20–35% RH.[138] Therefore, mixed perovskites are recommended when fabricating PSCs in ambient conditions and any further studies should focus more on the utilization of this composition considering the excellent stability and performance.

iv) Suitable antisolvents in the fabrication process enables the formation of high-quality perovskite films under ambient conditions. In the one-step spin-coating method, antisolvents can reduce the solubility of the perovskite in other solvents and accelerate its nucleation due to supersaturation, where EtOAc was shown to provide the highest PCEs (>17%) in ambient conditions under medium humidity (30-40% RH).[166] In the case of higher humidity (60–70% RH), MeOAc has been shown to be the best option producing a PCE of 16.3%.[164] In the two-step spin-coating method, IPA should be used to solubilize cationic salts since it provides the least harmful effects to the underlying PbI_2 layer.[172] Screening other solvents and their mixtures as an antisolvent for ambient PSC fabrication is still an important direction for future research investigation.

v) Additive engineering provides a simple approach to modify the precursor solution, which coordinates with the composition of the perovskite, enhancing film crystallization and final device stability. In the one-step spin-coating method, the most promising additive used in ambient fabrication is 2-pyridylthiourea which promotes excellent film morphology and device stability where at RH between 50–60%, PSCs can obtain PCEs over 18%.[29] For the two-step spin-coating method, the addition of BTA[143] or ZnO NP[112] additives produced PSCs with PCEs of 17.56% and 18.34%, respectively, at a RH of 60%. Additive engineering is a strategy which remains very promising and given there are so many unexplored additives, this strategy is effectively in its infancy. Future work exploiting halide additives (particularly chlorides) or amino acid additives with different alkyl chain lengths would be beneficial for the future development of this strategy.

vi) Preheating the substrate prior to perovskite deposition was frequently reported to improve the quality of the perovskite film, thus the efficiency of PSCs. Preheating was found to have positive effects on nucleation and reduce the sensitivity of antisolvents. It is therefore recommended that future work which investigates the underlying mechanism of this effect is explored since it has clearly shown to be one of the most promising strategies for fabricating PSCs under both low and high humidity.

Most methods performed under moisture exposure produce PSCs with PCEs exceeding 15%, and compared with the devices fabricated under nitrogen environment, had better long-term stability. These investigations illustrate that by following the strategies summarized in in this review, PSCs can still obtain efficiencies over 20% outside of a glovebox, and thus lower the cost of PSC fabrication. As an alternative to a glovebox, fabricating PSCs in a dry box with well-controlled humidity could prove to be a much more affordable route to fabricate high quality perovskite films. Designing a dry box with an excellent ventilation system (with a dry air flow system) would be very valuable. Another limiting factor is the respective CTLs, which are often air sensitive or utilize air-sensitive additives (such as Li-TFSI in Spiro-OMeTAD). While handling sensitive CTLs in a controlled environment would minimize some detrimental effects, using air stable metal oxide transport layers or carbon-based materials is a more promising long-term solution.

The tremendous potential of low temperature carbon-based inks, which effectively replace the HTM and metal electrode in n–i–p PSCs, should also be further explored. Although their efficiencies are (in most cases) not exceeding 15%, their simple, low-cost processing provides an exciting stable alternative HTM/electrode which is free from hygroscopic dopants.[268,301] Their poor efficiencies are typically attributed to poor contact at the perovskite/carbon interface, which is usually a result of 1) pinholes or blemishes in the carbon ink due to the nature of the evaporating solvents, and 2) the perovskite layer containing pinholes not filled by the carbon ink.[302] Given that research into carbon-based inks is in its infancy, it is predicted that the addition of nanomaterials (such as functionalized graphene and carbon nanotubes) will improve the hole selectivity and contact between the perovskite/carbon ink, thus improving the efficiency of ambient PSCs.[301] A wide range of nanocarbons have already provided many beneficial results in both dye sensitized solar cells (DSSCs)[303–308] and PSCs,[309–316] suggesting that the use of such nanomaterials in carbon inks will provide a bright future for the fabrication ambient PSCs.

Although great progress has been made in the fabrication of PSCs in ambient air, there is still a lot of room for improvement. As introduced in this review, PSCs fabricated under ambient conditions obtain better long-term stability, but the perovskite films still decompose slowly in an ambient environment. Furthermore, the highest quality perovskite films and PSCs are typically produced using spin-coating which may have some drawbacks when it comes to upscaling costs. Despite the exciting progress of PSCs fabricated in ambient conditions, the PCEs are still typically lower compared to PSCs fabricated in an inert environment. Moreover, most of the methods required a controlled humidity environment where if uncontrolled, resulted in poor perovskite films and PSCs with low PCEs. Despite this, the initial efficiency of PSCs fabricated in ambient air was only 15.7% but has now exceeded 20%, indicating that excellent progress has been made in this field. **Table 1** provides a summary of all the notable achievements for PSCs fabricated in ambient conditions. There is little doubt further developments in PSCs fabricated in ambient conditions will be seen. While this review focuses predominately on fabricating high efficiency PSCs in an ambient atmosphere, the durability and testing conditions of PSCs should also be carefully considered. For example, the consensus statement for stability assessment and reporting for perovskite PV based on the International Summit on Organic Photovoltaic Stability (ISOS) protocols should be used.[317] In addition, PSCs should be subject to strict testing standards such as those in accordance with the IEC 61215:2016 standards, which will further strengthen the viability of commercial PSCs. During the

© 2020 The Authors. Published by Wiley-VCH GmbH

Table 1. Summary of perovskite solar cells fabricated under different humidity.

Method			RH [%]	PCE [%]	Reference
Compositional engineering	Mixed-cation and/or mixed-halide perovskites	$FA_{0.4}MA_{0.6}PbI_3$	30	10.86	[134]
		$FA_{0.9}Cs_{0.1}PbI_3$	55	16.5	[137]
		$FA_{0.8}MA_{0.15}Cs_{0.05}PbI_{2.55}Br_{0.45}$	50	18.2	[156]
		$Cs_{0.05}(MA_{0.17}FA_{0.83})_{0.95}Pb(I_{0.83}Br_{0.17})_3$	25	20.8	[138]
		$MAPbI_{3-x}(SCN)_x$	70	13.49	[58]
		$MAPbI_{3-x}(SCN)_x$ with 3.5% KSCN	N/A	16.59	[155]
Solvent engineering	One-step spin-coating method	75% chlorobenzene and 25% ethanol	40	14.0	[171]
		Diethyl ether	50	16.9	[90]
		Ethyl acetate	75	14.5	[165]
		Ethyl acetate	35	17.41	[168]
		Ethyl acetate	37.5	17.83	[166]
		Ethyl acetate	20–30	16.24	[167]
		Propyl acetate	52	17.78	[93]
		Methyl acetate	60–70	16.3	[164]
		Chlorobenzene	N/A	11.23	[170]
	Two-step spin-coating method	Isopropanol	50–60	16.27	[172]
		Ethanol	50	11.22	[173]
Additive engineering	One-step spin-coating method, use additive in perovskite precursor	2-Pyridylthiourea	50–60	18.2	[29]
		Dry-HCl	30	17.72	[187]
		Hydrogen iodide	50	17.2	[319]
		Diiodomethane	60	16.5	[183]
		Ammonium chloride	45	15.6	[182]
		33 wt% hydrochloric acid	60	14.28	[188]
		5% polysaccharide agarose	N/A	14.66	[184]
		MA (ethanol solvent) and MACl	10–15	20.3	[185]
	Two-step spin-coating method, use additive in PbI_2 precursor	*n*-Butylamine	25	16	[111]
		n-Butylamine additive with short-time dipping reaction (STDR) method	60–80	17.56	[143]
		4-*tert*-butylpyridine	50	12.6	[190]
		4-*tert*-butylpyridine	40–50	16.16	[192]
		33 wt% hydrochloric acid	60	14.76	[188]
		ZnO nanoparticles	60	18.34	[112]
		Tetrahydrofuran	50	15	[193]
large-scale fabrication	Substrate heating method	Preheated at 50 °C	50	15.76	[198]
		Preheated at 50 °C	40	18.38	[199]
		Preheated at 80 °C	70	18.11	[60]
		Preheated at 85 °C	50	15.91	[200]
		Preheated at 70 °C	90	19.5	[98]
		Preheated at 100 °C	15–25	18.0	[201]
	Slot-die coating method	CHP + DMSO additive	N/A	12.52	[207]
		Preheated at 70 °C	60	12.3	[209]
		MA/FA/Cs PSCs	40	10.57	[210]
		Gas flow assisting	45	15.57	[219]
	Doctor blading method		15–25	10.44	[69]

© 2020 The Authors. Published by Wiley-VCH GmbH

Table 1. Continued.

Method			RH [%]	PCE [%]	Reference
		Preheated at 120 °C	45	11.29	[211]
			40	10.92	[212]
		NiO_x as HTL	45	15.34	[214]
		GBL/DMSO solvent	35–55	15.6	[215]
	Spray coating method	Preheated at 75 °C	N/A	11	[216]
		Preheated at 75 °C	50	13.54	[217]
		Hot air blowing	30	13.5	[196]
Other methods	Gas flow assisting method	Humid air flowing	42–48	16.32	[220]
		N_2 gas, drop-casting with NH_4Cl additive	45	19.48	[219]
		LPCVD method	60	12.73	[59]
		Hot air/vapor-assisted deposition	35	18.90	[221]
		Crystalline perovskite powder	22	18.07	[222]
		Intermediate assisted method	60–80	15.56	[224]
		methylammonium acetate solvent	80	18.42	[225]
	Bath immersion method	Secondary crystal growth method	40	17.3	[226]
		Air knife-assisted recrystallization	60	19.39	[227]
		Crystal engineering	50–75	18.4	[229]
		Crystal engineering using doctor-blading method	50–75	17.77	[229]
		Prenucleation method	40	19.5	[62]
		HCOOCs precursor solution	30	16.14	[230]
		Aqueous $Pb(NO_3)_2$ precursor	N/A	16.50	[228]
Structure engineering	ETL	ZnO nanoparticles	N/A	15.7	[119]
		ZnO with aging method	50	14.25	[237]
	HTL	NiO-based	40	20.7	[295]
	HTL-free carbon-based		N/A	16.25	[271]
			50	15.06	[272]
			50	11.6	[273]
Interface engineering	Al_2O_3/NiO interface between the ETL (TiO_2) and perovskite		45–55	18.14	[298]
	[EMIM]PF_6 between ETL (ZnO) and perovskite		47.5	13.5	[300]
	DA-TiO_2		50	16.36	[113]
	Al_2O_3/Cu:NiO interface between ETL (SnO_2) and $MAPbI_{3-x}Cl_x$–Cu:NiO–carbon–graphite		68	18.6	[320]
	Phenethylammonium iodide passivation		30–40	23.32	[120]

preparation of this review, Shi et al.[318] used an encapsulation scheme using a mixed-cation mixed-halide perovskite absorber layer which survived more than 1800 h of damp heat test and 75 cycles of humidity freeze test, exceeding the requirement of IEC61215:2016. This exceptional achievement of stability and durability further demonstrates the exciting future of perovskite research.

This review has provided an overview of the key factors in the degradation of perovskite films in an ambient environment. Methods established in the literature that have reported PSCs under ambient conditions have been discussed and an overview of all the most successful routes, particularly of high efficiency, have been extensively summarized. This review summarizes all the recent progress and provides important insights into the future development of the ambient fabrication of PSCs, which is crucial for the upscaling and future commercialization of this exciting technology.

Acknowledgements

T.J.M. would like to thank the Royal Commission for the Exhibition of 1851 for their financial support through an 1851 Research Fellowship. I.P.P. would like to acknowledge the EPSRC Centres for Doctoral Training for their financial support (EP/L015862/1).

Conflict of Interest

The authors declare no conflict of interest.

Keywords

air-stable, ambient fabrication, device performance, efficiency, perovskite solar cells, photovoltaics, stability

Received: August 20, 2020
Published online: September 18, 2020

© 2020 The Authors. Published by Wiley-VCH GmbH

[1] L. M. Gonçalves, V. de Zea Bermudez, H. A. Ribeiro, A. M. Mendes, *Energy Environ. Sci.* **2008**, *1*, 655.
[2] J. A. Crook, L. A. Jones, P. M. Forster, R. Crook, *Energy Environ. Sci.* **2011**, *4*, 3101.
[3] V. Bagalini, B. Y. Zhao, R. Z. Wang, U. Desideri, *Research* **2019**, *2019*, 1.
[4] F. Ambroz, T. J. Macdonald, T. Nann, *Adv. Energy Mater.* **2017**, *7*, 1602093.
[5] K. Yoshikawa, H. Kawasaki, W. Yoshida, T. Irie, K. Konishi, K. Nakano, T. Uto, D. Adachi, M. Kanematsu, H. Uzu, K. Yamamoto, *Nat. Energy* **2017**, *2*, 1.
[6] M. A. Green, Y. Hishikawa, E. D. Dunlop, D. H. Levi, J. Hohl-Ebinger, M. Yoshita, A. W. Y. Ho-Baillie, *Prog. Photovoltaics* **2019**, *27*, 3.
[7] A. Richter, M. Hermle, S. W. Glunz, *IEEE J. Photovoltaics* **2013**, *3*, 1184.
[8] Z. Wang, Z. Song, Y. Yan, S. (Frank) Liu, D. Yang, *Adv. Sci.* **2019**, *6*, 1801704.
[9] B. O'Regan, M. Gratzel, *Nature* **1991**, *353*, 737.
[10] T. J. Macdonald, F. Ambroz, M. Batmunkh, Y. Li, D. Kim, C. Contini, R. Poduval, H. Liu, J. G. Shapter, I. Papakonstantinou, I. P. Parkin, *Mater. Today Energy* **2018**, *9*, 254.
[11] M. M. Tavakoli, M. Nasilowski, J. Zhao, M. G. Bawendi, J. Kong, *Small Methods* **2019**, *3*, 1900449.
[12] O. E. Semonin, J. M. Luther, S. Choi, H.-Y. Chen, J. Gao, A. J. Nozik, M. C. Beard, *Science* **2011**, *334*, 1530.
[13] J. Zhang, L. Zhu, Z. Wei, *Small Methods* **2017**, *1*, 1700258.
[14] Y. Lin, Y. Firdaus, M. I. Nugraha, F. Liu, S. Karuthedath, A.-H. Emwas, W. Zhang, A. Seitkhan, M. Neophytou, H. Faber, E. Yengel, I. McCulloch, L. Tsetseris, F. Laquai, T. D. Anthopoulos, *Adv. Sci.* **2020**, *7*, 1903419.
[15] T. J. Macdonald, M. Batmunkh, C. Lin, J. Kim, D. D. Tune, F. Ambroz, X. Li, S. Xu, C. Sol, I. Papakonstantinou, M. A. McLachlan, I. P. Parkin, J. G. Shapter, J. R. Durrant, *Small Methods* **2019**, *3*, 1900164.
[16] M. M. Lee, J. Teuscher, T. Miyasaka, T. N. Murakami, H. J. Snaith, *Science* **2012**, *338*, 643.
[17] L. Etgar, P. Gao, Z. Xue, Q. Peng, A. K. Chandiran, B. Liu, Md. K. Nazeeruddin, M. Grätzel, *J. Am. Chem. Soc.* **2012**, *134*, 17396.
[18] H.-S. Kim, C.-R. Lee, J.-H. Im, K.-B. Lee, T. Moehl, A. Marchioro, S.-J. Moon, R. Humphry-Baker, J.-H. Yum, J. E. Moser, M. Grätzel, N.-G. Park, *Sci. Rep.* **2012**, *2*, 591.
[19] S. D. Stranks, G. E. Eperon, G. Grancini, C. Menelaou, M. J. P. Alcocer, T. Leijtens, L. M. Herz, A. Petrozza, H. J. Snaith, *Science* **2013**, *342*, 341.
[20] G. Xing, N. Mathews, S. Sun, S. S. Lim, Y. M. Lam, M. Grätzel, S. Mhaisalkar, T. C. Sum, *Science* **2013**, *342*, 344.
[21] J. Burschka, N. Pellet, S.-J. Moon, R. Humphry-Baker, P. Gao, M. K. Nazeeruddin, M. Grätzel, *Nature* **2013**, *499*, 316.
[22] M. Saliba, T. Matsui, J.-Y. Seo, K. Domanski, J.-P. Correa-Baena, M. K. Nazeeruddin, S. M. Zakeeruddin, W. Tress, A. Abate, A. Hagfeldt, M. Grätzel, *Energy Environ. Sci.* **2016**, *9*, 1989.
[23] G. E. Eperon, S. D. Stranks, C. Menelaou, M. B. Johnston, L. M. Herz, H. J. Snaith, *Energy Environ. Sci.* **2014**, *7*, 982.
[24] Y. Li, L. Meng, Y. (Michael) Yang, G. Xu, Z. Hong, Q. Chen, J. You, G. Li, Y. Yang, Y. Li, *Nat. Commun.* **2016**, *7*, 1.
[25] M. Cai, Y. Wu, H. Chen, X. Yang, Y. Qiang, L. Han, *Adv. Sci.* **2017**, *4*, 1600269.
[26] D. Vaitukaityte, Z. Wang, T. Malinauskas, A. Magomedov, G. Bubniene, V. Jankauskas, V. Getautis, H. J. Snaith, *Adv. Mater.* **2018**, *30*, 1803735.
[27] A. Kojima, K. Teshima, Y. Shirai, T. Miyasaka, *J. Am. Chem. Soc.* **2009**, *131*, 6050.
[28] Best Research-Cell Efficiency Chart | Photovoltaic Research | NREL, https://www.nrel.gov/pv/cell-efficiency.html (accessed: May 2020).
[29] M. Sun, F. Zhang, H. Liu, X. Li, Y. Xiao, S. Wang, *J. Mater. Chem. A* **2017**, *5*, 13448.
[30] F. Hao, C. C. Stoumpos, D. H. Cao, R. P. H. Chang, M. G. Kanatzidis, *Nat. Photonics* **2014**, *8*, 489.
[31] V. M. Goldschmidt, *Die Naturwiss.* **1926**, *14*, 477.
[32] T. Leijtens, K. Bush, R. Cheacharoen, R. Beal, A. Bowring, M. D. McGehee, *J. Mater. Chem. A* **2017**, *5*, 11483.
[33] W. Travis, E. N. K. Glover, H. Bronstein, D. O. Scanlon, R. G. Palgrave, *Chem. Sci.* **2016**, *7*, 4548.
[34] R. D. Shannon, C. T. Prewitt, *Acta Crystallogr., Sect. B: Struct. Crystallogr. Cryst. Chem.* **1969**, *25*, 925.
[35] R. D. Shannon, *Acta Crystllogr., Sect. A: Found. Crystallogr.* **1976**, *32*, 751.
[36] X. Zheng, Y. Hou, C. Bao, J. Yin, F. Yuan, Z. Huang, K. Song, J. Liu, J. Troughton, N. Gasparini, C. Zhou, Y. Lin, D.-J. Xue, B. Chen, A. K. Johnston, N. Wei, M. N. Hedhili, M. Wei, A. Y. Alsalloum, P. Maity, B. Turedi, C. Yang, D. Baran, T. D. Anthopoulos, Y. Han, Z.-H. Lu, O. F. Mohammed, F. Gao, E. H. Sargent, O. M. Bakr, *Nat. Energy* **2020**, *5*, 131.
[37] H. Wei, J. Huang, *Nat. Commun.* **2019**, *10*, 1066.
[38] Q. Van Le, H. W. Jang, S. Y. Kim, *Small Methods* **2018**, *2*, 1700419.
[39] J. Miao, F. Zhang, *J. Mater. Chem. C* **2019**, *7*, 1741.
[40] Y. Lin, P. Pattanasattayavong, T. D. Anthopoulos, *Adv. Mater.* **2017**, *29*, 1702838.
[41] J. Lee, H. Kang, G. Kim, H. Back, J. Kim, S. Hong, B. Park, E. Lee, K. Lee, *Adv. Mater.* **2017**, *29*, 1606363.
[42] Y. Cheng, F. So, S.-W. Tsang, *Mater. Horiz.* **2019**, *6*, 1611.
[43] X. Li, D. Bi, C. Yi, J.-D. Décoppet, J. Luo, S. M. Zakeeruddin, A. Hagfeldt, M. Grätzel, *Science* **2016**, *353*, 58.
[44] W. Chen, Y. Wu, Y. Yue, J. Liu, W. Zhang, X. Yang, H. Chen, E. Bi, I. Ashraful, M. Gratzel, L. Han, *Science* **2015**, *350*, 944.
[45] S. Hong, J. Lee, H. Kang, G. Kim, S. Kee, J.-H. Lee, S. Jung, B. Park, S. Kim, H. Back, K. Yu, K. Lee, *Sci. Adv.* **2018**, *4*, eaat3604.
[46] D.-K. Lee, D.-N. Jeong, T. K. Ahn, N.-G. Park, *ACS Energy Lett.* **2019**, *4*, 2393.
[47] G. Jang, H. Kwon, S. Ma, S. Yun, H. Yang, J. Moon, *Adv. Energy Mater.* **2019**, *9*, 1901719.
[48] J. A. Christians, P. A. Miranda Herrera, P. V. Kamat, *J. Am. Chem. Soc.* **2015**, *137*, 1530.
[49] K. Domanski, E. A. Alharbi, A. Hagfeldt, M. Grätzel, W. Tress, *Nat. Energy* **2018**, *3*, 61.
[50] Y.-H. Kye, C.-J. Yu, U.-G. Jong, Y. Chen, A. Walsh, *J. Phys. Chem. Lett.* **2018**, *9*, 2196.
[51] H. Yuan, E. Debroye, K. Janssen, H. Naiki, C. Steuwe, G. Lu, M. Moris, E. Orgiu, H. Uji-i, F. De Schryver, P. Samorì, J. Hofkens, M. Roeffaers, *J. Phys. Chem. Lett.* **2016**, *7*, 561.
[52] I. Zimmermann, P. Gratia, D. Martineau, G. Grancini, J.-N. Audinot, T. Wirtz, M. K. Nazeeruddin, *J. Mater. Chem. A* **2019**, *7*, 8073.
[53] C. Tian, A. Mei, S. Zhang, H. Tian, S. Liu, F. Qin, Y. Xiong, Y. Rong, Y. Hu, Y. Zhou, S. Xie, H. Han, *Nano Energy* **2018**, *53*, 160.
[54] J. Lee, J. Kim, C.-L. Lee, G. Kim, T. K. Kim, H. Back, S. Jung, K. Yu, S. Hong, S. Lee, S. Kim, S. Jeong, H. Kang, K. Lee, *Adv. Energy Mater.* **2017**, *7*, 1700226.
[55] Y. Deng, X. Zheng, Y. Bai, Q. Wang, J. Zhao, J. Huang, *Nat. Energy* **2018**, *3*, 560.
[56] C.-T. Lin, F. De Rossi, J. Kim, J. Baker, J. Ngiam, B. Xu, S. Pont, N. Aristidou, S. A. Haque, T. Watson, M. A. McLachlan, J. R. Durrant, *J. Mater. Chem. A* **2019**, *7*, 3006.
[57] A. Mei, X. Li, L. Liu, Z. Ku, T. Liu, Y. Rong, M. Xu, M. Hu, J. Chen, Y. Yang, M. Gratzel, H. Han, *Science* **2014**, *345*, 295.
[58] Q. Tai, P. You, H. Sang, Z. Liu, C. Hu, H. L. W. Chan, F. Yan, *Nat. Commun.* **2016**, *7*, 11105.
[59] P. Luo, Z. Liu, W. Xia, C. Yuan, J. Cheng, Y. Lu, *ACS Appl. Mater. Interfaces* **2015**, *7*, 2708.

© 2020 The Authors. Published by Wiley-VCH GmbH

[60] Y. Cheng, X. Xu, Y. Xie, H.-W. Li, J. Qing, C. Ma, C.-S. Lee, F. So, S.-W. Tsang, *Sol. RRL* **2017**, *1*, 1700097.
[61] L.-L. Gao, C.-X. Li, C.-J. Li, G.-J. Yang, *J. Mater. Chem. A* **2017**, *5*, 1548.
[62] K. Zhang, Z. Wang, G. Wang, J. Wang, Y. Li, W. Qian, S. Zheng, S. Xiao, S. Yang, *Nat. Commun.* **2020**, *11*, 1006.
[63] J. You, Y. (Michael) Yang, Z. Hong, T.-B. Song, L. Meng, Y. Liu, C. Jiang, H. Zhou, W.-H. Chang, G. Li, Y. Yang, *Appl. Phys. Lett.* **2014**, *105*, 183902.
[64] W. Zhang, M. Saliba, D. T. Moore, S. K. Pathak, M. T. Hörantner, T. Stergiopoulos, S. D. Stranks, G. E. Eperon, J. A. Alexander-Webber, A. Abate, A. Sadhanala, S. Yao, Y. Chen, R. H. Friend, L. A. Estroff, U. Wiesner, H. J. Snaith, *Nat. Commun.* **2015**, *6*, 6142.
[65] Y. Shao, Z. Xiao, C. Bi, Y. Yuan, J. Huang, *Nat. Commun.* **2014**, *5*, 5784.
[66] J. Xu, A. Buin, A. H. Ip, W. Li, O. Voznyy, R. Comin, M. Yuan, S. Jeon, Z. Ning, J. J. McDowell, P. Kanjanaboos, J.-P. Sun, X. Lan, L. N. Quan, D. H. Kim, I. G. Hill, P. Maksymovych, E. H. Sargent, *Nat. Commun.* **2015**, *6*, 7081.
[67] A. Walsh, D. O. Scanlon, S. Chen, X. G. Gong, S.-H. Wei, *Angew. Chem., Int. Ed.* **2015**, *54*, 1791.
[68] K. X. Steirer, P. Schulz, G. Teeter, V. Stevanovic, M. Yang, K. Zhu, J. J. Berry, *ACS Energy Lett.* **2016**, *1*, 360.
[69] Z. Yang, C.-C. Chueh, F. Zuo, J. H. Kim, P.-W. Liang, A. K.-Y. Jen, *Adv. Energy Mater.* **2015**, *5*, 1500328.
[70] J. M. Frost, K. T. Butler, F. Brivio, C. H. Hendon, M. van Schilfga arde, A. Walsh, *Nano Lett.* **2014**, *14*, 2584.
[71] J. Yang, B. D. Siempelkamp, D. Liu, T. L. Kelly, *ACS Nano* **2015**, *9*, 1955.
[72] A. M. A. Leguy, Y. Hu, M. Campoy-Quiles, M. I. Alonso, O. J. Weber, P. Azarhoosh, M. van Schilfgaarde, M. T. Weller, T. Bein, J. Nelson, P. Docampo, P. R. F. Barnes, *Chem. Mater.* **2015**, *27*, 3397.
[73] J. Zhao, B. Cai, Z. Luo, Y. Dong, Y. Zhang, H. Xu, B. Hong, Y. Yang, L. Li, W. Zhang, C. Gao, *Sci. Rep.* **2016**, *6*, 1976.
[74] S. Emami, L. Andrade, A. Mendes, *U. Porto J. Eng.* **2018**, *1*, 52.
[75] G. Niu, W. Li, F. Meng, L. Wang, H. Dong, Y. Qiu, *J. Mater. Chem. A* **2014**, *2*, 705.
[76] D. Bryant, N. Aristidou, S. Pont, I. Sanchez-Molina, T. Chotchuna ngatchaval, S. Wheeler, J. R. Durrant, S. A. Haque, *Energy Environ. Sci.* **2016**, *9*, 1655.
[77] N. Aristidou, I. Sanchez-Molina, T. Chotchuangchutchaval, M. Brown, L. Martinez, T. Rath, S. A. Haque, *Angew. Chem., Int. Ed.* **2015**, *54*, 8208.
[78] N. Aristidou, C. Eames, I. Sanchez-Molina, X. Bu, J. Kosco, M. S. Islam, S. A. Haque, *Nat. Commun.* **2017**, *8*, 15218.
[79] S.-W. Lee, S. Kim, S. Bae, K. Cho, T. Chung, L. E. Mundt, S. Lee, S. Park, H. Park, M. C. Schubert, S. W. Glunz, Y. Ko, Y. Jun, Y. Kang, H.-S. Lee, D. Kim, *Sci. Rep.* **2016**, *6*, 38150.
[80] S. Ito, S. Tanaka, K. Manabe, H. Nishino, *J. Phys. Chem. C* **2014**, *118*, 16995.
[81] IEC 61215-1: 2016 | IEC Webstore | rural electrification, solar power, solar panel, photovoltaic, PV, smart city, LVDC, https://webstore.iec.ch/publication/24312 (accessed: July 2020).
[82] K. A. Bush, A. F. Palmstrom, Z. J. Yu, M. Boccard, R. Cheacharoen, J. P. Mailoa, D. P. McMeekin, R. L. Z. Hoye, C. D. Bailie, T. Leijtens, I. M. Peters, M. C. Minichetti, N. Rolston, R. Prasanna, S. Sofia, D. Harwood, W. Ma, F. Moghadam, H. J. Snaith, T. Buonassisi, Z. C. Holman, S. F. Bent, M. D. McGehee, *Nat. Energy* **2017**, *2*, 17009.
[83] B. Philippe, B.-W. Park, R. Lindblad, J. Oscarsson, S. Ahmadi, E. M. J. Johansson, H. Rensmo, *Chem. Mater.* **2015**, *27*, 1720.
[84] B. Conings, J. Drijkoningen, N. Gauquelin, A. Babayigit, J. D'Haen, L. D'Olieslaeger, A. Ethirajan, J. Verbeeck, J. Manca, E. Mosconi, F. D. Angelis, H.-G. Boyen, *Adv. Energy Mater.* **2015**, *5*, 1500477.
[85] E. J. Juarez-Perez, Z. Hawash, S. R. Raga, L. K. Ono, Y. Qi, *Energy Environ. Sci.* **2016**, *9*, 3406.
[86] N. J. Jeon, J. H. Noh, Y. C. Kim, W. S. Yang, S. Ryu, S. I. Seok, *Nat. Mater.* **2014**, *13*, 897.
[87] M. Xiao, F. Huang, W. Huang, Y. Dkhissi, Y. Zhu, J. Etheridge, A. Gray-Weale, U. Bach, Y.-B. Cheng, L. Spiccia, *Angew. Chem., Int. Ed.* **2014**, *53*, 9898.
[88] G. E. Eperon, V. M. Burlakov, P. Docampo, A. Goriely, H. J. Snaith, *Adv. Funct. Mater.* **2014**, *24*, 151.
[89] H. S. Jung, N.-G. Park, *Small* **2015**, *11*, 10.
[90] F. Wang, Z. Ye, H. Sarvari, S. M. Park, A. Abtahi, K. Graham, Y. Zhao, Y. Wang, Z. D. Chen, S. Li, *J. Power Sources* **2019**, *412*, 359.
[91] S. Pathak, A. Sepe, A. Sadhanala, F. Deschler, A. Haghighirad, N. Sakai, K. C. Goedel, S. D. Stranks, N. Noel, M. Price, S. Hüttner, N. A. Hawkins, R. H. Friend, U. Steiner, H. J. Snaith, *ACS Nano* **2015**, *9*, 2311.
[92] H. Gao, C. Bao, F. Li, T. Yu, J. Yang, W. Zhu, X. Zhou, G. Fu, Z. Zou, *ACS Appl. Mater. Interfaces* **2015**, *7*, 9110.
[93] D. Angmo, X. Peng, A. Seeber, C. Zuo, M. Gao, Q. Hou, J. Yuan, Q. Zhang, Y. Cheng, D. Vak, *Small* **2019**, *15*, 1904422.
[94] R. Chang, J. Zhang, S. Ullah, Z. Zhu, Y. Chen, H. Guo, J. Gu, *Thin Solid Films* **2019**, *690*, 137563.
[95] G. E. Eperon, S. N. Habisreutinger, T. Leijtens, B. J. Bruijnaers, J. J. van Franeker, D. W. deQuilettes, S. Pathak, R. J. Sutton, G. Grancini, D. S. Ginger, R. A. J. Janssen, A. Petrozza, H. J. Snaith, *ACS Nano* **2015**, *9*, 9380.
[96] L. Contreras-Bernal, C. Aranda, M. Valles-Pelarda, T. T. Ngo, S. Ramos-Terrón, J. J. Gallardo, J. Navas, A. Guerrero, I. Mora-Seró, J. Idígoras, J. A. Anta, *J. Phys. Chem. C* **2018**, *122*, 5341.
[97] G. Wang, D. Liu, J. Xiang, D. Zhou, K. Alameh, B. Ding, Q. Song, *RSC Adv.* **2016**, *6*, 43299.
[98] F. Wang, T. Zhang, Y. Wang, D. Liu, P. Zhang, H. Chen, L. Ji, L. Chen, Z. D. Chen, J. Wu, X. Liu, Y. Li, Y. Wang, S. Li, *J. Mater. Chem. A* **2019**, *7*, 12166.
[99] B. Wang, Z.-G. Zhang, S. Ye, H. Rao, Z. Bian, C. Huang, Y. Li, *J. Mater. Chem. A* **2016**, *4*, 17267.
[100] H. Zhou, Q. Chen, G. Li, S. Luo, T.-b. Song, H.-S. Duan, Z. Hong, J. You, Y. Liu, Y. Yang, *Science* **2014**, *345*, 542.
[101] M. Lv, X. Dong, X. Fang, B. Lin, S. Zhang, X. Xu, J. Ding, N. Yuan, *RSC Adv.* **2015**, *5*, 93957.
[102] Z. Wang, S. Yuan, D. Li, F. Jin, R. Zhang, Y. Zhan, M. Lu, S. Wang, Y. Zheng, J. Guo, Z. Fan, L. Chen, *Opt. Express* **2016**, *24*, A1431.
[103] W. Zhou, Y. Zhao, C. Shi, H. Huang, J. Wei, R. Fu, K. Liu, D. Yu, Q. Zhao, *J. Phys. Chem. C* **2016**, *120*, 4759.
[104] X. Gong, M. Li, X.-B. Shi, H. Ma, Z.-K. Wang, L.-S. Liao, *Adv. Funct. Mater.* **2015**, *25*, 6671.
[105] T. He, Z. Liu, Y. Zhou, H. Ma, *Sol. Energy Mater. Sol. Cells* **2018**, *176*, 280.
[106] D. Liu, C. J. Traverse, P. Chen, M. Elinski, C. Yang, L. Wang, M. Young, R. R. Lunt, *Adv. Sci.* **2018**, *5*, 1700484.
[107] R. Brenes, D. Guo, A. Osherov, N. K. Noel, C. Eames, E. M. Hutter, S. K. Pathak, F. Niroui, R. H. Friend, M. S. Islam, H. J. Snaith, V. Bulović, T. J. Savenije, S. D. Stranks, *Joule* **2017**, *1*, 155.
[108] Z. Ren, A. Ng, Q. Shen, H. C. Gokkaya, J. Wang, L. Yang, W.-K. Yiu, G. Bai, A. B. Djurišić, W. W. Leung, J. Hao, W. K. Chan, C. Surya, *Sci. Rep.* **2015**, *4*, 6752.
[109] S.-C. Liu, Z. Li, Y. Yang, X. Wang, Y.-X. Chen, D.-J. Xue, J.-S. Hu, *J. Am. Chem. Soc.* **2019**, *141*, 18075.
[110] H. Han, *Sci. Bull.* **2020**, *65*, 335.
[111] J. Wu, J.-J. Dong, S.-X. Chen, H.-Y. Hao, J. Xing, H. Liu, *Nanoscale Res. Lett.* **2018**, *13*, 293.
[112] W.-T. Wang, J. Sharma, J.-W. Chen, C.-H. Kao, S.-Y. Chen, C.-H. Chen, Y.-C. Feng, Y. Tai, *Nano Energy* **2018**, *49*, 109.
[113] P. Zhai, R. Cheng, L. Ren, Y.-T. Huang, H. Lee, S.-P. Feng, *Sol. RRL* **2018**, *2*, 1800103.
[114] J. Huang, S. Tan, P. D. Lund, H. Zhou, *Energy Environ. Sci.* **2017**, *10*, 2284.

© 2020 The Authors. Published by Wiley-VCH GmbH

[115] B. Yang, O. Dyck, J. Poplawsky, J. Keum, S. Das, A. Puretzky, T. Aytug, P. C. Joshi, C. M. Rouleau, G. Duscher, D. B. Geohegan, K. Xiao, *Angew. Chem., Int. Ed.* **2015**, *54*, 14862.
[116] J. B. Patel, R. L. Milot, A. D. Wright, L. M. Herz, M. B. Johnston, *J. Phys. Chem. Lett.* **2016**, *7*, 96.
[117] Y. Xu, L. Zhu, J. Shi, X. Xu, J. Xiao, J. Dong, H. Wu, Y. Luo, D. Li, Q. Meng, *ChemPhysChem* **2016**, *17*, 112.
[118] C.-G. Wu, C.-H. Chiang, Z.-L. Tseng, Md. K. Nazeeruddin, A. Hagfeldt, M. Grätzel, *Energy Environ. Sci.* **2015**, *8*, 2725.
[119] D. Liu, T. L. Kelly, *Nat. Photonics* **2014**, *8*, 133.
[120] Q. Jiang, Y. Zhao, X. Zhang, X. Yang, Y. Chen, Z. Chu, Q. Ye, X. Li, Z. Yin, J. You, *Nat. Photonics* **2019**, *13*, 460.
[121] Q. Wang, Q. Dong, T. Li, A. Gruverman, J. Huang, *Adv. Mater.* **2016**, *28*, 6734.
[122] S. S. Shin, E. J. Yeom, W. S. Yang, S. Hur, M. G. Kim, J. Im, J. Seo, J. H. Noh, S. I. Seok, *Science* **2017**, *356*, 167.
[123] C. Lin, J. Lee, J. Kim, T. J. Macdonald, J. Ngiam, B. Xu, M. Daboczi, W. Xu, S. Pont, B. Park, H. Kang, J. Kim, D. J. Payne, K. Lee, J. R. Durrant, M. A. McLachlan, *Adv. Funct. Mater.* **2019**, 1906763.
[124] T. Baikie, Y. Fang, J. M. Kadro, M. Schreyer, F. Wei, S. G. Mhaisalkar, M. Graetzel, T. J. White, *J. Mater. Chem. A* **2013**, *1*, 5628.
[125] Z. Song, S. C. Watthage, A. B. Phillips, B. L. Tompkins, R. J. Ellingson, M. J. Heben, *Chem. Mater.* **2015**, *27*, 4612.
[126] T. Oku, M. Zushi, Y. Imanishi, A. Suzuki, K. Suzuki, *Appl. Phys. Express* **2014**, *7*, 121601.
[127] P. Luo, W. Xia, S. Zhou, L. Sun, J. Cheng, C. Xu, Y. Lu, *J. Phys. Chem. Lett.* **2016**, *7*, 3603.
[128] S. Pont, D. Bryant, C.-T. Lin, N. Aristidou, S. Wheeler, X. Ma, R. Godin, S. A. Haque, J. R. Durrant, *J. Mater. Chem. A* **2017**, *5*, 9553.
[129] S. Colella, E. Mosconi, P. Fedeli, A. Listorti, F. Gazza, F. Orlandi, P. Ferro, T. Besagni, A. Rizzo, G. Calestani, G. Gigli, F. De Angelis, R. Mosca, *Chem. Mater.* **2013**, *25*, 4613.
[130] Y. Sun, J. Peng, Y. Chen, Y. Yao, Z. Liang, *Sci. Rep.* **2017**, *7*, 46193.
[131] J.-P. Correa-Baena, A. Abate, M. Saliba, W. Tress, T. Jesper Jacobsson, M. Grätzel, A. Hagfeldt, *Energy Environ. Sci.* **2017**, *10*, 710.
[132] D. P. McMeekin, G. Sadoughi, W. Rehman, G. E. Eperon, M. Saliba, M. T. Horantner, A. Haghighirad, N. Sakai, L. Korte, B. Rech, M. B. Johnston, L. M. Herz, H. J. Snaith, *Science* **2016**, *351*, 151.
[133] Y. Zhao, H. Tan, H. Yuan, Z. Yang, J. Z. Fan, J. Kim, O. Voznyy, X. Gong, L. N. Quan, C. S. Tan, J. Hofkens, D. Yu, Q. Zhao, E. H. Sargent, *Nat. Commun.* **2018**, *9*, 1607.
[134] J. Duan, Z. Liu, Y. Zhang, K. Liu, T. He, F. Wang, J. Dai, P. Zhou, *Opt. Mater.* **2018**, *85*, 55.
[135] P. Holzhey, P. Yadav, S.-H. Turren-Cruz, M. Grätzel, A. Hagfeldt, M. Saliba, *Mater. Today* **2019**, *29*, 10.
[136] Z. Li, M. Yang, J.-S. Park, S.-H. Wei, J. J. Berry, K. Zhu, *Chem. Mater.* **2016**, *28*, 284.
[137] J.-W. Lee, D.-H. Kim, H.-S. Kim, S.-W. Seo, S. M. Cho, N.-G. Park, *Adv. Energy Mater.* **2015**, *5*, 1501310.
[138] T. Singh, T. Miyasaka, *Adv. Energy Mater.* **2018**, *8*, 1700677.
[139] S. T. Williams, F. Zuo, C.-C. Chueh, C.-Y. Liao, P.-W. Liang, A. K.-Y. Jen, *ACS Nano* **2014**, *8*, 10640.
[140] K. Odysseas Kosmatos, L. Theofylaktos, E. Giannakaki, D. Deligiannis, M. Konstantakou, T. Stergiopoulos, *Energy Environ. Mater.* **2019**, *2*, 79.
[141] Q. Chen, H. Zhou, Y. Fang, A. Z. Stieg, T.-B. Song, H.-H. Wang, X. Xu, Y. Liu, S. Lu, J. You, P. Sun, J. McKay, M. S. Goorsky, Y. Yang, *Nat. Commun.* **2015**, *6*, 7269.
[142] L. Fan, Y. Ding, J. Luo, B. Shi, X. Yao, C. Wei, D. Zhang, G. Wang, Y. Sheng, Y. Chen, A. Hagfeldt, Y. Zhao, X. Zhang, *J. Mater. Chem. A* **2017**, *5*, 7423.
[143] L. Zhang, X. Zhang, Y. Yu, X. Xu, J. Tang, X. He, J. Wu, Z. Lan, *Sol. Energy* **2017**, *155*, 942.
[144] Y. Zhou, Z. Zhou, M. Chen, Y. Zong, J. Huang, S. Pang, N. P. Padture, *J. Mater. Chem. A* **2016**, *4*, 17623.
[145] W.-J. Yin, J.-H. Yang, J. Kang, Y. Yan, S.-H. Wei, *J. Mater. Chem. A* **2015**, *3*, 8926.
[146] S. R. Raga, M.-C. Jung, M. V. Lee, M. R. Leyden, Y. Kato, Y. Qi, *Chem. Mater.* **2015**, *27*, 1597.
[147] G. Niu, X. Guo, L. Wang, *J. Mater. Chem. A* **2015**, *3*, 8970.
[148] Z. Cheng, J. Lin, *CrystEngComm* **2010**, *12*, 2646.
[149] A. Senocrate, G. Y. Kim, M. Grätzel, J. Maier, *ACS Energy Lett.* **2019**, *4*, 2859.
[150] L. Gil-Escrig, A. Miquel-Sempere, M. Sessolo, H. J. Bolink, *J. Phys. Chem. Lett.* **2015**, *6*, 3743.
[151] J. H. Noh, S. H. Im, J. H. Heo, T. N. Mandal, S. I. Seok, *Nano Lett.* **2013**, *13*, 1764.
[152] A. J. Knight, A. D. Wright, J. B. Patel, D. P. McMeekin, H. J. Snaith, M. B. Johnston, L. M. Herz, *ACS Energy Lett.* **2019**, *4*, 75.
[153] M. C. Brennan, S. Draguta, P. V. Kamat, M. Kuno, *ACS Energy Lett.* **2018**, *3*, 204.
[154] A. Aziz, N. Aristidou, X. Bu, R. J. E. Westbrook, S. A. Haque, M. S. Islam, *Chem. Mater.* **2020**, *32*, 400.
[155] Z. Zhang, Y. Zhou, Y. Cai, H. Liu, Q. Qin, X. Lu, X. Gao, L. Shui, S. Wu, J.-M. Liu, *J. Power Sources* **2018**, *377*, 52.
[156] M.-C. Tang, Y. Fan, D. Barrit, X. Chang, H. X. Dang, R. Li, K. Wang, D.-M. Smilgies, S. (Frank) Liu, S. D. Wolf, T. D. Anthopoulos, K. Zhao, A. Amassian, *J. Mater. Chem. A* **2020**, *8*, 1095.
[157] Technology Standards Department of State Bureau of Environmental Protection of China, Environmental Quality Standard for Soils GB 15618-1995, State Bureau of Environmental Protection of China, **1995**.
[158] J. Li, H.-L. Cao, W.-B. Jiao, Q. Wang, M. Wei, I. Cantone, J. Lü, A. Abate, *Nat. Commun.* **2020**, *11*, 310.
[159] A. Babayigit, D. Duy Thanh, A. Ethirajan, J. Manca, M. Muller, H.-G. Boyen, B. Conings, *Sci. Rep.* **2016**, *6*, 18721.
[160] P. B. Tchounwou, C. G. Yedjou, A. K. Patlolla, D. J. Sutton, in *Molecular, Clinical and Environmental Toxicology* (Ed: A. Luch), Springer, Basel **2012**, pp. 133–164.
[161] K. Nishimura, M. A. Kamarudin, D. Hirotani, K. Hamada, Q. Shen, S. Iikubo, T. Minemoto, K. Yoshino, S. Hayase, *Nano Energy* **2020**, *74*, 104858.
[162] M. Xiao, L. Zhao, M. Geng, Y. Li, B. Dong, Z. Xu, L. Wan, W. Li, S. Wang, *Nanoscale* **2018**, *10*, 12141.
[163] J. W. Jung, S. T. Williams, A. K.-Y. Jen, *RSC Adv.* **2014**, *4*, 62971.
[164] F. Yang, G. Kapil, P. Zhang, Z. Hu, M. A. Kamarudin, T. Ma, S. Hayase, *ACS Appl. Mater. Interfaces* **2018**, *10*, 16482.
[165] J. Troughton, K. Hooper, T. M. Watson, *Nano Energy* **2017**, *39*, 60.
[166] W. Zhang, Y. Li, X. Liu, D. Tang, X. Li, X. Yuan, *Chem. Eng. J.* **2020**, *379*, 122298.
[167] L. Shi, H. Hao, J. Dong, T. Zhong, C. Zhang, J. Hao, J. Xing, H. Liu, *Nanomaterials* **2019**, *9*, 915.
[168] Z. Zhang, X. Luo, J. Ding, J. Zhang, *J. Solid State Chem.* **2019**, *274*, 199.
[169] N. Lin, J. Qiao, H. Dong, F. Ma, L. Wang, *J. Mater. Chem. A* **2015**, *3*, 22839.
[170] F. Yang, D.-W. Kang, Y.-S. Kim, *RSC Adv.* **2017**, *7*, 19030.
[171] D. Gedamu, I. M. Asuo, D. Benetti, M. Basti, I. Ka, S. G. Cloutier, F. Rosei, R. Nechache, *Sci. Rep.* **2018**, *8*, 12885.
[172] W.-T. Wang, S. K. Das, Y. Tai, *ACS Appl. Mater. Interfaces* **2017**, *9*, 10743.
[173] N. Cheng, P. Liu, S. Bai, Z. Yu, W. Liu, S.-S. Guo, X.-Z. Zhao, *J. Power Sources* **2016**, *319*, 111.
[174] Y. Xie, F. Shao, Y. Wang, T. Xu, D. Wang, F. Huang, *ACS Appl. Mater. Interfaces* **2015**, *7*, 12937.
[175] T. Zhang, M. Yang, Y. Zhao, K. Zhu, *Nano Lett.* **2015**, *15*, 3959.
[176] Y. Zhao, K. Zhu, *J. Mater. Chem. A* **2015**, *3*, 9086.
[177] F. Zhang, K. Zhu, *Adv. Energy Mater.* **2020**, *10*, 1902579.
[178] T. Li, Y. Pan, Z. Wang, Y. Xia, Y. Chen, W. Huang, *J. Mater. Chem. A* **2017**, *5*, 12602.

© 2020 The Authors. Published by Wiley-VCH GmbH

[179] J.-W. Lee, H.-S. Kim, N.-G. Park, *Acc. Chem. Res.* **2016**, *49*, 311.
[180] C. Aranda, C. Cristobal, L. Shooshtari, C. Li, S. Huettner, A. Guerrero, *Sustainable Energy Fuels* **2017**, *1*, 540.
[181] N. Ahn, D.-Y. Son, I.-H. Jang, S. M. Kang, M. Choi, N.-G. Park, *J. Am. Chem. Soc.* **2015**, *137*, 8696.
[182] Y. Rong, X. Hou, Y. Hu, A. Mei, L. Liu, P. Wang, H. Han, *Nat. Commun.* **2017**, *8*, .
[183] K. Ankireddy, A. H. Ghahremani, B. Martin, G. Gupta, T. Druffel, *J. Mater. Chem. A* **2018**, *6*, 9378.
[184] Y. Yang, T. Chen, D. Pan, J. Gao, C. Zhu, F. Lin, C. Zhou, Q. Tai, S. Xiao, Y. Yuan, Q. Dai, Y. Han, H. Xie, X. Guo, *Nano Energy* **2020**, *67*, 104246.
[185] X. Huang, R. Chen, G. Deng, F. Han, P. Ruan, F. Cheng, J. Yin, B. Wu, N. Zheng, *J. Am. Chem. Soc.* **2020**, *142*, 6149.
[186] J. Pan, C. Mu, Q. Li, W. Li, D. Ma, D. Xu, *Adv. Mater.* **2016**, *28*, 8309.
[187] Z. Yang, J. Pan, Y. Liang, Q. Li, D. Xu, *Small* **2018**, *14*, 1802240.
[188] G. Li, T. Zhang, Y. Zhao, *J. Mater. Chem. A* **2015**, *3*, 19674.
[189] Y. Wu, A. Islam, X. Yang, C. Qin, J. Liu, K. Zhang, W. Peng, L. Han, *Energy Environ. Sci.* **2014**, *7*, 2934.
[190] C. Liu, W. Ding, X. Zhou, J. Gao, C. Cheng, X. Zhao, B. Xu, *J. Phys. Chem. C* **2017**, *121*, 6546.
[191] N. Eustathopoulos, M. G. Nicholas, B. Drevet, *Wettability at High Temperatures*, 1st ed., Vol. *3*, Elsevier, Amsterdam **1999**,
[192] W.-H. Chen, L. Qiu, Z. Zhuang, L. Song, P. Du, J. Xiong, F. Ko, *J. Power Sources* **2019**, *442*, 227216.
[193] B. Chaudhary, A. Kulkarni, A. K. Jena, M. Ikegami, T. Miyasaka, *Energy Technol.* **2020**, *8*, 1900990.
[194] Y. Rong, Y. Ming, W. Ji, D. Li, A. Mei, Y. Hu, H. Han, *J. Phys. Chem. Lett.* **2018**, *9*, 2707.
[195] A. T. Mallajosyula, K. Fernando, S. Bhatt, A. Singh, B. W. Alphenaar, J.-C. Blancon, W. Nie, G. Gupta, A. D. Mohite, *Appl. Mater. Today* **2016**, *3*, 96.
[196] J. Su, H. Cai, X. Ye, X. Zhou, J. Yang, D. Wang, J. Ni, J. Li, J. Zhang, *ACS Appl. Mater. Interfaces* **2019**, *11*, 10689.
[197] Z. Wang, X. Liu, Y. Lin, Y. Liao, Q. Wei, H. Chen, J. Qiu, Y. Chen, Y. Zheng, *J. Mater. Chem. A* **2019**, *7*, 2773.
[198] H.-S. Ko, J.-W. Lee, N.-G. Park, *J. Mater. Chem. A* **2015**, *3*, 8808.
[199] K. Huang, H. Li, C. Zhang, Y. Gao, T. Liu, J. Zhang, Y. Gao, Y. Peng, L. Ding, J. Yang, *Sol. RRL* **2019**, *3*, 1800318.
[200] L. Liang, Z. Li, F. Zhou, Q. Wang, H. Zhang, Z. Xu, L. Ding, S. (Frank) Liu, Z. Jin, *J. Mater. Chem. A* **2019**, *7*, 26776.
[201] T. Singh, M. Ikegami, T. Miyasaka, *ACS Appl. Energy Mater.* **2018**, *1*, 6741.
[202] R. Patidar, D. Burkitt, K. Hooper, D. Richards, T. Watson, *Mater. Today Commun.* **2020**, *22*, 100808.
[203] A. Verma, D. Martineau, E. Hack, M. Makha, E. Turner, F. Nüesch, J. Heier, *J. Mater. Chem. C* **2020**, *8*, 6124.
[204] J. B. Whitaker, D. H. Kim, B. W. Larson, F. Zhang, J. J. Berry, M. F. A. M. van Hest, K. Zhu, *Sustainable Energy Fuels* **2018**, *2*, 2442.
[205] Y. Galagan, F. Di Giacomo, H. Gorter, G. Kirchner, I. de Vries, R. Andriessen, P. Groen, *Adv. Energy Mater.* **2018**, *8*, 1801935.
[206] J. Ciro, M. A. Mejía-Escobar, F. Jaramillo, *Sol. Energy* **2017**, *150*, 570.
[207] Y.-S. Jung, K. Hwang, Y.-J. Heo, J.-E. Kim, D. Lee, C.-H. Lee, H.-I. Joh, J.-S. Yeo, D.-Y. Kim, *ACS Appl. Mater. Interfaces* **2017**, *9*, 27832.
[208] Y.-J. Jeon, S. Lee, R. Kang, J.-E. Kim, J.-S. Yeo, S.-H. Lee, S.-S. Kim, J.-M. Yun, D.-Y. Kim, *Sci. Rep.* **2015**, *4*, 6953.
[209] Y.-C. Huang, C.-F. Li, Z.-H. Huang, P.-H. Liu, C.-S. Tsao, *Sol. Energy* **2019**, *177*, 255.
[210] C. Gong, S. Tong, K. Huang, H. Li, H. Huang, J. Zhang, J. Yang, *Sol. RRL* **2020**, *4*, 1900204.
[211] H. Wu, C. Zhang, K. Ding, L. Wang, Y. Gao, J. Yang, *Org. Electron.* **2017**, *45*, 302.
[212] Y. Peng, Y. Cheng, C. Wang, C. Zhang, H. Xia, K. Huang, S. Tong, X. Hao, J. Yang, *Org. Electron.* **2018**, *58*, 153.
[213] M. Yang, Y. Zhou, Y. Zeng, C.-S. Jiang, N. P. Padture, K. Zhu, *Adv. Mater.* **2015**, *27*, 6363.
[214] D. Wang, J. Zheng, X. Wang, J. Gao, W. Kong, C. Cheng, B. Xu, *J. Energy Chem.* **2019**, *38*, 207.
[215] Z. Bi, X. Rodríguez-Martínez, C. Aranda, E. Pascual-San-José, A. R. Goñi, M. Campoy-Quiles, X. Xu, A. Guerrero, *J. Mater. Chem. A* **2018**, *6*, 19085.
[216] A. T. Barrows, A. J. Pearson, C. K. Kwak, A. D. F. Dunbar, A. R. Buckley, D. G. Lidzey, *Energy Environ. Sci.* **2014**, *7*, 2944.
[217] Z. Bi, Z. Liang, X. Xu, Z. Chai, H. Jin, D. Xu, J. Li, M. Li, G. Xu, *Sol. Energy Mater. Sol. Cells* **2017**, *162*, 13.
[218] M. Zhang, H. Yu, J.-H. Yun, M. Lyu, Q. Wang, L. Wang, *Chem. Commun.* **2015**, *51*, 10038.
[219] C. Zuo, D. Vak, D. Angmo, L. Ding, M. Gao, *Nano Energy* **2018**, *46*, 185.
[220] B. Lei, V. O. Eze, T. Mori, *Jpn. J. Appl. Phys.* **2015**, *54*, 100305.
[221] J. Yin, H. Qu, J. Cao, H. Tai, J. Li, N. Zheng, *J. Mater. Chem. A* **2016**, *4*, 13203.
[222] R. Singh, S. Sandhu, H. Yadav, J.-J. Lee, *ACS Appl. Mater. Interfaces* **2019**, *11*, 29941.
[223] H.-J. Yen, P.-W. Liang, C.-C. Chueh, Z. Yang, A. K.-Y. Jen, H.-L. Wang, *ACS Appl. Mater. Interfaces* **2016**, *8*, 14513.
[224] X. Xu, C. Ma, Y.-M. Xie, Y. Cheng, Y. Tian, M. Li, Y. Ma, C.-S. Lee, S.-W. Tsang, *J. Mater. Chem. A* **2018**, *6*, 7731.
[225] L. Chao, Y. Xia, B. Li, G. Xing, Y. Chen, W. Huang, *Chem* **2019**, *5*, 995.
[226] L. Zheng, L. Xiao, Y. Wang, H. Yang, *Org. Electron.* **2018**, *58*, 119.
[227] R. Cheng, C.-C. Chung, H. Zhang, Z. Zhou, P. Zhai, Y.-T. Huang, H. Lee, S.-P. Feng, *Small* **2019**, *15*, 1804465.
[228] P. Zhai, T.-S. Su, T.-Y. Hsieh, W.-Y. Wang, L. Ren, J. Guo, T.-C. Wei, *Nano Energy* **2019**, *65*, 104036.
[229] N. Yaghoobi Nia, F. Giordano, M. Zendehdel, L. Cinà, A. L. Palma, P. G. Medaglia, S. M. Zakeeruddin, M. Grätzel, A. Di Carlo, *Nano Energy* **2020**, *69*, 104441.
[230] C. Duan, J. Cui, M. Zhang, Y. Han, S. Yang, H. Zhao, H. Bian, J. Yao, K. Zhao, Z. Liu, S. (Frank) Liu, *Adv. Energy Mater.* **2020**, *10*, 2000691.
[231] A. Klasen, P. Baumli, Q. Sheng, E. Johannes, S. A. Bretschneider, I. M. Hermes, V. W. Bergmann, C. Gort, A. Axt, S. A. L. Weber, H. Kim, H.-J. Butt, W. Tremel, R. Berger, *J. Phys. Chem. C* **2019**, *123*, 13458.
[232] E. Jiang, J. Yan, Y. Ai, N. Li, B. Yan, Y. Zeng, J. Sheng, J. Ye, *Mater. Today Energy* **2019**, *12*, 389.
[233] F. Zhang, W. Ma, H. Guo, Y. Zhao, X. Shan, K. Jin, H. Tian, Q. Zhao, D. Yu, X. Lu, G. Lu, S. Meng, *Chem. Mater.* **2016**, *28*, 802.
[234] Q. Zhang, C. S. Dandeneau, X. Zhou, G. Cao, *Adv. Mater.* **2009**, *21*, 4087.
[235] J. Yang, B. D. Siempelkamp, E. Mosconi, F. De Angelis, T. L. Kelly, *Chem. Mater.* **2015**, *27*, 4229.
[236] Y. Guo, X. Li, L. L. Kang, X. He, Z. Q. Ren, J. D. Wu, J. Y. Qi, *RSC Adv.* **2016**, *6*, 62522.
[237] Y. Guo, L. Kang, M. Zhu, Y. Zhang, X. Li, P. Xu, *Chem. Eng. J.* **2018**, *336*, 732.
[238] P. Docampo, J. M. Ball, M. Darwich, G. E. Eperon, H. J. Snaith, *Nat. Commun.* **2013**, *4*, 761.
[239] J.-Y. Jeng, Y.-F. Chiang, M.-H. Lee, S.-R. Peng, T.-F. Guo, P. Chen, T.-C. Wen, *Adv. Mater.* **2013**, *25*, 3727.
[240] S. Yamane, J. Mizukado, Y. Suzuki, M. Sakurai, L. Chen, H. Suda, *Chem. Lett.* **2015**, *44*, 339.
[241] Z. Xiao, J. Yao, D. Yang, F. Wang, S. Huang, L. Gan, Z. Jia, Z. Jiang, X. Yang, B. Zheng, G. Yuan, S. Zhang, Z. Wang, *J. Am. Chem. Soc.* **2007**, *129*, 16149.
[242] M. O. Reese, A. M. Nardes, B. L. Rupert, R. E. Larsen, D. C. Olson, M. T. Lloyd, S. E. Shaheen, D. S. Ginley, G. Rumbles, N. Kopidakis, *Adv. Funct. Mater.* **2010**, *20*, 3476.

© 2020 The Authors. Published by Wiley-VCH GmbH

[243] H. K. H. Lee, A. M. Telford, J. A. Röhr, M. F. Wyatt, B. Rice, J. Wu, A. de Castro Maciel, S. M. Tuladhar, E. Speller, J. McGettrick, J. R. Searle, S. Pont, T. Watson, T. Kirchartz, J. R. Durrant, W. C. Tsoi, J. Nelson, Z. Li, *Energy Environ. Sci.* **2018**, *11*, 417.
[244] A. S. Anselmo, A. Dzwilewski, K. Svensson, E. Moons, *Chem. Phys. Lett.* **2016**, *652*, 220.
[245] R. Hansson, C. Lindqvist, L. K. E. Ericsson, A. Opitz, E. Wang, E. Moons, *Phys. Chem. Chem. Phys.* **2016**, *18*, 11132.
[246] Y. Bai, Q. Dong, Y. Shao, Y. Deng, Q. Wang, L. Shen, D. Wang, W. Wei, J. Huang, *Nat. Commun.* **2016**, *7*, 12806.
[247] D. Yang, X. Zhang, K. Wang, C. Wu, R. Yang, Y. Hou, Y. Jiang, S. Liu, S. Priya, *Nano Lett.* **2019**, *19*, 3313.
[248] W. Chen, Y. Wu, Y. Yue, J. Liu, W. Zhang, X. Yang, H. Chen, E. Bi, I. Ashraful, M. Grätzel, L. Han, *Science* **2015**, *350*, 944.
[249] L. Q. Zhang, X. W. Zhang, Z. G. Yin, Q. Jiang, X. Liu, J. H. Meng, Y. J. Zhao, H. L. Wang, *J. Mater. Chem. A* **2015**, *3*, 12133.
[250] G. Kakavelakis, T. Maksudov, D. Konios, I. Paradisanos, G. Kioseoglou, E. Stratakis, E. Kymakis, *Adv. Energy Mater.* **2017**, *7*, 1602120.
[251] J. You, L. Meng, T.-B. Song, T.-F. Guo, Y. Yang, W.-H. Chang, Z. Hong, H. Chen, H. Zhou, Q. Chen, Y. Liu, N. De Marco, Y. Yang, *Nat. Nanotechnol.* **2016**, *11*, 75.
[252] W. Tress, N. Marinova, T. Moehl, S. M. Zakeeruddin, M. K. Nazeeruddin, M. Grätzel, *Energy Environ. Sci.* **2015**, *8*, 995.
[253] W. Tress, K. Leo, M. Riede, *Adv. Funct. Mater.* **2011**, *21*, 2140.
[254] W. Tress, S. Corvers, K. Leo, M. Riede, *Adv. Energy Mater.* **2013**, *3*, 873.
[255] C. Chen, S. Zhang, S. Wu, W. Zhang, H. Zhu, Z. Xiong, Y. Zhang, W. Chen, *RSC Adv.* **2017**, *7*, 35819.
[256] F. Lamberti, T. Gatti, E. Cescon, R. Sorrentino, A. Rizzo, E. Menna, G. Meneghesso, M. Meneghetti, A. Petrozza, L. Franco, *Chem* **2019**, *5*, 1806.
[257] J. H. Noh, N. J. Jeon, Y. C. Choi, Md. K. Nazeeruddin, M. Grätzel, S. I. Seok, *J. Mater. Chem. A* **2013**, *1*, 11842.
[258] H. Sarvari, X. Wang, Y. Wang, P. Zhang, S. Li, V. P. Singh, Z. Chen, *IEEE J. Photovoltaics* **2018**, *8*, 1051.
[259] S. Fantacci, F. De Angelis, M. K. Nazeeruddin, M. Grätzel, *J. Phys. Chem. C* **2011**, *115*, 23126.
[260] S. Wang, W. Yuan, Y. S. Meng, *ACS Appl. Mater. Interfaces* **2015**, *7*, 24791.
[261] Z. Hawash, L. K. Ono, Y. Qi, *Adv. Mater. Interfaces* **2016**, *3*, 1600117.
[262] M. Stolterfoht, P. Caprioglio, C. M. Wolff, J. A. Márquez, J. Nordmann, S. Zhang, D. Rothhardt, U. Hörmann, Y. Amir, A. Redinger, L. Kegelmann, F. Zu, S. Albrecht, N. Koch, T. Kirchartz, M. Saliba, T. Unold, D. Neher, *Energy Environ. Sci.* **2019**, *12*, 2778.
[263] E. H. Jung, N. J. Jeon, E. Y. Park, C. S. Moon, T. J. Shin, T.-Y. Yang, J. H. Noh, J. Seo, *Nature* **2019**, *567*, 511.
[264] A. Shit, A. K. Nandi, *Phys. Chem. Chem. Phys.* **2016**, *18*, 10182.
[265] M. Batmunkh, C. J. Shearer, M. J. Biggs, J. G. Shapter, *J. Mater. Chem. A* **2015**, *3*, 9020.
[266] N. Arora, M. I. Dar, S. Akin, R. Uchida, T. Baumeler, Y. Liu, S. M. Zakeeruddin, M. Grätzel, *Small* **2019**, *15*, 1904746.
[267] X. Meng, J. Zhou, J. Hou, X. Tao, S. H. Cheung, S. K. So, S. Yang, *Adv. Mater.* **2018**, *30*, 1706975.
[268] H. Chen, S. Yang, *Adv. Mater.* **2017**, *29*, 1603994.
[269] Z. Ku, Y. Rong, M. Xu, T. Liu, H. Han, *Sci. Rep.* **2013**, *3*, 3132.
[270] C.-T. Lin, J. Ngiam, B. Xu, Y.-H. Chang, T. Du, T. J. Macdonald, J. R. Durrant, M. A. McLachlan, *J. Mater. Chem. A* **2020**, *8*, 8684.
[271] J. Zhou, J. Wu, N. Li, X. Li, Y.-Z. Zheng, X. Tao, *J. Mater. Chem. A* **2019**, *7*, 17594.
[272] P. Liu, Y. Gong, Y. Xiao, M. Su, S. Kong, F. Qi, H. Zhang, S. Wang, X. Sun, C. Wang, X.-Z. Zhao, *Chem. Commun.* **2019**, *55*, 218.
[273] N. Cheng, P. Liu, F. Qi, Y. Xiao, W. Yu, Z. Yu, W. Liu, S.-S. Guo, X.-Z. Zhao, *J. Power Sources* **2016**, *332*, 24.
[274] D. Papadatos, D. Sygkridou, E. Stathatos, *Mater. Lett.* **2020**, *268*, 127621.
[275] X. Chang, W. Li, L. Zhu, H. Liu, H. Geng, S. Xiang, J. Liu, H. Chen, *ACS Appl. Mater. Interfaces* **2016**, *8*, 33649.
[276] M. I. Hossain, F. H. Alharbi, N. Tabet, *Sol. Energy* **2015**, *120*, 370.
[277] N. Arora, M. I. Dar, A. Hinderhofer, N. Pellet, F. Schreiber, S. M. Zakeeruddin, M. Grätzel, *Science* **2017**, *358*, 768.
[278] X. Jiang, D. Wang, Z. Yu, W. Ma, H.-B. Li, X. Yang, F. Liu, A. Hagfeldt, L. Sun, *Adv. Energy Mater.* **2019**, *9*, 1803287.
[279] G. Murugadoss, H. Kanda, S. Tanaka, H. Nishino, S. Ito, H. Imahori, T. Umeyama, *J. Power Sources* **2016**, *307*, 891.
[280] V. I. Madogni, B. Kounouhéwa, A. Akpo, M. Agbomahéna, S. A. Hounkpatin, C. N. Awanou, *Chem. Phys. Lett.* **2015**, *640*, 201.
[281] E. Voroshazi, B. Verreet, A. Buri, R. Müller, D. Di Nuzzo, P. Heremans, *Org. Electron.* **2011**, *12*, 736.
[282] A. Seemann, H.-J. Egelhaaf, C. J. Brabec, J. A. Hauch, *Org. Electron.* **2009**, *10*, 1424.
[283] F. Hou, Z. Su, F. Jin, X. Yan, L. Wang, H. Zhao, J. Zhu, B. Chu, W. Li, *Nanoscale* **2015**, *7*, 9427.
[284] D. B. Kim, J. C. Yu, Y. S. Nam, D. W. Kim, E. D. Jung, S. Y. Lee, S. Lee, J. H. Park, A.-Y. Lee, B. R. Lee, D. Di Nuzzo, R. H. Friend, M. H. Song, *J. Mater. Chem. C* **2016**, *4*, 8161.
[285] J. C. Yu, J. A. Hong, E. D. Jung, D. B. Kim, S.-M. Baek, S. Lee, S. Cho, S. S. Park, K. J. Choi, M. H. Song, *Sci. Rep.* **2018**, *8*, 1070.
[286] S. H. Chang, K.-F. Lin, K. Y. Chiu, C.-L. Tsai, H.-M. Cheng, S.-C. Yeh, W.-T. Wu, W.-N. Chen, C.-T. Chen, S.-H. Chen, C.-G. Wu, *Sol. Energy* **2015**, *122*, 892.
[287] D. Zhao, M. Sexton, H.-Y. Park, G. Baure, J. C. Nino, F. So, *Adv. Energy Mater.* **2015**, *5*, 1401855.
[288] O. Malinkiewicz, C. Roldán-Carmona, A. Soriano, E. Bandiello, L. Camacho, M. K. Nazeeruddin, H. J. Bolink, *Adv. Energy Mater.* **2014**, *4*, 1400345.
[289] Q. Wang, C. Bi, J. Huang, *Nano Energy* **2015**, *15*, 275.
[290] C. Bi, Q. Wang, Y. Shao, Y. Yuan, Z. Xiao, J. Huang, *Nat. Commun.* **2015**, *6*, 7747.
[291] W. Zhang, J. Smith, R. Hamilton, M. Heeney, J. Kirkpatrick, K. Song, S. E. Watkins, T. Anthopoulos, I. McCulloch, *J. Am. Chem. Soc.* **2009**, *131*, 10814.
[292] S. Barard, M. Heeney, L. Chen, M. Cölle, M. Shkunov, I. McCulloch, N. Stingelin, M. Philips, T. Kreouzis, *J. Appl. Phys.* **2009**, *105*, 013701.
[293] J. Veres, S. Ogier, G. Lloyd, D. de Leeuw, *Chem. Mater.* **2004**, *16*, 4543.
[294] S. S. Mali, H. Kim, H. H. Kim, S. E. Shim, C. K. Hong, *Mater. Today* **2018**, *21*, 483.
[295] M. M. Tavakoli, H. T. Dastjerdi, D. Prochowicz, P. Yadav, R. Tavakoli, M. Saliba, Z. Fan, *J. Mater. Chem. A* **2019**, *7*, 14753.
[296] S. Ye, H. Rao, Z. Zhao, L. Zhang, H. Bao, W. Sun, Y. Li, F. Gu, J. Wang, Z. Liu, Z. Bian, C. Huang, *J. Am. Chem. Soc.* **2017**, *139*, 7504.
[297] W. Kong, W. Li, C. Liu, H. Liu, J. Miao, W. Wang, S. Chen, M. Hu, D. Li, A. Amini, S. Yang, J. Wang, B. Xu, C. Cheng, *ACS Nano* **2019**, *13*, 1625.
[298] Y. Wang, T. Mahmoudi, W.-Y. Rho, H.-Y. Yang, S. Seo, K. S. Bhat, R. Ahmad, Y.-B. Hahn, *Nano Energy* **2017**, *40*, 408.
[299] Z. Yang, B. H. Babu, S. Wu, T. Liu, S. Fang, Z. Xiong, L. Han, W. Chen, *Sol. RRL* **2020**, *4*, 1900257.
[300] W. Zhang, Z. Ren, Y. Guo, X. He, X. Li, *Electrochim. Acta* **2018**, *268*, 539.
[301] M. Hadadian, J.-H. Smått, J.-P. Correa-Baena, *Energy Environ. Sci.* **2020**, *13*, 1377.
[302] L. Fagiolari, F. Bella, *Energy Environ. Sci.* **2019**, *12*, 3437.
[303] J. D. Roy-Mayhew, I. A. Aksay, *Chem. Rev.* **2014**, *114*, 6323.
[304] D. H. Seo, M. Batmunkh, J. Fang, A. T. Murdock, S. Yick, Z. Han, C. J. Shearer, T. J. Macdonald, M. Lawn, A. Bendavid, J. G. Shapter, K. (Ken) Ostrikov, *FlatChem* **2018**, *8*, 1.
[305] S. Casaluci, M. Gemmi, V. Pellegrini, A. D. Carlo, F. Bonaccorso, *Nanoscale* **2016**, *8*, 5368.
[306] M. Batmunkh, M. J. Biggs, J. G. Shapter, *Small* **2015**, *11*, 2963.
[307] T. J. Macdonald, D. D. Tune, M. R. Dewi, C. T. Gibson, J. G. Shapter, T. Nann, *ChemSusChem* **2015**, *8*, 3396.

© 2020 The Authors. Published by Wiley-VCH GmbH

[308] B. He, Q. Tang, T. Liang, Q. Li, *J. Mater. Chem. A* **2014**, *2*, 3119.
[309] P. O'Keeffe, D. Catone, A. Paladini, F. Toschi, S. Turchini, L. Avaldi, F. Martelli, A. Agresti, S. Pescetelli, A. E. Del Rio Castillo, F. Bonaccorso, A. Di Carlo, *Nano Lett.* **2019**, *19*, 684.
[310] C. Zhang, S. Wang, H. Zhang, Y. Feng, W. Tian, Y. Yan, J. Bian, Y. Wang, S. Jin, S. M. Zakeeruddin, M. Grätzel, Y. Shi, *Energy Environ. Sci.* **2019**, *12*, 3585.
[311] M. Acik, S. B. Darling, *J. Mater. Chem. A* **2016**, *4*, 6185.
[312] M. Batmunkh, T. J. Macdonald, C. J. Shearer, M. Bat-Erdene, Y. Wang, M. J. Biggs, I. P. Parkin, T. Nann, J. G. Shapter, *Adv. Sci.* **2017**, *4*, 1600504.
[313] S. N. Habisreutinger, T. Leijtens, G. E. Eperon, S. D. Stranks, R. J. Nicholas, H. J. Snaith, *Nano Lett.* **2014**, *14*, 5561.
[314] S. N. Habisreutinger, N. K. Noel, B. W. Larson, O. G. Reid, J. L. Blackburn, *ACS Energy Lett.* **2019**, *4*, 1872.
[315] A. S. R. Bati, L. Yu, S. A. Tawfik, M. J. S. Spencer, P. E. Shaw, M. Batmunkh, J. G. Shapter, *iScience* **2019**, *14*, 100.
[316] C. Wu, K. Wang, M. Batmunkh, A. S. R. Bati, D. Yang, Y. Jiang, Y. Hou, J. G. Shapter, S. Priya, *Nano Energy* **2020**, *70*, 104480.
[317] M. V. Khenkin, E. A. Katz, A. Abate, G. Bardizza, J. J. Berry, C. Brabec, F. Brunetti, V. Bulović, Q. Burlingame, A. Di Carlo, R. Cheacharoen, Y.-B. Cheng, A. Colsmann, S. Cros, K. Domanski, M. Dusza, C. J. Fell, S. R. Forrest, Y. Galagan, D. Di Girolamo, M. Grätzel, A. Hagfeldt, E. von Hauff, H. Hoppe, J. Kettle, H. Köbler, M. S. Leite, S. (Frank) Liu, Y.-L. Loo, J. M. Luther, C.-Q. Ma, M. Madsen, M. Manceau, M. Matheron, M. McGehee, R. Meitzner, M. K. Nazeeruddin, A. F. Nogueira, Ç. Odabaşı, A. Osherov, N.-G. Park, M. O. Reese, F. De Rossi, M. Saliba, U. S. Schubert, H. J. Snaith, S. D. Stranks, W. Tress, P. A. Troshin, V. Turkovic, S. Veenstra, I. Visoly-Fisher, A. Walsh, T. Watson, H. Xie, R. Yıldırım, S. M. Zakeeruddin, K. Zhu, M. Lira-Cantu, *Nat. Energy* **2020**, *5*, 35.
[318] L. Shi, M. P. Bucknall, T. L. Young, M. Zhang, L. Hu, J. Bing, D. S. Lee, J. Kim, T. Wu, N. Takamure, D. R. McKenzie, S. Huang, M. A. Green, A. W. Y. Ho-Baillie, *Science* **2020**, *368*, eaba2412.
[319] J. H. Heo, D. H. Song, H. J. Han, S. Y. Kim, J. H. Kim, D. Kim, H. W. Shin, T. K. Ahn, C. Wolf, T.-W. Lee, S. H. Im, *Adv. Mater.* **2015**, *27*, 3424.
[320] Y. Wang, T. Mahmoudi, W.-Y. Rho, Y.-B. Hahn, *Nano Energy* **2019**, *64*, 103964.
[321] K. Momma, F. Izumi, *J. Appl. Cryst.* **2011**, *44*, 1272.



Yuan Zhang received a B.S. degree in chemistry at the University of Sheffield in 2018, and M.S. degree in materials for energy and environment at University College London in 2019. He will be starting his Ph.D. in the School of Engineering and Materials Science at Queen Mary University of London in 2021. He is interested in the fabrication of perovskite solar cells and piezoelectric energy harvesters.



Munkhbayar Batmunkh is a research fellow in the Centre for Clean Environment and Energy at Griffith University, Australia. He also worked at the University of Queensland (2018–2019) and Flinders University (2017–2018), and was a visiting scholar in Virginia Tech in the USA. He studied for "Bachelor of Science" (2006–2010) at the National University of Mongolia, in Mongolia and "Master of Engineering" (2010–2012) at Gyeongsang National University, in South Korea, before completing his Ph.D. in chemical engineering in 2017 at the University of Adelaide (Australia). His research interests include functional nanomaterials (e.g., nanocarbons and 2D materials) for energy related applications such as solar cells, smart photovoltaic windows, and catalysis.



Thomas J. Macdonald is currently an 1851 Research Fellow in the Department of Chemistry at Imperial College London. He is also a visiting Research Fellow in the Chemistry Department at University College London. Prior to this, he was a Ramsay Memorial Fellow at University College London working on nanomaterials for energy conversion. He obtained his Ph.D. at the University of South Australia in 2016 working in the research group of Prof. Thomas Nann. He has a strong interest in renewable energy conversion and has extensive experience in the synthesis of functional nanomaterials and the fabrication of third-generation photovoltaics.

© 2020 The Authors. Published by Wiley-VCH GmbH